

*phd thesis*

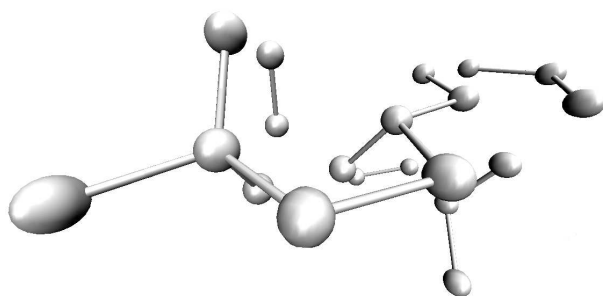
---

---

**Long-time simulations of viscous liquids**  
*from strong correlations to crystallization*

---

---



Ulf Rørbæk Pedersen

Supervisor: Thomas B. Schrøder

*Danish National Research Foundation Centre "Glass and Time",  
IMFUFA, Department of Science, Systems and Models,  
Roskilde University, Denmark*

January 30, 2009



---

## Abstract

This philosophiæ doctor thesis has thirteen companion papers. The major part is a theoretical and simulation study of a class of liquids referred to as strongly correlating liquids. However, one chapter is dedicated to a study of thermodynamic fluctuations of simulated phospholipid membranes, and another to a simulation study of crystallization of a binary mixture. The thesis also includes a short introduction to supercooled viscous liquids and molecular dynamics simulations. The final chapter is an outlook. The conclusions are as follows:

A class of model liquids exhibit strong correlation in the thermal fluctuations of the virial and potential energy at constant volume. The origin of the correlation is explained for the Lennard-Jones liquid. The pair energy can to a good approximation be replaced by an inverse power-law plus a linear term. At constant volume only the inverse power-law gives a contribution to fluctuations, thereby explaining the correlation. Two quantities characterize a strongly correlating liquid: i) A correlation coefficient,  $R$ , that determine the degree of correlation and ii) a slope,  $\gamma$ , that determine the proportionality between virial and potential energy. If the correlation coefficient is close to unity the liquid is strongly correlating and  $3\gamma$  equals the exponent of the inverse power-law.

For viscous liquids, the correlation coefficient equals the inverse square-root of a Prigogine-Defay ratio defined from three response functions. Also the slope can be determined from response functions. Literature values of the classical Prigogine-Defay suggests that van der Waals bonded liquids in general are strongly correlating.

Strongly correlating viscous liquids are more simple than viscous liquids in general: i) Slow dynamics are determined by a single relaxing parameter. Thus, time- and frequency-dependent response functions of a given ensemble are proportional. ii) Scale invariance is inherited from soft-sphere liquids though the effective inverse-power law. Thus, state points with the same value of  $\rho^\gamma/T$  have the same scaled structure and dynamics. These conclusions are verified in simulations.

Slow thermal fluctuations of volume and energy of simulated phospholipid membranes are strongly correlated. The origin of the strong correlation can be traced to the van der Waals bonded core of the membranes and, thus, have the same origin as simple strongly correlating liquids.

The last part of the thesis reports crystallization into the MgZn<sub>2</sub> Laves phase of the binary Lennard-Jones mixture suggested by Wahnström [1991]. The crystallization mechanism from the supercooled melt is investigated in detail.

---

*Abstract in danish:*

Denne philosophiæ doctor afhandling er ledsaget af tretten artikler. Hoveddelen er et teoretisk og simulerings studie af en klasse af væsker refereret til som stærkt korrelerede væsker. Dog er et kapitel dedikeret til et studie af termiske fluktuationer af simulerede phospholipidmembraner, og et kapitel til et simuleringsstudie af krystallisering af en binær blanding. Afhandlingen inkluderer også en kort introduktion til underafkølede viskøse væsker samt molekyledynamik simuleringer. Det sidste kapitel omhandler fremtidige undersøgelser. Følgende er konkluderet:

En klasse af modelvæsker udviser ved konstant volumen en stærk korrelation i de termiske fluktuationer af virial og potentiel energi. Korrelationens ophav er forklaret for Lennard-Jones væsken. Parenergien kan med god tilnærmelse erstattes med en inverts potensfunktion plus et lineært led. Ved konstant volumen er det kun den inverse potensfunktion som giver bidrag til fluktuationer, og derved forklarer korrelationen. To størrelser karakteriserer en stærkt korreleret væske: i) En korrelationskoefficient,  $R$ , som bestemmer graden af korrelation og ii) en hældning,  $\gamma$ , som bestemmer proportionaliteten mellem virial og potentiel energi. Hvis korrelationskoefficienten er tæt på én, er væsken stærkt korrelerende og  $3\gamma$  er lig med eksponenten af den inverse potensfunktion.

For viskøse væsker er korrelationskoefficienten lig med den inverse kvadratrods af en Prigogine-Defay kvotient defineret ud fra tre responsfunktioner. Hældningen kan også bestemmes ud fra responsfunktioner. Værdier af den klassiske Prigogine-Defay kvotient fra litteraturen indikerer, at van der Waals væsker i almindelighed er stærkt korrelerede.

Stærkt korrelerede viskøse væsker er simple end viskøse væsker i almindelighed: i) Langsom dynamik er styret af en enkelt relakserende parameter. Derved er de tids- og frekvensafhængige responsfunktioner for et givet ensemble proportionale. ii) Skaleringsinvarians af *soft sphere*-væsker nedarves gennem den inverse potensfunktion. Derfor har tilstande med samme værdi af  $\rho^\gamma/T$  den samme skallerede struktur og dynamik. Simuleringer bekræfter disse konklusioner.

Simulerede phospholipidmembraners langsomme termiske fluktuationer af volumen og energi er stærkt korrelerede. Forklaringen på den stærke korrelation skal findes i den indre van der Waalske del af membranen. Derved er oprindelsen den samme som for de stærkt korrelerede simple væsker.

Den sidste del af afhandlingen beretter om krystallisering ind i  $\text{MgZn}_2$  Laves-fasen af den binære Lennard-Jones blanding foreslået af Wahnström [1991]. Mekanismen for krystallisering af den underafkølede smelte er undersøgt i detaljer.

# Preface

This is the philosophiæ doctor (Ph.D.) thesis of Ulf Rørbæk Pedersen. The Ph.D. was initiated February 1st 2006 and the thesis was submitted January 30th 2009, thus lasting the three years of the Danish Ph.D. program.

The thesis have thirteen companion papers (listed below). The purpose of the thesis is to guide the reader though these papers. The reader will, however, have to consult the papers to get the full story. Also, parts of the thesis goes beyond the papers.

## Papers

Companion papers are listed below and reprinted in Appendix B.

**Paper I:** Niels L. Ellegaard, Tage Christensen, Peder Voetmann Christiansen, Niels Boye Olsen, Ulf R. Pedersen, Thomas B. Schröder, Jeppe C. Dyre (2007) *Single-order-parameter description of glass-forming liquids: A one-frequency test*. J. Chem. Phys 126, 074502

**Paper II:** Ulf R. Pedersen, Nicholas P. Bailey, Jeppe C. Dyre, Thomas B. Schröder (2007) *Crystallization of the Wahnström Binary Lennard-Jones Liquid*. arXiv:0706.0813

**Paper III:** Ulf R. Pedersen, Nicholas P. Bailey, Thomas B. Schröder, Jeppe C. Dyre (2008) *Strong pressure-energy correlations in van der Waals liquids*. Phys. Rev. Lett. 100, 015701

**Paper IV:** Ulf R. Pedersen, Tage Christensen, Thomas B. Schröder, Jeppe C. Dyre (2008) *Feasibility of a single-parameter description of equilibrium viscous liquid dynamics*. Phys. Rev. E 77, 011201

**Paper V:** Ulf R. Pedersen, Günther H. Peters, Thomas B. Schröder, Jeppe C. Dyre (2008) *Volume-energy correlations in the slow degrees of freedom of computer-simulated phospholipid membranes*. AIP Conf. Proc. 982, 407-409

**Paper VI:** Nicholas P. Bailey, Tage Chistensen, Bo Jakobsen, Kristine Niss, Niels Boye Olsen, Ulf R. Pedersen, Thomas B. Schröder, Jeppe C. Dyre (2008) *Glass-forming liquids: one or more 'order' parameters?* Journal of physics-condensed matter 20, 244113

**Paper VII:** Thomas B. Schröder, Ulf R. Pedersen, Jeppe C. Dyre (2008) *Density scaling in a strongly correlating viscous liquid*. arXiv:0803.2199 [cond-mat.soft]

- Paper VIII:** Nicholas P. Bailey, Ulf R. Pedersen, Nicoletta Gnan, Thomas B. Schröder, Jeppe C. Dyre (2008) *Pressure-energy correlations in liquids. I. Results from computer simulations*. J. Chem. Phys. 129, 184507
- Paper IX:** Nicholas P. Bailey, Ulf R. Pedersen, Nicoletta Gnan, Thomas B. Schröder, Jeppe C. Dyre (2008) *Pressure-energy correlations in liquids. II. Analysis and consequences*. J. Chem. Phys. 129, 184508 (2008)
- Paper X:** Ulf R. Pedersen, Günther H. Peters, Thomas B. Schröder, Jeppe C. Dyre (2008) *Computer simulations of phospholipid-membrane thermodynamic fluctuations*. arXiv:0811.3317 [physics.bio-ph]
- Paper XI:** Søren Toxvaerd, Ulf R. Pedersen, Thomas B. Schröder, Jeppe C. Dyre (2008) *Stability of supercooled binary liquid mixtures*. arXiv:0811.1117v1 [cond-mat.soft]
- Paper XII:** Ulf R. Pedersen, Thomas B. Schröder, Jeppe C. Dyre (2008) *Termiske fluktuationer — er der noget nyt under Solen?* (in danish) Kvant: Tidsskrift for fysik og astronomi 16(4), 26-29. Dec 2008
- Paper XIII:** Thomas B. Schröder, Ulf R. Pedersen, Nicholas Bailey, Søren Toxværd, Jeppe C. Dyre (2008) *Hidden scale invariance in molecular van der Waals liquids: A simulation study* arXiv:0812.4960v1 [cond-mat.soft]

## Oral and poster presentations

Results of this thesis have also been presented at the following conferences and meetings.

Oral presentations:

- Copenhagen 2008** *Long-lived structural fluctuations and crystallization of a binary Lennard-Jones mixture*. Presented at the international workshop Fragility of Viscous Liquids: Cause(s) and Consequences [Carlsberg Academy, Copenhagen, Denmark, October 8-10, 2008].
- Nyborg Strand 2008** *Volume-energy correlations in the slow degrees of freedom of phospholipid membranes*. Presented at the Danish Physical Society Annual Meeting [Nyborg Strand Hotel, Denmark, June 17-18, 2008].
- Søminestationen 2007** *Crystallization of the Wahnström binary Lennard-Jones liquid*. Presented at Viscous Liquids and the Glass Transition VI [Søminestationen, Holbæk, Denmark, June 29 - July 1, 2007].
- Søminestationen 2006** *A tumbling model of toluene*. Presented at Viscous Liquids and the Glass Transition V [Søminestationen, Holbæk, Denmark, May 26-28, 2006].

Poster presentations:

- Kyoto 2008** *Density scaling as a property of strongly correlating viscous liquids and Long-lived structural fluctuations and crystallization of a binary mixture*. Two posters presented at Unifying Concepts in Glass Physics IV (UCGP2008) [Kyoto, Japan, November 25-28 2008].

- Sitges 2008** *Equilibrium fluctuations of volume and energy of simulated phospholipid membranes.* Presented at the XXI Sitges Conference on Statistical mechanics: Statistical Mechanics of Molecular Biophysics [Sitges, Barcelona, Spain, June 2-6, 2008].
- Andalo 2008** *Long-lived structural fluctuations and crystallization of a binary Lennard-Jones mixture.* Presented at XI International Workshop on Complex Systems [Andalo, Italy, March 17-20, 2008].
- Sendai 2007** *Volume-energy correlations in the slow degrees of freedom of phospholipid membranes.* Presented at the 5th International Workshop on Complex Systems [Sendai International Center, Sendai, Japan, September 25-28, 2007].
- Holderness 2007** *Strong pressure-energy correlations in model liquids.* Presented at The Physics and Chemistry of Liquids (Gordon Conference) [Holderness School, New Hampshire, July 29 - August 3, 2007].
- Pisa 2006** *The dynamical Prigogine-Defay ratio: Is the glass transition controlled by one or more order-parameters?* Presented at IV Workshop on Non Equilibrium Phenomena in Supercooled Fluids, Glasses and Amorphous Materials [Pisa, Italy, September 17-22, 2006].
- Nyborg Strand 2006** *Molecular Dynamic Simulations of Viscous Toluene.* Presented at the Danish Physical Society Annual Meeting [Nyborg Strand Hotel, Denmark, June 1-2, 2006].

## Acknowledgments

This Ph.D. was financed by the Danish National Research Foundation Center for Viscous Liquids Dynamics “Glass and Time”.

First, I would like to thank the members of “Glass and Time” group: Jon Papini, Ditte Gundermann, Tina Hecksher, Nicolette Gnan, Claudio Maggi, Albena Nielsen, Ib Høst Pedersen, Torben Rasmussen, Ebbe Hyldahl Larsen, Preben Olsen, Elin Emborg, Heine Larsen, Brian Igarashi, Neslihan Saglanmak, Bo Jakobsen, Nicholas P. Bailey, Kristine Niss, Søren Toxværd, Thomas B. Schrøder, Tage Christensen, Niels B. Olsen, and Jeppe C. Dyre. It has been nice to experience the expansion of the group with more clever heads. A special thanks is given to Heine Larsen for managing computers and Elin Emborg for practical matters. I would like to thank everybody at IMFUFA for providing a pleasant working environment. A special thank is given to Jørgen Larsen for helping with questions related to statistics.

I would like to thank Henning Osholm Sørensen for help with identifying the crystal structure of the Wahnström binary Lennard-Jones mixture.

The study of phospholipid membranes was done in collaboration with Günther H. Peters who is an expert in simulations of phospholipid membranes. Simulations of phospholipid membranes were performed at the Danish Center for Scientific Computing at the University of Southern Denmark. Also thanks to Richard M. Venable for kindly providing a configuration of an ordered membrane.

## PREFACE

---

In March-April 2007 I spent one month visiting the Francesco Sciortino group at La Sapienza in Rome. I would like to thank them for the hospitality and nice discussions.

In September-November 2007 I visited Peter Harrowell at the School of Chemistry at the University of Sydney, where I also had the pleasure to meet Toby Hudson and Asaph Widmer-Cooper. I really enjoyed the enlightening discussion and warm humor of the Aussies. The study of the crystallisation of the Wahnström binary Lennard-Jones liquid is done in collaboration with Peter Harrowell.

Before handing in the thesis Nicolas P. Bailey and Thomas B. Schröder read all of the thesis and gave many useful comments and suggestions.

Finally I would like to thank the International Earth Rotation Service for giving an extra second after Jan 1st 00:59:59 2009. In the final phase of writing a thesis some extra time is always welcome.

# Contents

<b>Preface</b>	<b>v</b>
Papers . . . . .	v
Oral and poster presentations . . . . .	vi
Acknowledgments . . . . .	vii
<b>Contents</b>	<b>ix</b>
<b>1 Introduction</b>	<b>1</b>
1.1 Supercooled viscous liquids . . . . .	1
1.2 Molecular dynamics simulations . . . . .	4
1.2.1 Simulated systems . . . . .	6
1.3 Outline of thesis . . . . .	10
<b>2 Strongly correlating liquids</b>	<b>13</b>
2.1 An example: The Lennard-Jones Liquid . . . . .	13
2.2 A class of strongly correlating liquids . . . . .	17
2.3 Supercritical Argon . . . . .	17
<b>3 Origin of strong correlations</b>	<b>19</b>
3.1 Effective inverse power-law pair potential . . . . .	19
3.2 Approximate inverse power-law plus linear term pair potential . . . . .	24
3.3 Low temperature limit of crystal . . . . .	25
3.4 Weeks-Chandler-Andersen . . . . .	26
<b>4 Strongly correlating viscous liquids</b>	<b>29</b>
4.1 A single order-parameter of viscous liquids . . . . .	29
4.1.1 Dynamic Prigogine-Defay ratio, $\Lambda(\omega)$ . . . . .	30
4.1.2 Connecting Prigogine-Defay ratio to a correlation coefficient . . . . .	33
4.1.3 Rethinking the classical Prigogine-Defay ratio . . . . .	40
4.2 Hidden scale invariance . . . . .	41
<b>5 Volume-energy fluctuations of phospholipid membranes</b>	<b>49</b>
5.1 Motivation . . . . .	49
5.2 A simulation study . . . . .	51
<b>6 Stability of a binary mixture</b>	<b>59</b>
6.1 The Wahnström binary Lennard-Jones mixture . . . . .	59
6.2 The crystal . . . . .	61

## CONTENTS

---

6.3	Mechanism of crystallization . . . . .	62
6.4	Long-lived structural fluctuations stabilizing the liquid . . . . .	67
6.5	Kob-Andersen binary Lennard-Jones mixture . . . . .	72
<b>7</b>	<b>Outlook</b>	<b>75</b>
	<b>Bibliography</b>	<b>77</b>
<b>A</b>	<b>Calculations</b>	<b>87</b>
A.1	Energy-pressure correlations in a soft-sphere liquid . . . . .	87
A.2	Fitting inverse power-law to the generalized Lennard-Jones potential . . . . .	87
<b>B</b>	<b>Papers</b>	<b>89</b>
B.1	Paper I . . . . .	91
B.2	Paper II . . . . .	99
B.3	Paper III . . . . .	103
B.4	Paper IV . . . . .	107
B.5	Paper V . . . . .	113
B.6	Paper VI . . . . .	117
B.7	Paper VII . . . . .	125
B.8	Paper VIII . . . . .	131
B.9	Paper IX . . . . .	145
B.10	Paper X . . . . .	165
B.11	Paper XI . . . . .	181
B.12	Paper XII . . . . .	195
B.13	Paper XIII . . . . .	199

# Chapter 1

## Introduction

The purpose of this chapter is to give a short introduction to the field of supercooled viscous liquids (Section 1.1) and molecular dynamics simulations (Section 1.2). Section 1.3 gives an outline of the remainder of the thesis.

### 1.1 Supercooled viscous liquids

Imagine we are cooling a liquid as shown in Figure 1.1. Below some temperature  $T_m$  the free energy per particle of the crystal  $\mu_{\text{cry}}$  becomes lower than that of the liquid  $\mu_{\text{liq}}$ . According to thermodynamics, the molecules should now form a crystal to lower the free energy. However, making this experiment, in a computer or in the laboratory, the crystal might first form below  $T_m$  or never. The liquid is said to be supercooled at  $T < T_m$ .

To get insight on supercooling, recall classical nucleation theory in its simplest form [Volmer and Weber, 1926, Becker and Doring, 1935]. Imagine that for some reason a spherical crystallite had actually formed in the liquid at  $T < T_m$ . Let  $N_c$  be the number of particles,  $r_c$  the radius and  $\rho_c = \frac{N_c}{\frac{4}{3}\pi r_c^3}$  the density of the crystallite. The stability of this crystallite is given by the Gibbs free energy  $G$  relative to the liquid. Bulk particles in a crystalline environment will give a negative volume contribution;  $G_{\text{vol}} = -\frac{4}{3}\pi r_c^3 \rho_c \Delta\mu$  where  $\Delta\mu = \mu_{\text{liq}} - \mu_{\text{cry}}$ . However, the solid-liquid surface tension  $\gamma_\infty$  will give a positive surface contribution;  $G_{\text{surf}} = 4\pi r_c^2 \gamma_\infty$ , thereby destabilizing the crystallite. Surface area scales as  $r_c^2$  and volume as  $r_c^3$ , so if the crystallite is big enough, the negative volume contribution dominates and the crystallite will grow;  $\frac{\partial}{\partial r_c} \Delta G < 0$  for large  $r_c$  where  $\Delta G = G_{\text{surf}} + G_{\text{vol}}$ . However, at some critical size the surface contribution and the volume contribution will balance out.  $\frac{\partial}{\partial r_c} \Delta G = 0$ , when

$$r_c^* = \frac{2\gamma_\infty}{\rho_c \Delta\mu} \quad \text{and} \quad \Delta G^* = \frac{16\pi\gamma_\infty^3}{3\rho_c^2 (\Delta\mu)^2} \quad (1.1)$$

Crystallites smaller than  $r_c^*$  are unstable. The crystallite leading to crystallization is referred to as the critical nucleus. Remember that  $\Delta\mu(T_m) \equiv 0$  by definition, thus, the size  $r_c^*$  and barrier height  $\Delta G^*$  of the critical nucleus is infinitely large at the melting temperature. Therefore all liquids can be supercooled since all crystallites are unstable at  $T_m$ . If we wait long enough at  $T < T_m$  a thermal fluctuation will eventually form the critical nucleus and the

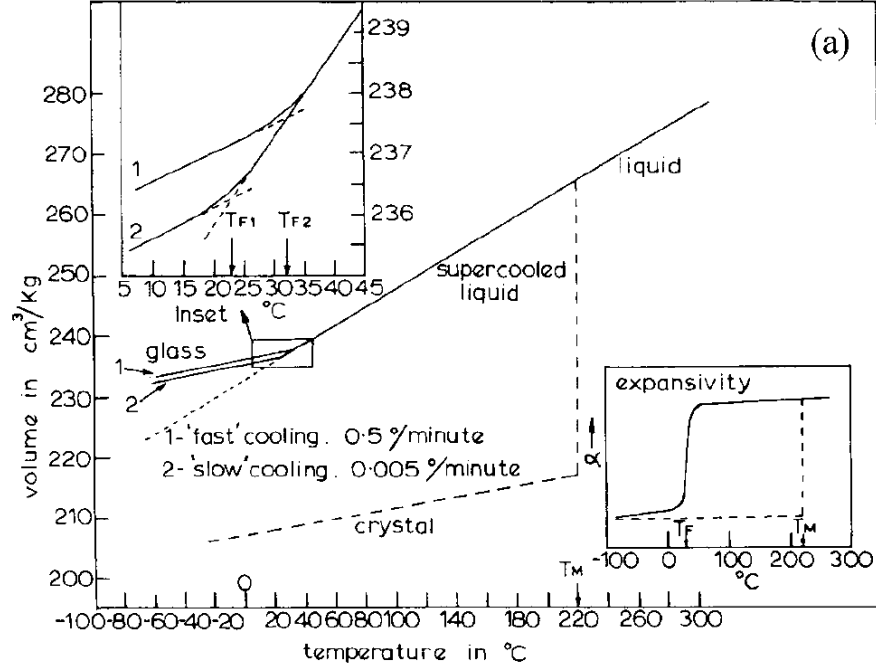


Figure 1.1: Volume of Selenium in different phases. At cooling rates of 0.5 degree per minute and 0.005 degree per minute crystallization is avoided. At these cooling rates, nothing special is observed when passing the melting temperature at  $T_m = 220$  °C. Note the change of slope at temperature  $T_{F1}$  and  $T_{F2}$  enlarge on the upper inset. This is a result of a glass transition. The figure is reprinted from Reference [Dyre, 2006], however, the original figure is from Reference [Owen, 1985] with data from Dzhaililo and Rzaev [1967].

liquid will find its true equilibrium state. However, in the time of an experiment or simulation this might never occur. Therefore, the liquid is said to be in a metastable equilibrium since the liquid behaves as if it was in a true equilibrium. It should be noted that classical nucleation theory is only adequate close to  $T_m$  [Debenedetti, 2006].

Now, consider a liquid where crystallization do not occur. As the thermal energy is lowered it becomes more difficult for particles to overcome energy barriers associated with flow events. The liquid becomes highly viscous. If we disturb the system it will take some time for the liquid to find its new (metastable) equilibrium state, characterized by a structural relaxation time  $\tau_\alpha$ . At some temperature<sup>1</sup>, referred to as the glass transition temperature  $T_g$ ,  $\tau_\alpha$  will become longer than the time-scales of the experiment or computer simulation. Structure cannot relax, and the liquid falls out of (metastable) equilibrium. The liquid is now in a so-called glassy state as shown in Figures

<sup>1</sup>To make  $T_g$  well-defined, it is often defined as  $\tau_\alpha(T_g) = 100$  seconds. Here we will loosely define  $T_g$  as the temperature where we cannot bring the system to its (metastable) equilibrium state.

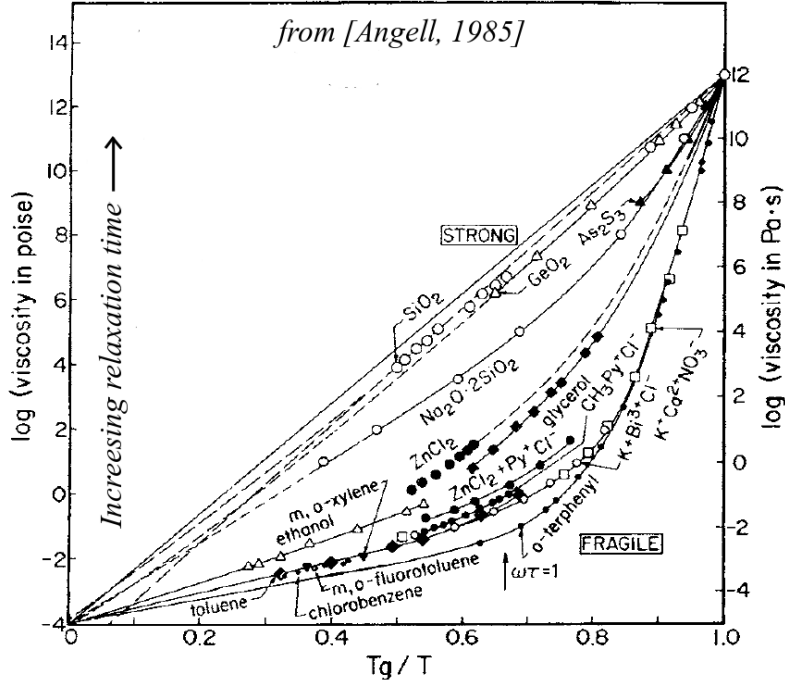


Figure 1.2: Logarithm of viscosity as a function of inverse temperature for several liquids. A straight line in this plot corresponds to an Arrhenius law, Equation 1.2.  $T_g$  is defined as  $\eta(T_g) = 10^{12}$  Pa·s. According to the Maxwell model [see Dyre, 2006], the relaxation time is given by  $\tau_\alpha = \eta/G_\infty$ . If assuming that the instantaneous shear modulus  $G_\infty$  is constant, then viscosity is proportional to the relaxation time,  $\tau_\alpha(T) \propto \eta(T)$ . Note that some liquids, like  $\text{SiO}_2$ , follows the Arrhenius law to a good approximation, while others, like o-terphenyl (OTP), have a significant non-Arrhenius growth of structural relaxation. See also Figure 1.8. This figure is originally from Reference [Angell, 1985] (data of heat-capacity is removed from original figure for clarity) and reprinted from [Dyre, 2006].

1.1. The *solid* glass is different from the *solid* crystal, since the structure is not ordered, but has inherited the disordered structure of the liquid.

Let us take a look at the temperature dependency of  $\tau_\alpha$ . In a situation where there is only one energy barrier  $E_A$ , the relaxation time would follow an Arrhenius law [Debenedetti and Stillinger, 2001]

$$\tau_\alpha(T) = \tau_0 \exp\left(\frac{-E_A}{k_B T}\right). \quad (1.2)$$

Figure 1.2 shows (a measure of) relaxations times as a function of inverse temperature for a broad collection of liquids. Structural relaxation of some liquids, like the covalent bonded  $\text{SiO}_2$ , follow this equation to a good approximation. Presumably,  $E_A$  is related to breaking bonds needed for flow. Others liquids,

like the van der Waals bonded o-terphenyl (OTP), have a more dramatic increase of  $\tau_\alpha$ . Apparently, the energy barriers for this kind of liquids increase as the liquid is cooled;  $\frac{\partial}{\partial(1/T)} E_A(T) > 0$ . Many theoretical descriptions even predict a divergence of  $E_A(T)$  at some finite temperature  $T_0$ . Experimental data, however, neither confirms nor rejects such a divergence [Hecksher et al., 2008]. Generally, changing volume  $V$  will also influence  $\tau_\alpha$ , so we should write  $\tau_\alpha(V, T)$ . Explaining the non-Arrhenius behavior of fragile liquids is one of the great puzzles of viscous liquids [Dyre, 2006].

Another great puzzle of viscous liquids relates to how various quantities relax to equilibrium after a disturbance. Let  $\Delta A(t) = A(t) - \langle A \rangle$  be the distance to equilibrium of some observable like internal energy, pressure or volume. Again, consider a simple situation where the liquid only have to overcome a single energy barrier to relax. In this scenario relaxation would be exponential,

$$\Delta A(t) = A_0 \exp\left(-\frac{t}{\tau_\alpha}\right) \quad (1.3)$$

However, virtually no liquids behave this way suggesting some distribution of energy barriers.

The studies presented in this thesis utilize molecular dynamics simulations of supercooled viscous liquids. An introduction to this is given in the following section.

## 1.2 Molecular dynamics simulations

Computers can make an incredible amount of repetitive calculations. For this reason, computational methods play an important role in the field of condensed matter. A popular method is molecular dynamics simulations [ten Wolde and Frenkel, 1998, Allen and Tildesley, 1987]. To illustrate the basic concept of this method, imagine that we want to simulate a liquid of Argon atoms. Our first assumption will be that dynamics can be described using classical mechanics. Next, we need some model of forces between atoms, referred to as the force-field. For simplicity we will assume that Argon atoms only interact pairwise with a force  $F_{ij}(r_{ij})$ , where  $r_{ij}$  is the distance between particle  $i$  and  $j$ . Imagine we have a box with  $N$  particles. We need to consider what to do with the walls of the box. We could put some repulsive interactions at the walls, however, then we would be investigating a liquid close to a wall. For a better simulation of bulk properties we can make use of periodic boundaries as illustrated in Figure 1.3. The result is that there is no wall, although, due to the limited size of the system, there can still be finite size effects.

From an initial configuration of positions and velocities we can integrate the classical equations of motion numerically. A numerical integration consists of a simple repetitive calculation and is therefore ideal for computers. There are numerous algorithms for numerical integrations. A crucial choice is the size of numerical time step,  $dt^{\text{step}}$ . A large time-step is preferable, since we are interested in long times. The fastest vibrations, however, set an upper limit for the time step. The longest times of the simulation is determined by the available computer power and the complexity of the system. At present day, a system of 1000 particles can be investigated in a time-window of  $10^{-14}$  seconds to  $10^{-4}$  seconds (Figure 1.7).

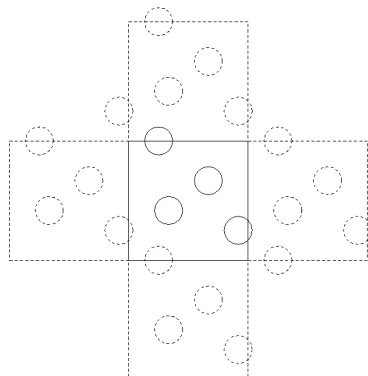


Figure 1.3: Illustration of four particles confined in a box with periodic boundaries. Image boxes are displayed with dashed lines.

In a simulation as presented here the number of particles, volume and total energy are constant. Thus, such a simulation is of the  $NVE$  ensemble. Algorithms<sup>2</sup> have been developed to keep temperature and/or pressure constant, making  $NVT$  and  $NpT$  simulations possible. In long-time simulations a thermostat is preferable since numerical errors make the total energy drift in  $NVE$ .

Before we can perform an actual simulation we need to specify a force-field. In the following we will think in terms of pair energy,  $U_{ij}(r)$ . This is just another way of writing the force. It is natural to choose to have zero energy at  $r_{ij} = \infty$  and therefore  $U_{ij}(r) = \int_r^\infty F_{ij}(r) dr$ .

Now, let us think of a good expression for  $U_{ij}(r)$ . Recall that “induced dipole”-“induced dipole” attraction, known as London dispersion forces, act between all atoms [Atkins and de Paula, 2002, or a similar standard textbook]. The pair energy associated with this is  $U_{ij}^{\text{London}} \propto -r^{-6}$ . Bringing two atoms close together will result in a repulsion since electron-clouds cannot overlap. For this we should choose some function with a steep divergence at  $r = 0$ . Traditionally  $U_{ij}^{\text{rep}} \propto r^{-12}$  is used. Putting this together we obtain the so-called Lennard-Jones potential [Lennard-Jones, 1931],

$$U_{ij}^{\text{LJ}}(r) = 4\varepsilon \left( \left( \frac{\sigma}{r} \right)^{12} - \left( \frac{\sigma}{r} \right)^6 \right). \quad (1.4)$$

We will refer to this as the Lennard-Jones liquid. Note that  $\varepsilon$  defines the energy scale,  $\sigma$  the length scale and unit of mass is defined by the mass  $m$  of the particles. Dimensionless versions of physical quantities can be defined from these three. As an example, a dimensionless time can be defined as

$$t' = t \sqrt{\frac{\varepsilon}{m\sigma^2}} \quad (1.5)$$

Some good values for Argon are  $\varepsilon = 0.997$  kJ/mol,  $\sigma = 0.34$  nm and  $m = 39.95$  u [van der Spoel et al., 2006]. Using this we have  $t = t' 2.15$  ps.

<sup>2</sup>In the simulations presented in this theses, the Nosé-Hoover thermostat [Nosé, 1984, Hoover, 1985] and the Nosé-Hoover Langevin barostat [Feller et al., 1995] are used.

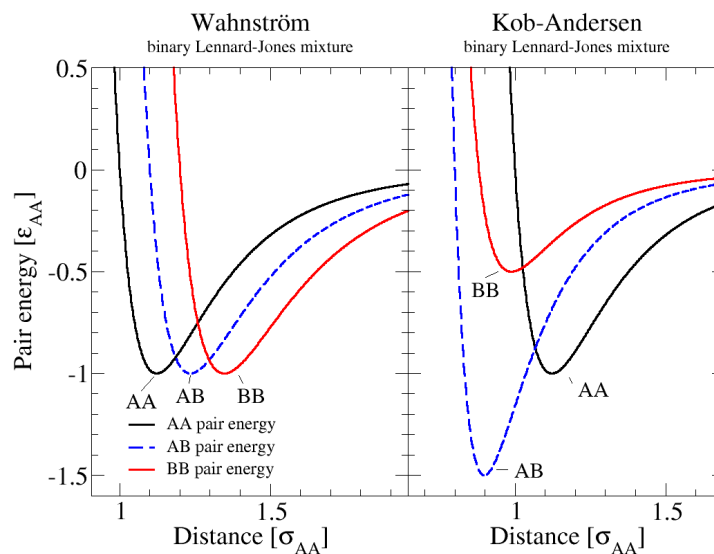


Figure 1.4: Pair potentials of two binary Lennard-Jones mixture; the parameter suggested by Wahnström [1991] and Kob and Andersen [1994]. The parameters for the Wahnström mixture are  $\sigma_{BB} = 1.2\sigma_{AA}$ ,  $\sigma_{AB} = 1.1\sigma_{AA}$ ,  $\varepsilon_{AA} = \varepsilon_{AB} = \varepsilon_{BB}$ ,  $m_B = 2m_A$  and  $N_A = N_B = 512$  ( $\chi_B = 0.5$ ) in a volume  $V = (11.094\sigma_{AA})^3$ . The parameters for the Kob-Andersen mixture are  $\sigma_{BB} = 0.88\sigma_{AA}$ ,  $\sigma_{AB} = 0.80\sigma_{AA}$ ,  $\varepsilon_{BB} = 0.5\varepsilon_{AA}$ ,  $\varepsilon_{AB} = 1.5\varepsilon_{AA}$ ,  $m_A = m_B$ ,  $N_A = 800$ ,  $N_B = 200$  ( $\chi_B = 0.2$ ) in a volume  $V = (9.4\sigma_{AA})^3$ . The Kob-Andersen mixture is by far the most well-studied.

The Lennard-Jones liquid can easily form a (defected) face center cubic crystal and it has limited use in the study of supercooled viscous liquids since crystallization will occur before it becomes viscous. Clarke [1979] did, however, investigate the glass transition. Crystallization can be avoided by make more complicated models. It is desirable to keep models as simple as possible, so they are computationally cheap. The following subsection briefly describes the models investigated in this thesis.

### 1.2.1 Simulated systems

Below is a list of models I have simulated. Where nothing else is noted, simulations were performed using the Gromacs software package [van der Spoel et al., 2006]. Analysis of the trajectories were done using the Gromacs software package, home-made Octave scripts [<http://www.gnu.org/software/octave/>] and home-made FORTRAN90 code. Pictures of configurations are made using VMD [Humphrey et al., 1996] assisted with home-made code.

**Lennard-Jones liquid:** 864 Lennard-Jones particles.

**Kob-Andersen binary Lennard-Jones mixture:** 800 type A and 200 type B Lennard-Jones particles. The parameters for the three kinds of pair

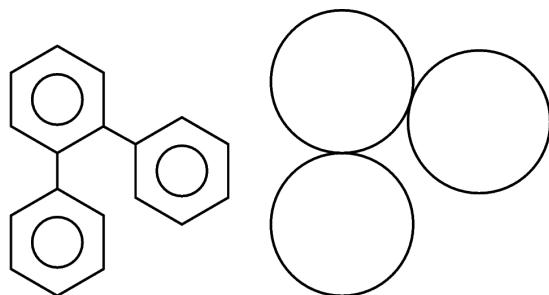


Figure 1.5: The chemical structure of o-terphenyl (OTP),  $C_6H_4(C_6H_5)_2$ , and a representation of the model suggested by Lewis and Wahnström [1994] where circles represent Lennard-Jones particles. The Lennard-Jones parameters are  $\varepsilon = (600 \text{ K})k_B$ ,  $\sigma = 0.483 \text{ nm}$  and  $m = 76.768 \text{ u}$ . The center of the Lennard-Jones particles are located in the corners of rigid isosceles triangle with two sides of length  $\sigma$  and one angle of  $75^\circ$ .

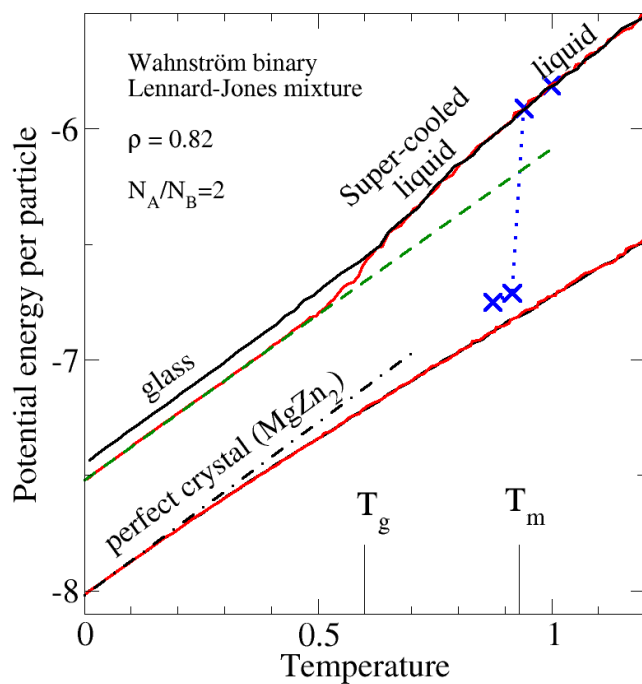


Figure 1.6: The potential energy in different phases of the Wahnström binary Lennard-Jones liquid at  $\chi_B = 1/3$ . Note that traditionally the  $\chi_B = 1/2$  composition is simulated (see Figure 1.4). See Chapter 6 and Paper II for more about the stability of this mixture. Note that the phenomenology is the same as seen in Figure 1.1 for Selenium. Similar phenomenology is found for liquids in general.

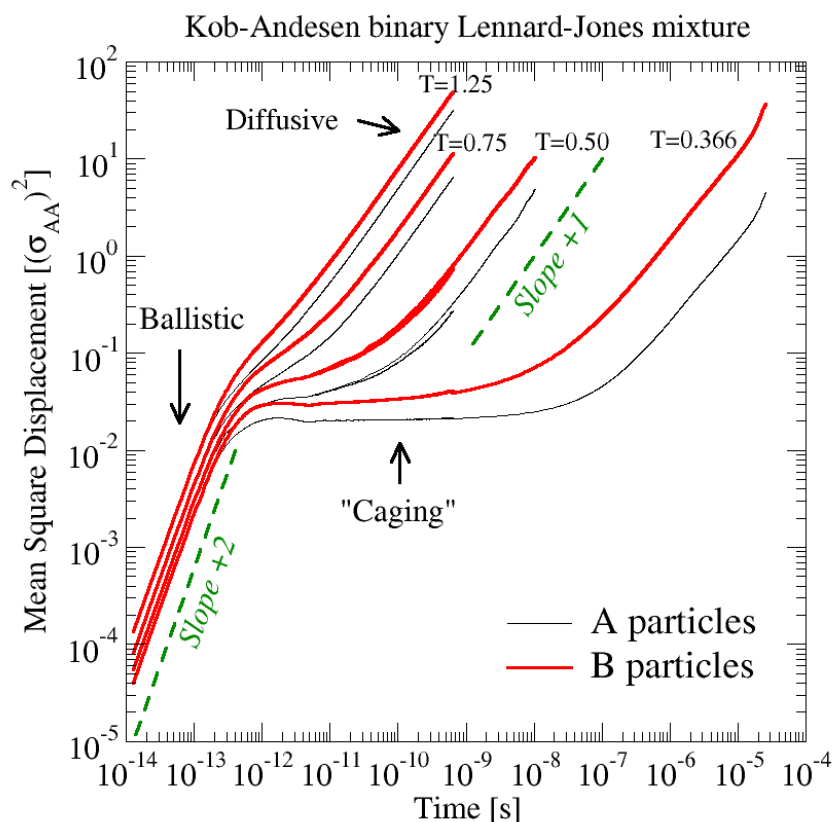


Figure 1.7: Mean square displacement,  $\langle(\Delta r(t))^2\rangle = \langle(|\vec{r}(t) - \vec{r}(0)|)^2\rangle$ , of A and B particles of the Kob-Andersen binary Lennard-Jones mixture. At ultra short times particles have not “felt” each other, and displacements are ballistic,  $\langle(\Delta r(t))^2\rangle = (v_m t)^2$  where  $v_m$  is the root mean square velocity. At long-times displacements become diffusive,  $\langle(\Delta r(t))^2\rangle = 6Dt$ , where  $D$  is the diffusion constant. At low temperatures,  $T < 0.5$ , particles become “caged” in the intermediate region.

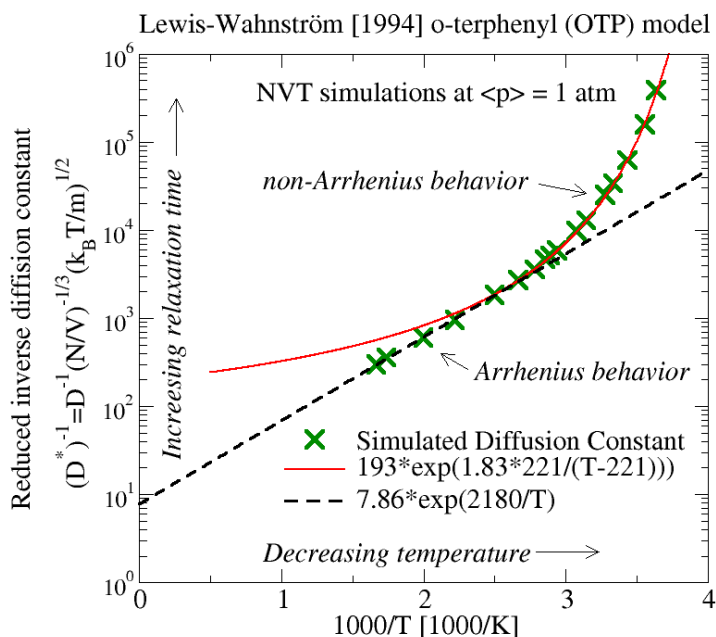


Figure 1.8: Reduced inverse diffusion constant  $(D^*)^{-1} = D^{-1}(N/V)^{-1/3}(k_B T/m)^{1/2}$  as a function of inverse temperature in a simulation of the Lewis-Wahnström model of OTP.  $(D^*)^{-1}$  relates to some characteristic “diffusion” time. A straight line in this plot corresponds to an Arrhenius law, Equation 1.2. Note that at high temperature  $(D^*)^{-1}$  follows an Arrhenius law, but not at lower temperature. A non-Arrhenius behavior at low temperature is also found for experimental data of OTP (see o-terphenyl (OTP) in Figure 1.2).

energies,  $U_{AA}^{LJ}(r)$ ,  $U_{BB}^{LJ}(r)$ ,  $U_{AB}^{LJ}(r)$ , are  $\sigma_{BB} = 0.88\sigma_{AA}$ ,  $\sigma_{AB} = 0.80\sigma_{AA}$ ,  $\varepsilon_{BB} = 0.5\varepsilon_{AA}$ ,  $\varepsilon_{AB} = 1.5\varepsilon_{AA}$ . The pair potentials are shown in Figure 1.4. This model was suggested by Kob and Andersen [1994] and is one of the most well-studied model viscous liquids.

**Wahnström binary Lennard-Jones mixture:** 500 type A and 500 type B Lennard-Jones particles with the interaction parameters  $\sigma_{BB} = 1.2\sigma_{AA}$ ,  $\sigma_{AB} = 1.1\sigma_{AA}$ ,  $\varepsilon_{AA} = \varepsilon_{AB} = \varepsilon_{BB}$  and masses  $m_B = 2m_A$ . The pair potentials are shown in Figure 1.4. This model was suggested by Wahnström [1991].

**Lewis-Wahnström OTP model:** Lewis and Wahnström [1994] suggested to connect three identical Lennard-Jones particles with rigid bonds as a toy model of o-terphenyl (OTP). The LINCS algorithm [Hess et al., 1997] is used for making rigid bonds (in all the models). See Figure 1.5 for more details about this model.

**Asymmetric dumbbells:** A system of asymmetric dumbbells as a toy model of toluene, where a phenyl-group,  $C_6H_5-$ , and the methyl-group,  $-CH_3$

where represented as Lennard-Jones particles.

**Seven-site model of toluene:** A model of toluene,  $C_6H_5CH_3$ , where  $CH_x$  groups (where  $x$  is either 0, 1, or 3) are simulated as Lennard-Jones particles connected by rigid bonds. The UA-OPLS parameter set [Jorgensen et al., 1984] were used for bond lengths and interaction parameters.

**SPC/E water:** Three-site model of water suggested by Berendsen et al. [1987].

**GROMOS methanol:** Three-site model of methanol,  $CH_3OH$ , where  $CH_3$ , O and H are simulated as charged Lennard-Jones spheres. The GROMOS parameter set [van Gunsteren et al., 1996] was used for bond lengths and interaction parameters.

**Phospholipid membranes:** Seven phospholipid membranes were simulated using a modified version of the all-atom CHARMM27 [Foloppe and MacKerell, 2000] parameter set. See Chapter 5, References [Pedersen, 2005, Pedersen et al., 2006, 2007, Sonne et al., 2007], and/or Paper X for more details. As a part of my master thesis [Pedersen, 2005] I simulated one of these membranes, however, the simulations presented in this thesis are conducted by Günther H. Peters (using the NAMD2 program [Kale et al., 1999]).

Model liquids shows the same phenomenology as real liquids. Figures 1.6 to 1.7 exemplifies this. Figure 1.6 shows the potential energy in different phases of the Wahnström binary Lennard-Jones mixture. At the investigated cooling rates of the liquid, crystallization is avoided and a glass transition is observed. Recall that this is the same phenomenology as shown in Figure 1.1.

Figure 1.7 shows the root mean square displacement  $\langle(\Delta r(t))^2\rangle = \langle(|\vec{r}(t) - \vec{r}(0)|)^2\rangle$  of particles of the Kob-Andersen Lennard-Jones liquid. At short times displacements are ballistic and at long times they are diffusive. From this last part of the curve, the diffusion constant  $D$  can be determined,  $\langle(\Delta r(t))^2\rangle = 6Dt$ . At low temperatures an intermediate plateau appears, where particles do not move. At  $T = 0.366$  particles are “caged” from  $10^{-12}$  to  $10^{-7}$  seconds (in Argon units).

Figure 1.8 shows the diffusion constant of molecules of the Lewis-Wahnström OTP model at different temperatures. At high-temperatures, the diffusion constant follows an Arrhenius law. However, at low-temperatures, diffusion is clearly non-Arrhenius. This is in good agreement of what is observed for real OTP as seen in Figure 1.2 (labeled o-terphenyl).

### 1.3 Outline of thesis

In Chapter 2 it is shown that some model liquids exhibit strong correlations in the thermal fluctuations of configurational parts of pressure and energy in the  $NVT$  ensemble. Such liquids are referred to as strongly correlating liquids. Chapter 3 explains the origin of the strong correlation. In Chapter 4 it is argued, on the basis of the previous chapters, that strong correlating *viscous* liquids are more simple than viscous liquids in general. This is exemplified by the so-called Progovine-Defay ratio being close to unity (Section 4.1), and scale invariance of structure and dynamics (Section 4.2).

Thermodynamic fluctuations of phospholipid membranes also exhibit strong correlations. These correlations are reported and explained in Chapter 5.

Chapter 6 reports and investigates crystallization from the melt of some of the investigated models. Before the presented study, these models had not been reported to crystallize from the melt. Crystallization of the Wahnström binary Lennard-Jones liquid is investigated in details.

The final chapter is an outlook.



## Chapter 2

# Strongly correlating liquids

Consider a system of  $N$  particles in a fixed volume  $V$ . Total energy  $E$  is a sum of a kinetic part (kinetic energy) that is only a function of the momenta,  $\vec{Q} = \{\vec{q}_1, \vec{q}_2, \dots, \vec{q}_N\}$ , and a configurational part (potential energy) that is only a function of positions,  $\vec{R} = \{\vec{r}_1, \vec{r}_2, \dots, \vec{r}_N\}$ ;

$$E(\vec{Q}, \vec{R}) = K(\vec{Q}) + U(\vec{R}). \quad (2.1)$$

In the same way, pressure  $p$  is a sum of a kinetic and a configurational part,

$$p(\vec{Q}, \vec{R}) = Nk_B T(\vec{Q})/V + W(\vec{R})/V, \quad (2.2)$$

where  $T(\vec{Q})$  is the instantaneous temperature.  $W/V$  and  $U$  are the configurational part of pressure and energy respectively. Note that  $W$  is in units of energy. If thermal fluctuations of  $W$  and  $U$  are strongly correlated in time, this is referred to as a *strongly correlated liquid*. The remainder of this chapter discuss such  $W$ - $U$  correlations in model liquids and super critical Argon. The main references for this chapter are Paper III and Paper VIII.

### 2.1 An example: The Lennard-Jones Liquid

Probably the most well-studied model liquid is the (single component) Lennard-Jones liquid, where particles interact pairwise via the Lennard-Jones potential [Lennard-Jones, 1931]:

$$U_{ij}^{LJ} = 4\epsilon \left( \left( \frac{\sigma}{r_{ij}} \right)^{12} - \left( \frac{\sigma}{r_{ij}} \right)^6 \right), \quad (2.3)$$

where  $r_{ij}$  is the distance between particle  $i$  and  $j$  (see also Section 1.2). The virial of a system of pairwise interactions particles is

$$W = \frac{1}{3} \sum_{i \neq j} r_{ij} F_{ij} = \sum_{i \neq j} W_{ij} \quad (2.4)$$

where  $F_{ij} = -\frac{d}{dr} U_{ij}$  is the force between particle  $i$  and  $j$ . It is convenient to define a pair virial as

$$W_{ij} = -\frac{r_{ij}}{3} \frac{d}{dr} U_{ij}. \quad (2.5)$$

## 2. STRONGLY CORRELATING LIQUIDS

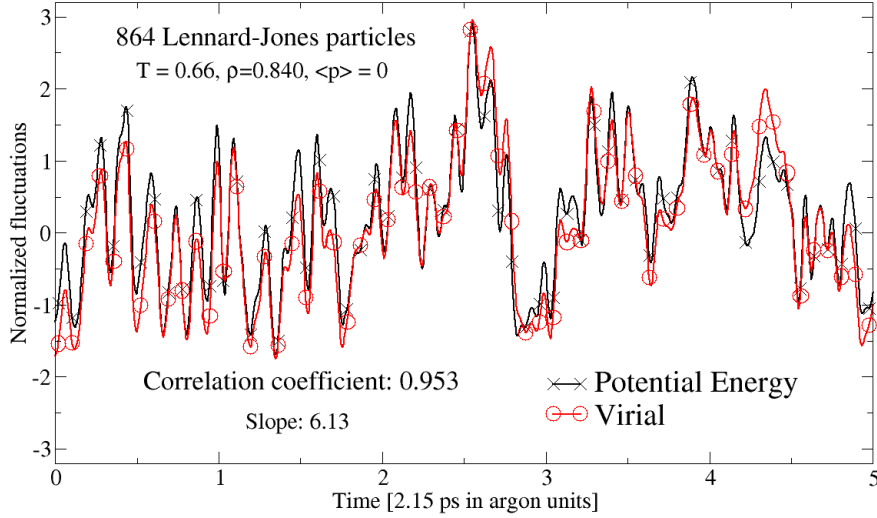


Figure 2.1: Instantaneous normalized fluctuations of virial and potential energy in a single component Lennard-Jones liquid.  $W(t)$  and  $U(t)$  are strongly correlated. This figure is the same as Figure 1A in Paper III, but for another simulation.

For the Lennard-Jones potential this is

$$W_{ij}^{LJ} = 8\varepsilon \left( 2 \left( \frac{\sigma}{r_{ij}} \right)^{12} - \left( \frac{\sigma}{r_{ij}} \right)^6 \right). \quad (2.6)$$

Figure 2.1 shows a time series of normalized fluctuations (with respect to the standard deviation  $\sigma$ ) of virial  $W(t)$  and potential energy  $U(t)$  in a constant  $NVT$  simulation at  $T = 0.66$  ( $T = 80$  K in Argon units) and  $\rho = 0.840$  ( $\langle p \rangle = 0$ ). Virial and potential energy are strongly correlated. This is quantified by the correlation coefficient,

$$R_{WU} \equiv \frac{\langle \Delta W \Delta U \rangle}{\sqrt{\langle (\Delta W)^2 \rangle \langle (\Delta U)^2 \rangle}} = 0.953, \quad (2.7)$$

being close to unity.

Figure 2.2 shows a scatter plot of virial versus potential energy for some more state points. The cigar-form of the scatter-blobs for a given state-point indicates a strong correlation. Note also the constant density paths. The slope of these paths is around 6 ( $\pm 10\%$ ) and the same value as the “slope” of a single state point defined as

$$\gamma_{WU} \equiv \sqrt{\frac{\langle (\Delta W)^2 \rangle}{\langle (\Delta U)^2 \rangle}} \quad (2.8)$$

When pressure is held constant (and not volume), the correlation is weaker.

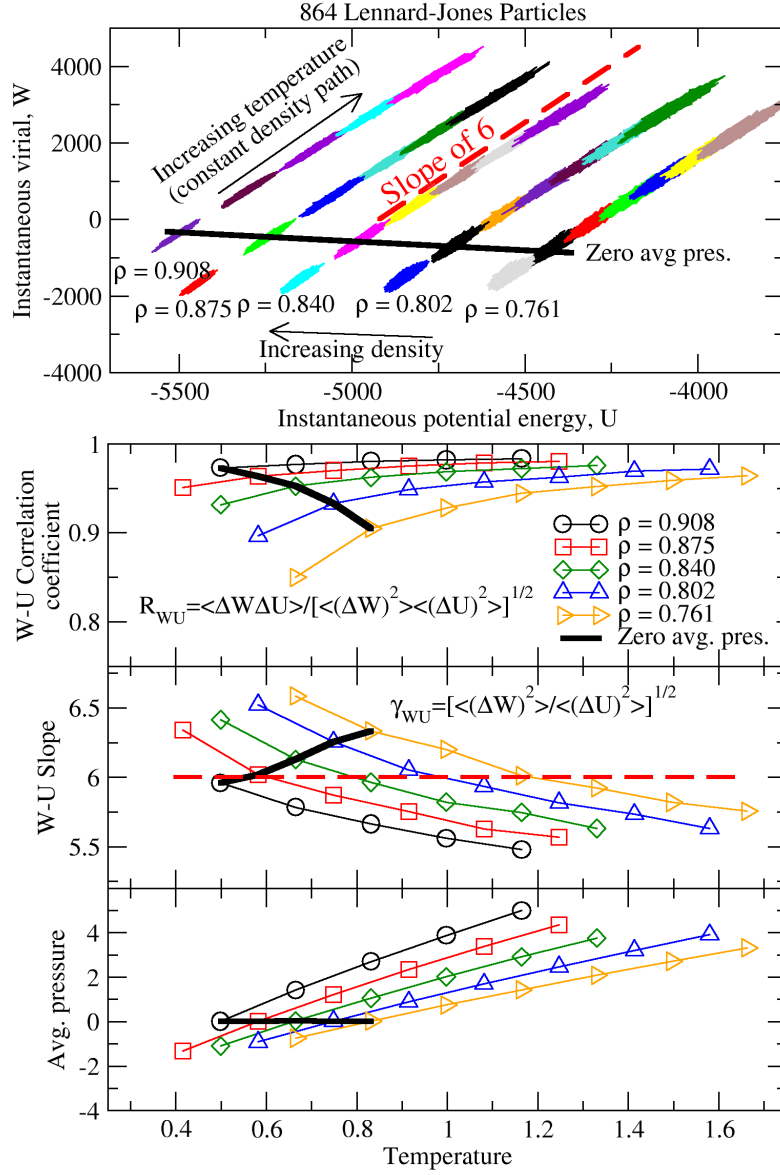


Figure 2.2: Scatter plot of virial and potential energy in a single component Lennard-Jones liquid at different state points. Simulations were done in the  $NVT$  ensemble. The lower panels show the  $W-U$  correlation coefficient  $R_{WU}$  (Equation 2.7), the  $W-U$  slope (Equation 2.8) and the average pressure.

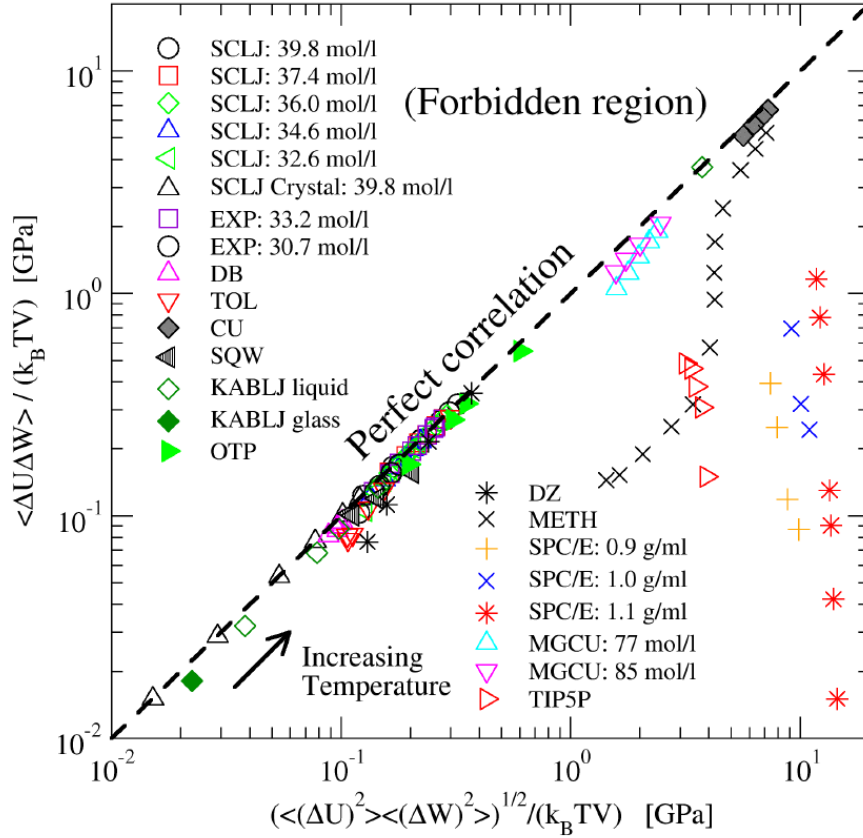


Figure 2.3:  $W$ - $U$  correlation plot of model liquids. The numerator plotted against the denominator of the correlation coefficient expressed in units of pressure (making them intensive quantities). The diagonal (dashed line) correspond to perfect correlation. Models of van der Waals bonded liquid are close to this line showing strong  $W$ - $U$  correlations, whereas hydrogen bonded liquids only have weak or no correlation. The simulated systems are the single component Lennard-Jones liquids (SCLJ), a model with exponential repulsion therm (EXP), a asymmetric dumbbell model (DB), model of Toluene using the UA-OPLS parameters (TOL) [Jorgensen et al., 1984], a model of pure Cu with a many body potential (CU) [Jacobsen et al., 1987, 1996], a binary mixture of particles with hard-core repulsion and a square-well attraction (SQW) [Zaccarelli et al., 2002, 2004], a binary Lennard-Jones mixture suggested by Kob and Andersen [1994, 1995a] (KABLJ), a ortho-terphenyl model suggested by Lewis and Wahnström [1994] (OTP), a single component glass former suggested by Dzugutov [1992], a model of methanol using the GROMOS parameters [van Gunsteren et al., 1996], a three-site model of water (SPC/E) [Berendsen et al., 1987], a model of  $Mg_{85}Cu_{15}$  [Bailey et al., 2004] and a five-site model of water (TIP5P) [Mahoney and Jorgensen, 2000]. Simulations of SCLJ and EXP where conducted by Thomas B. Schröder. Simulations of CU, DZ and MGCU where conducted by Nicholas P. Bailey. Simulations of SQW and TIP5P where conducted by Nicolette Gnan. The remaining simulations where conducted by the author, see Section 1.2.1. This figure is the same as Figure 10 in Paper VIII, where simulation details are also given.

## 2.2 A class of strongly correlating liquids

If strong  $W$ - $U$  correlations were only present in the Lennard-Jones liquid, they would not be so interesting. However, other liquids also exhibit strong  $W$ - $U$  correlations. Figure 2.3 show the nominator,  $\langle \Delta W \Delta U \rangle / (k_B T V)$ , versus the denominator,  $\sqrt{\langle (\Delta W)^2 \rangle \langle (\Delta U)^2 \rangle} / (k_B T V)$ , of the correlation coefficient, in units of pressure to make them intensive quantities, of 13 liquids. In this plot, the diagonal correspond to perfect correlation.

A large group of liquids are strongly correlating. This suggest that there exist a class of strongly correlating liquids (see Sections 3.1, 4.1.3 and 4.2 for more about this conjecture). Note that van der Waals bonded liquids belongs to this class, whereas hydrogen bonded liquids only have weak correlations. The weakening of correlation can be explained by competing interactions. Close to the density maximum of water  $W$  and  $U$  are uncorrelated,  $R_{WU} = 0$ . For more about this, see section C in Paper VIII.

## 2.3 Supercritical Argon

An experimental correlation coefficient of super-critical argon can be calculated<sup>1</sup>: Recall, that for particles with no internal degrees of freedom kinetic parts of pressure and energy is simply that of a mono-atomic ideal gas and that the fluctuation-dissipation theorem relates fluctuations to response functions [Allen and Tildesley, 1987]; For a mono-atomic system we can write

$$\langle (\Delta U)^2 \rangle / k_B T^2 = C_V - \frac{3}{2} N k_B, \quad (2.9)$$

$$\langle (\Delta W)^2 \rangle / k_B T = N k_B T + \langle W \rangle - V K_T + \langle X \rangle \quad (2.10)$$

and

$$\langle \Delta U \Delta W \rangle / k_B T^2 = V \beta_V - N k_B. \quad (2.11)$$

Note, that the so-called ‘‘hyper-virial’’  $X$  [Allen and Tildesley, 1987] goes into the relation between  $\langle (\Delta W)^2 \rangle$  and  $K_T$  (Eq. 2.10).  $X$  is not a thermodynamic quantity and cannot be measured.

Fortunately, it is possible to subtract  $X$  out of the equations (with some assumptions), as described in Paper VIII section IIIA. If  $T_{\text{ref}}$  is the temperature at some reference state-point (along a constant density path)  $c_V^{\text{conf}} = c_V - \frac{3}{2} N k_B T$ ,  $\beta_V^{\text{conf}} = \beta_V - N k_B / V$  and  $\langle p \rangle^{\text{conf}} = \langle p \rangle - \frac{N k_B T}{V}$  then the correlation coefficient is given by

$$R_{WU} \simeq \sqrt{\frac{B(T) - B(T_{\text{ref}})}{A(T) - A(T_{\text{ref}})}} \quad (2.12)$$

where

$$A(T) = \langle p \rangle - K_T + \frac{\langle p \rangle^{\text{conf}} \beta_V^{\text{conf}}}{c_V^{\text{conf}}}, \quad (2.13)$$

<sup>1</sup>There are two reasons for choosing Argon. 1st: A calculations on lighter noble gasses like Helium should include quantum effects. Here we ignore such quantum effects. 2nd: Heavier noble gasses is known to form compounds indicating that the Lennard-Jones potential is to simple (loosely speaking: the large electron cloud of the heavy noble gasses can make covalent bonds).

and

$$B(T) = T(\beta_V^{\text{conf}})^2/c_V^{\text{conf}}. \quad (2.14)$$

Figure 9 in Paper VIII shows experimental data from the NIST database [Lemmon et al., 2005] of super critical Argon where the diagonal corresponds to perfect correlation. The correlation is strong with a  $W$ - $U$  correlation coefficient of 0.96. This show that strongly correlating liquids exist in nature and not just the computer. Equation 2.12 also demonstrate that strongly correlating liquids are more simple than the general case. If we assume  $R = 1$ , a good approximation for strongly correlating liquids, we can predict a third response function from two others. This is not the general case.

## Chapter 3

# Origin of strong correlations

In this chapter it is shown that the origin of the strong correlation between virial and energy (in the constant volume ensemble) is a consequence of an effective inverse power-law of the pair-potential. This power-law describes the thermodynamical fluctuations of the NVT ensemble. See also Paper III, Paper VIII and Paper IX. The real pair potential cannot simply be approximated by an inverse power. This would give a wrong equation of state. However, a good approximation is an inverse power-law plus a linear term. The linear term does not contribute (significantly) to fluctuations at fixed volume.

### 3.1 Effective inverse power-law pair potential

First, consider a soft-sphere liquid [Hoover et al., 1970], where particles interact via an inverse power-law potential:

$$U_{ij}^{\text{pow}} = ar_{ij}^{-n}, \quad (3.1)$$

where  $n$  is some exponent and  $a$  is a prefactor. As shown in Appendix A.1, potential energy and virial are proportional

$$W^{\text{pow}}(t) = \gamma_{WU}^{\text{pow}} U^{\text{pow}}(t), \quad (3.2)$$

with a proportional constant (or slope) of

$$\gamma_{WU}^{\text{pow}} = n/3. \quad (3.3)$$

Then, recall that the Lennard-Jones potential is a sum of two inverse power-laws, where  $r^{-12}$  dominates at short distances. A possible explanation for the correlations could be that the  $r^{-12}$  term dominates fluctuations. However, this would give a slope of four, whereas the observed slope is around six. The reason for this is that particles are located close to the minimum, where both  $r^{-12}$  and  $r^{-6}$  terms play a role (Paper III, [Ben-Amotz and Stell, 2003]). Note, however, that the slope in Figure 2.2 does approach four with increasing pressure (where  $r^{-12}$  dominates).

Fluctuations of virial and potential energy (at constant volume) can be described by an effective inverse power-law with an exponent larger than 12. To show this, split the pair energy in an inverse power-law term plus a difference term,

$$U^{\text{LJ}} = U^{\text{pow}} + U^{\text{diff}}. \quad (3.4)$$

### 3. ORIGIN OF STRONG CORRELATIONS

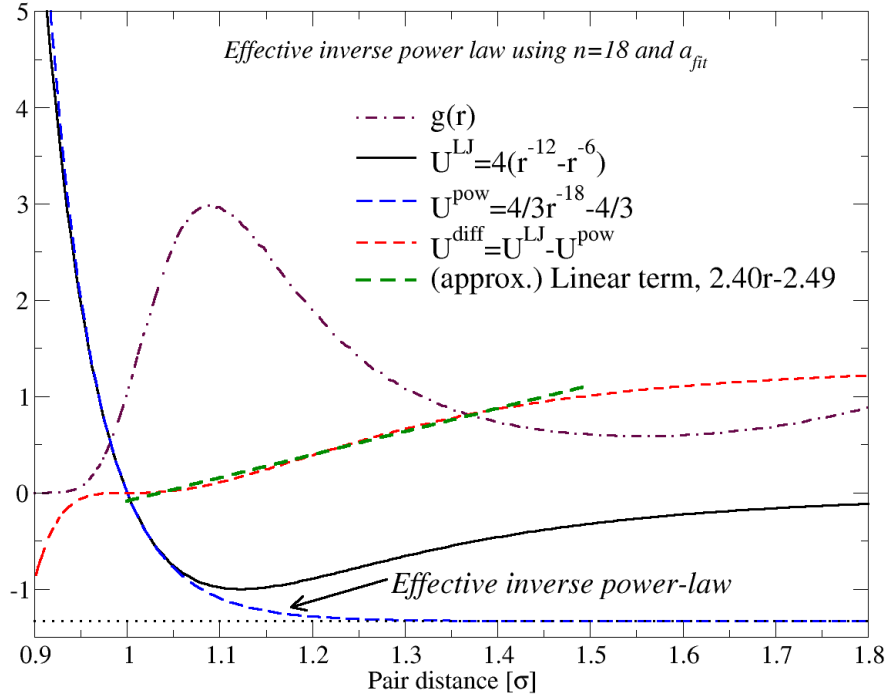


Figure 3.1: Effective inverse power-law  $U_{ij}^{\text{pow}} = \frac{4}{3}r^{-18} - \frac{4}{3}$  derived in Appendix A.2. See also Figure 3.5. The definition of the radial distribution function  $g(r)$  is given in Section 3.2.

and

$$W^{\text{LJ}} = W^{\text{pow}} + W^{\text{diff}}. \quad (3.5)$$

Then the variance of energy and virial can be written as

$$\langle (\Delta U^{\text{LJ}})^2 \rangle = \langle (\Delta U^{\text{pow}})^2 \rangle + \langle (\Delta U^{\text{diff}})^2 \rangle + 2\langle \Delta U^{\text{pow}} \Delta U^{\text{diff}} \rangle, \quad (3.6)$$

and

$$\langle (\Delta W^{\text{LJ}})^2 \rangle = \langle (\Delta W^{\text{pow}})^2 \rangle + \langle (\Delta W^{\text{diff}})^2 \rangle + 2\langle \Delta W^{\text{pow}} \Delta W^{\text{diff}} \rangle. \quad (3.7)$$

If an effective inverse power-law gives a good description of the fluctuations then

$$\Delta U^{\text{LJ}}(t) \simeq \Delta U^{\text{pow}}(t) \quad (3.8)$$

and

$$\Delta W^{\text{LJ}}(t) \simeq \Delta W^{\text{pow}}(t). \quad (3.9)$$

To quantify “ $\simeq$ ” in the above equations, we can investigate the pow-LJ correlation coefficients

$$R_{U^{\text{pow}}, U^{\text{LJ}}} \equiv \frac{\langle \Delta U^{\text{LJ}} \Delta U^{\text{pow}} \rangle}{\sqrt{\langle (\Delta U^{\text{LJ}})^2 \rangle \langle (\Delta U^{\text{pow}})^2 \rangle}}, \quad (3.10)$$

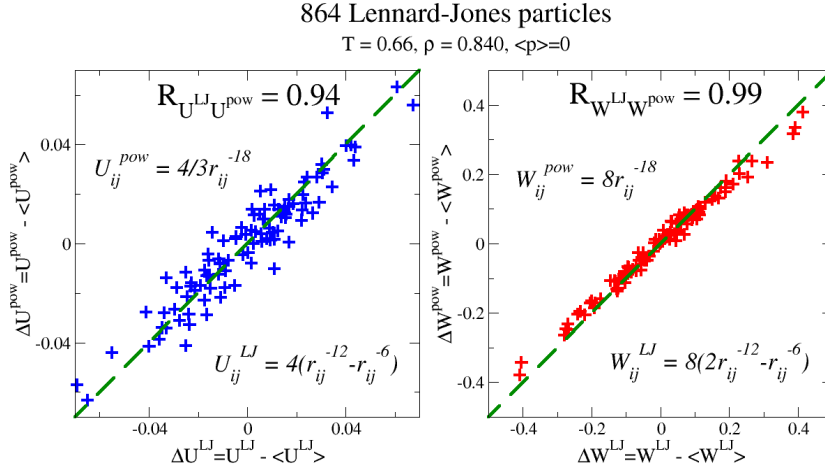


Figure 3.2: The panel on the left shows a scatter plot of  $\Delta U^{\text{pow}}$  versus  $\Delta U^{\text{LJ}}$  (Equation 3.4) and the panel on the right shows  $\Delta W^{\text{pow}}$  versus  $\Delta W^{\text{LJ}}$  (Equation 3.5) of configurations of the Lennard-Jones liquid at  $T = 0.66$  and  $\rho = 0.840$  ( $\langle p \rangle = 0$ ). The effective inverse power-law describes fluctuations of virial and energy to a good approximation (Equations 3.8 and 3.9).

and

$$R_{W^{\text{pow}}, W^{\text{LJ}}} \equiv \frac{\langle \Delta W^{\text{LJ}} \Delta W^{\text{pow}} \rangle}{\sqrt{\langle (\Delta W^{\text{LJ}})^2 \rangle \langle (\Delta W^{\text{pow}})^2 \rangle}} \quad (3.11)$$

and the amount of variance described by the effective power-law,

$$\gamma_{U^{\text{pow}}, U^{\text{LJ}}}^2 \equiv \frac{\langle (\Delta U^{\text{pow}})^2 \rangle}{\langle (\Delta U^{\text{LJ}})^2 \rangle}, \quad (3.12)$$

and

$$\gamma_{W^{\text{pow}}, W^{\text{LJ}}}^2 \equiv \frac{\langle (\Delta W^{\text{pow}})^2 \rangle}{\langle (\Delta W^{\text{LJ}})^2 \rangle}. \quad (3.13)$$

If the description is good, all of these should be close to unity.

As a first guess, we will assume that  $n = 18$  ( $\gamma = 6$ ) (as the  $W$ - $U$  slope on Figure 2.1 suggest), and get a pre-factor  $a$  by fitting the inverse-power law to the Lennard-Jones potential by matching 0th, 1st and 2nd derivative as described in Appendix A.2. This give the inverse power-law  $U_{ij}^{\text{pow}} = \frac{4}{3}(r_{ij}/\sigma)^{-18}$  shown on Figure 3.1. Figure 3.2 shows that this effective inverse power-law gives a pretty good description of the fluctuations.

In the following, a way to determine the best<sup>1</sup>  $n$  and  $a$  from fluctuations at one state-point will be given. Figure 3.3 shows Eqs. 3.10–3.13 as a function of  $n$ . In some range ( $\pm 10\%$ ) the power-law energy and virial are strongly correlated with the Lennard-Jones ( $R_{U^{\text{pow}}, U^{\text{LJ}}} > 0.93$  and  $R_{W^{\text{pow}}, W^{\text{LJ}}} > 0.96$ ) and dominates the fluctuations ( $\langle (\Delta U^{\text{LJ}})^2 \rangle \simeq \langle (\Delta U^{\text{pow}})^2 \rangle > \langle (\Delta U^{\text{diff}})^2 \rangle \simeq |\langle \Delta U^{\text{pow}} \Delta U^{\text{diff}} \rangle|$ ). Both virial and energy fluctuations should be described

<sup>1</sup>best: Effective inverse power-law that gives the best description of the fluctuating parts of energy and virial.

### 3. ORIGIN OF STRONG CORRELATIONS

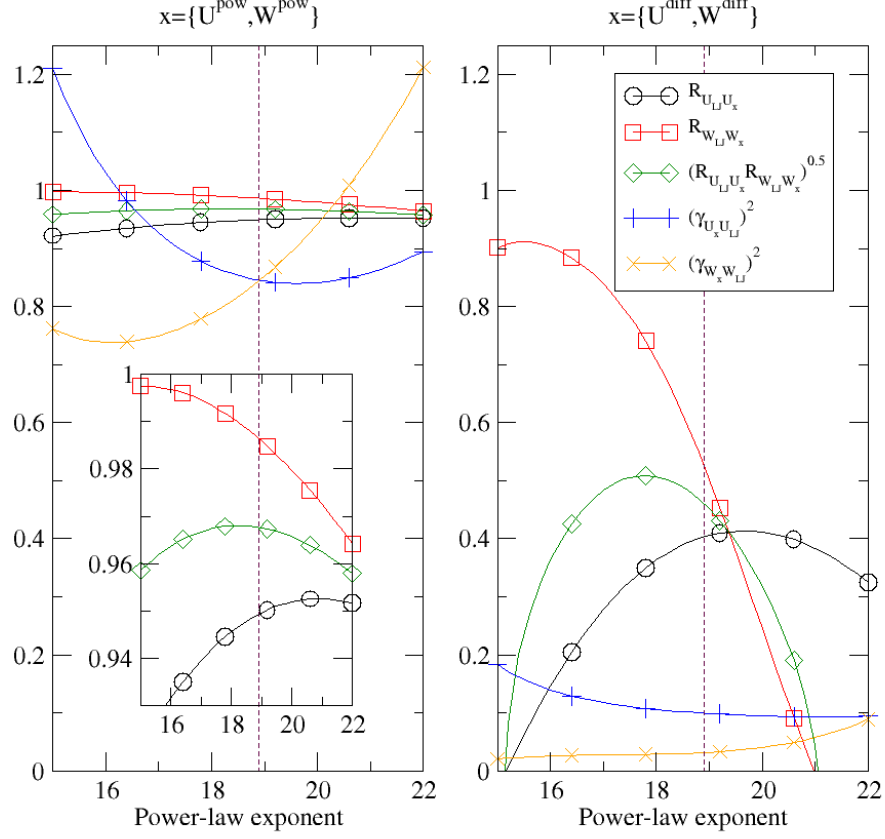


Figure 3.3: Eqs. 3.10 to 3.13 as a function of  $n$  (using  $a_{\text{fit}}$ ) of the Lennard-Jones liquids at  $T = 0.66$  and  $\rho = 0.840$ . The *optimization parameter*  $\sqrt{R_{U^{\text{pow}}, U^{\text{LJ}}} R_{W^{\text{pow}}, W^{\text{LJ}}}}$  have maximum, close to  $n = 18.9 = 3\sqrt{\frac{\langle(\Delta W)^2\rangle}{\langle(\Delta U)^2\rangle}}$ . However, note that  $\sqrt{R_{U^{\text{pow}}, U^{\text{LJ}}} R_{W^{\text{pow}}, W^{\text{LJ}}}}$  is close to unity in the entire investigated region. This suggest that a  $n$  not exactly 19.8 works pretty well. Also, note that covariances  $\langle\Delta U^{\text{pow}}\Delta U^{\text{diff}}\rangle/\langle(\Delta U^{\text{diff}})^2\rangle = 0.02$  and  $\langle\Delta W^{\text{pow}}\Delta W^{\text{diff}}\rangle/\langle(\Delta W^{\text{diff}})^2\rangle = 0.06$  are small at exponent  $n = 18.9$ .

by the effective inverse power-law (both  $R_{U^{\text{pow}}, U^{\text{LJ}}}$  and  $R_{W^{\text{pow}}, W^{\text{LJ}}}$  close to unity). Thus,  $\sqrt{R_{U^{\text{pow}}, U^{\text{LJ}}} R_{W^{\text{pow}}, W^{\text{LJ}}}}$  should be close to unity. Note that this optimization parameter have a maximum close to the exponent calculated from the  $W$ - $U$  slope ( $n = 3\gamma_{WU} = 18.9$ ). Thus, the apparent exponent can simply be calculated as

$$n = 3\sqrt{\frac{\langle(\Delta W)^2\rangle}{\langle(\Delta U)^2\rangle}} = 3\gamma_{WU} \quad (3.14)$$

The prefactor  $a$  can also be determined from the  $W$  and  $U$  fluctuations. The  $a_{\text{fit}}$  calculated in Appendix A.2 worked pretty well, however, a slight increase give a better fit. Figure 3.4 shows that an 8.8% increase gives the best

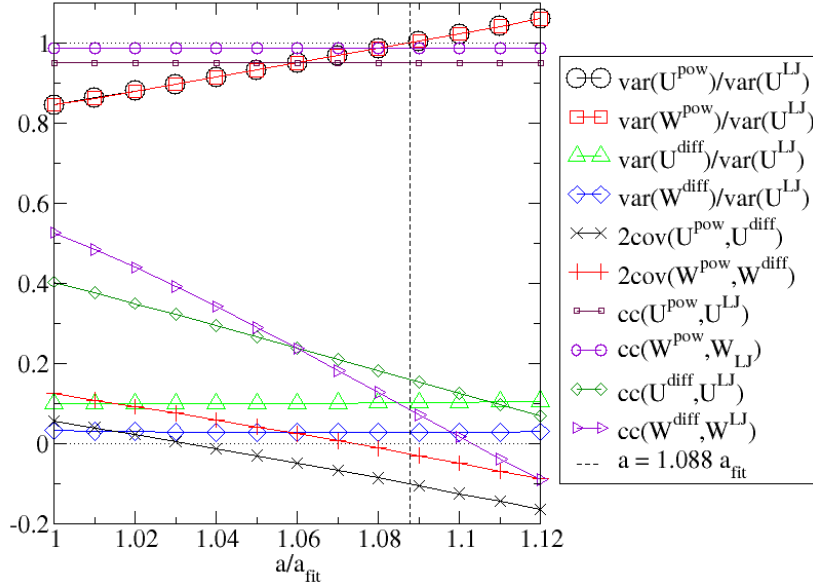


Figure 3.4: Eqs. 3.10 to 3.13 as a function of  $a/a_{\text{fit}}$  ( $n = 18.9$ ) of the Lennard-Jones liquids at  $T = 0.66$  and  $\rho = 0.840$ .  $T = 80$  K and  $\langle p \rangle = 0$ . At  $a_{\text{opt}} = 1.088a_{\text{fit}} = 1.389$  (dashed line) the variance of  $\Delta U^{\text{LJ}}(t)$  equals that of  $\Delta U^{\text{pow}}(t)$  and the variance of  $\Delta W^{\text{LJ}}(t)$  equals that of  $\Delta W^{\text{pow}}(t)$ . Also, at  $a_{\text{opt}}$  the variance of  $\Delta U^{\text{diff}}(t)$  and  $\Delta W^{\text{diff}}(t)$  and the correlation coefficient  $R_{U^{\text{LJ}}, U^{\text{diff}}}$  and  $R_{W^{\text{LJ}}, W^{\text{diff}}}$  are small.

description. It is possible to match (the magnitude of) both the potential energy and the virial,  $\langle (\Delta U^{\text{pow}})^2 \rangle / \langle (\Delta U^{\text{LJ}})^2 \rangle \simeq \langle (\Delta W^{\text{pow}})^2 \rangle / \langle (\Delta W^{\text{LJ}})^2 \rangle \simeq 1$ . Note that changing  $a$  do not effect the correlation coefficients  $R_{U^{\text{pow}}, U^{\text{LJ}}}$  and  $R_{W^{\text{pow}}, W^{\text{LJ}}}$ .

Figure 3.5 show  $U_{ij}^{\text{pow}}$  with exponent  $n = 18.9$  and  $a_{\text{opt}} = 1.088a_{\text{fit}} = 1.389$ . Note that  $U_{ij}^{\text{diff}}$  of this effective inverse power-law is well approximated by a straight line in the range of the first peak of the radial distribution function,  $g(r)$ . This will be discussed further in the next section.

So far it is only demonstrated that the effective power-law works for the 6-12 Lennard-Jones liquid. However, in Paper XIII it is argued that a similar fitting can be done for the assymmetric dumbbell model. Coslovich and Roland [2009] have recently shown that the description also works for the generalized Lennard-Jones potential,  $U_{ij}^{\text{gen.LJ}} = (nr^{-m} - mr^{-n})/(m - n)$ . It is reasonable that a similar inverse power-law matching can be done in similar systems. Therefore, a good conjecture is that the effective power-law explanation works for van der Waals bonded systems in general. More work is needed to clarify this.

Note that the Lennard-Jones potential cannot simply be replaced by an inverse power-law – only fluctuations (at fixed volume) can be described by a inverse power-law. The Lennard-Jones liquid does not have the same equation of states as the soft-sphere liquid. In the next section will discuss the role of

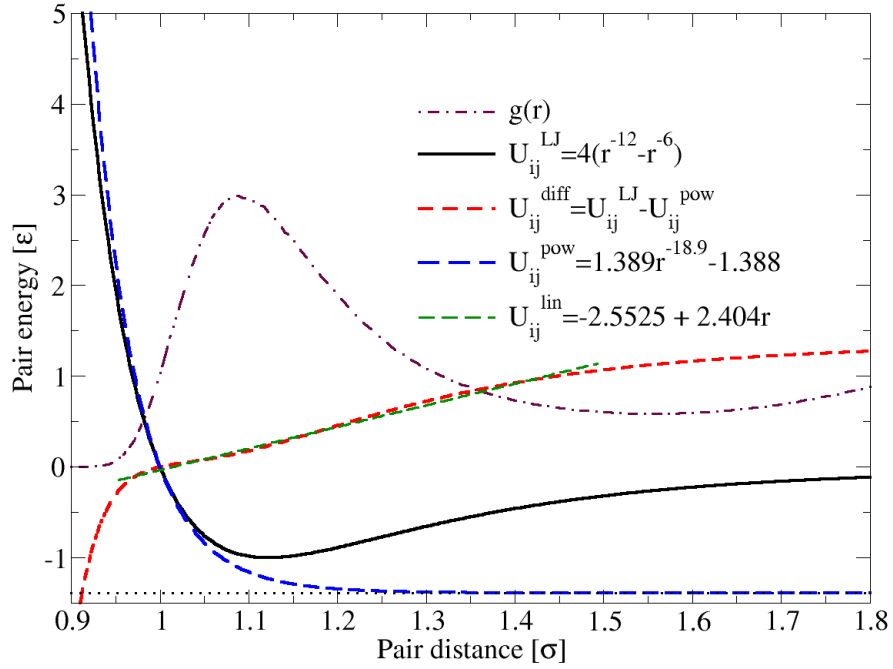


Figure 3.5: The optimal effective inverse power-law of  $U_{ij}^{\text{pow}} = 1.389r^{-18.9} - 1.388$  of the Lennard-Jones liquid at the state-point  $T = 0.66$  and  $\rho = 0.840$ .  $n = 18.9$  and  $a = 1.389$  are calculated from fluctuations as outline in Figure 3.3 and Figure 3.4. The definition of the radial distribution function  $g(r)$  is given in Section 3.2.

$U^{\text{diff}}$ .

### 3.2 Approximate inverse power-law plus linear term pair potential

The effective inverse power-law gives a good description of the pair potential at short distances,  $r < r_{\text{min}} (= 1.12\sigma)$ , but not at longer distances, as shown on Figure 3.1. At first glance, it is surprising that the effective power-law does so well after all. Even at zero pressure where particles are located close to the minimum of the Lennard-Jones potential. In the following, it will be discussed why  $U^{\text{diff}}$  does not contribute to the fluctuations at fixed volume. The whole system, and not just a single pair, has to be taken into account. See also Paper IX section II-D.

Define the instantaneous pair distribution function (or radial distribution function) as<sup>2</sup>

$$g(r, t) = \frac{1}{2N\rho} \sum_{i \neq j} \delta(r - r_{ij}(t)) \quad (3.15)$$

<sup>2</sup> $\delta(x)$  is Dirac delta function.

where

$$g(r) = \langle g(r, t) \rangle \quad (3.16)$$

is the traditional pair distribution function [Allen and Tildesley, 1987]. From  $g(r, t)$  we can calculate the potential energy at time  $t$  as

$$U(t) = (4\pi\rho N/2) \int_0^\infty U_{ij}(r)g(r, t)r^2 dr, \quad (3.17)$$

and

$$\Delta U(t) = (4\pi\rho N/2) \int_0^\infty U_{ij}(r)\Delta g(r, t)r^2 dr, \quad (3.18)$$

where

$$\Delta g(r, t) = g(r, t) - g(r). \quad (3.19)$$

$U^{\text{diff}}$ , shown on Figure 3.1, can be approximated with a linear function in the first shell regime (first peak of  $g(r)$ ). The same goes for  $W^{\text{diff}}$ . The fact that  $U^{\text{diff}}$  is nearly constant,  $\Delta U^{\text{diff}}(t) \simeq 0$ , suggests that

$$4\pi\rho N/2 \int_{\text{first shell}} r_{ij}\Delta g(r, t)r^2 dr \simeq 0 \quad (3.20)$$

or

$$\int_{\text{first shell}} r_{ij}\Delta\rho_b(r, t)r^2 dr \simeq 0 \quad (3.21)$$

where  $\rho_b(r, t) = (4\pi\rho N/2)\Delta g(r, t)$  is the bond density. In other words the number of bonds in first shell is constant, and the average first shell bond distance  $r_m(t) = \int_{\text{first shell}} r\rho_b(r, t)dr$  is constant. This is reasonable for a dense liquid in a fixed volume. Whenever a particle moves it will come closer to some particles and move further away from others – approximately without affecting  $r_m(t)$ .

If volume is changed we expect an overall change of the bond density, and  $U^{\text{diff}}$  will change. This is why the  $W-U$  scatter plot on Figure 2.2 has constant density paths,

$$W = \gamma_{WU}(U + U_0(\rho)) \quad (3.22)$$

Here, the argumentation of  $r_m$  being constant is somewhat imprecise. It is intuitively reasonable, but the “first shell” integral,  $\int_{\text{first shell}} \dots dr$ , is not well-defined. The following section discuss a one dimensional crystal where a clear argumentat can be made. Note, however, that the reasoning is of the same nature.

### 3.3 Low temperature limit of crystal

The correlation survives all the way down to the zero temperature limit of the crystal – even at negative pressure (Figure 4 in Paper IX). This low-temperature limit can be explained by approximating the pair potential by a Taylor expansion. In the following we will investigate  $W-U$  correlations of a one-dimensional crystal.

Think of a one-dimensional crystal with only nearest neighbor interactions (see also Paper IX section II-B-1). Let  $N$  be the number of particles in box of length (or “volume”)  $L$ . Make the box periodic so particle  $N + k$  is a mirror

### 3. ORIGIN OF STRONG CORRELATIONS

---

of particle  $k$ . The average pair distance will then be  $a = L/N$ . For simplicity put  $a$  at the minimum of the potential,  $U'_{ij}(a = r_m) = 0$ , and shift the minimum to zero,  $U_{ij}(r_m) = 0$ . In the low temperature limit we can make a Taylor expansion of the pair potential, keeping up to the third order in relative displacement. Define

$$S_p \equiv \sum_i^N (r_{i,i+1} - r_m)^p, \quad (3.23)$$

and write energy as (the third order term of energy is explicitly written here, since it goes into the second order term of virial)

$$U = \frac{1}{2}k_2S_2 + \frac{1}{6}k_3S_3 + O(S_4), \quad (3.24)$$

and virial as (see Paper IX for details)

$$W = -\frac{1}{3}(k_2r_mS_1 + (k_2 + \frac{1}{2}k_3r_m)S_2) + O(S_3), \quad (3.25)$$

where  $k_p$  is the  $p$ 'th derivative of the pair potential at  $r_m$ .

The lowest order term of the energy is second order  $S_2$ . To second order,  $W$  involves both  $S_1$  and  $S_2$ , so apparently there is no  $W-U$  correlation. However,  $S_1$  vanishes when volume is fixed: Fixed volume implies that  $\sum_i^N r_{i,i+1} = Nr_m = L$ , and  $S_1 = \sum_i^N (r_{i,i+1} - r_m) = \sum_i^N r_{i,i+1} - Nr_m = 0$ .

Combining Equations 3.24 and 3.25 (with  $S_1 = 0$  and throwing away  $O(S_3)$ ) we recover a  $W-U$  correlation,

$$W = -\frac{1}{3} \frac{k_2 + \frac{1}{2}k_3r_m}{\frac{1}{2}k_2} U. \quad (3.26)$$

For the Lennard-Jones potential (with  $r_m = 2^{1/6}\sigma$ ) the slope is  $-\frac{1}{3} \frac{k_2 + \frac{1}{2}k_3r_m}{\frac{1}{2}k_2} = 6.33$ . This is in good agreement with slope found in simulations (see Figure 2.2)<sup>3</sup>.

The three dimensional crystal is more complicated (see Paper IX section II-B-2 and II-B-3). Here, the correlation is not exact but the energy-virial correlation is close to unity (Figure in Paper IX) and slope is close to observed six.

Again, note the importance of fixed volume. In the one dimensional crystal the situation is more clear than the effective inverse power-law explanation (and the three dimensional crystal), but are of the same nature. When one bond gets shorter another must get longer. The volume constrain makes linear terms vanish. That is  $S_1 = 0$  or  $\int_{\text{first peak}} r \Delta\rho_b(r, t) dr \simeq 0$ .

#### 3.4 Weeks-Chandler-Andersen

The reader has perhaps noticed the similarities between the apparent inverse power-law and the celebrated 1971 paper by Andersen, Weeks, and Chandler [1971] (WCA). These authors argue that molecules of a liquid can be thought

---

<sup>3</sup>Traditionally, we think of the low-temperature limit of the crystal as harmonic. However, for the harmonic crystal ( $k_3 = 0$ ) the slope is  $-2/3$  and not close to six.

of as hard-core particles ( $U_{ij}^{\text{hs}}(r) = \infty$  for  $r < r_d$  and  $U_{ij}^{\text{hs}}(r) = 0$  elsewhere) with attraction that can be viewed as a perturbation.

The effective inverse power-law plus a linear term agrees with the WCA interpretation, that the repulsive region of the pair potential dominates liquid structure – an important result of WCA-paper. However, in the following chapter it will be demonstrated that an inverse power-law is more useful than a hard-core description. (One can think of a hard-core interactions as a approximation to the effective inverse power-law.)



## Chapter 4

# Strongly correlating viscous liquids

In this chapter it is demonstrated that strongly correlating *viscous* liquids are more simple than viscous liquids in general.

In the first section, it is argued that the glass-transition of strongly correlating *viscous* liquids is single-parameter in the Prigogine-Defay sense. The references for this section are Paper I, Paper IV, Paper VI and Paper IX. In addition, the section give some simple equations to illustrate possible scenarios of thermodynamic fluctuations and a rethinking of the (classical) Prigogine-Defay ratio  $\Pi^{\text{classic}}$ .

In the second section it is shown that strongly correlating viscous liquids have a scale invariant energy landscape. This provides a scaling-law of dynamics (exemplified by the diffusion constant  $D$ ) and structure (exemplified by the radial distribution function  $g(r)$ ). The references for this section are Paper VII and Paper XIII.

### 4.1 A single order-parameter of viscous liquids

The classical picture of a single order-parameter description of the glass transition was developed by Davies and Jones [1953a,b]. In these authors' picture, an important number is the so-called Prigogine-Defay ratio [Prigogine and Defay, 1954]. This ratio is calculated from the change of the (static) response function at the glass-transition. If  $\Delta c_p = c_p^{\text{liquid}} - c_p^{\text{glass}}$  is the change of the isobaric heat capacity per unit volume,  $\Delta \kappa_T = \kappa_T^{\text{liquid}} - \kappa_T^{\text{glass}}$  is the change of isothermal compressibility and  $\Delta \alpha_p = \alpha_p^{\text{liquid}} - \alpha_p^{\text{glass}}$  is the change of isobaric expansion coefficient, then the classical Prigogine-Defay ration is defined as<sup>1</sup>

$$\Pi_{pT}^{\text{classic}} = \frac{\Delta c_p \Delta \kappa_T}{T_g (\Delta \alpha_p)^2}. \quad (4.1)$$

In general  $\Pi_{pT}^{\text{classic}} \geq 1$  and  $\Pi_{pT}^{\text{classic}} = 1$  in the single parameter case. Since then, the topic has been debated in the glass community<sup>2</sup>. Moynihan et al.

---

<sup>1</sup>The superscript "classic" in equation 4.1 is normally not used, but is used here distinguish it from the later defined Prigogine-Defay ratios. The subscript  $pT$  is to emphasize that this ratio relates the natural response functions of the  $NpT$  ensemble - the ensemble preferred in an experimental situation. That is  $c_p$ ,  $\kappa_T$  and  $\alpha_p$ .

<sup>2</sup>See References [Davies and Jones, 1953a,b, DiMarzio, 1974, Goldstein, 1975, Gupta and Moynihan, 1976, Moynihan et al., 1976, Roe, 1977, Moynihan and Gupta, 1978, Lesikar and

[1976] concluded, on the basis of available experimental data, that the ratio typically takes values of  $2 < \Pi_{pT}^{\text{classic}} < 4$ . The conclusion from this is therefore that in general more than one order-parameter is needed. A collection of ratios available today are compiled in Table 4.1. Note that some Prigogine-Defay ratios are in fact close to unity. Table 4.1 is discussed in details in Section 4.1.3.

At this point, I have not explained to the reader what exactly is meant by “a single-order parameter”. The reason for this is that Roe [1977], Moynihan and Gupta [1978], Moynihan and Lesikar [1981] realized that the classical Prigogine-Defay ratio is not well-defined. Theoretical predictions solely based on  $\Pi_{pT}^{\text{classic}}$  are therefore problematic. The solution to this was a (well-defined) revised Prigogine-Defay ratio. This ratio relates to the frequency dependent response functions of the equilibrium liquid (disregarding the crystal) and is defined as

$$\Pi_{pT}^{\text{linear}} = \frac{[c_p(\omega \rightarrow 0) - c_p(\omega \rightarrow \infty)][\kappa_T(\omega \rightarrow 0) - \kappa_T(\omega \rightarrow \infty)]}{T[\alpha_p(\omega \rightarrow 0) - \alpha_p(\omega \rightarrow \infty)]^2} \quad (4.2)$$

where  $\omega \rightarrow \infty$  refers to high-, and  $\omega \rightarrow 0$  to the low frequency limit. Unfortunately, it is difficult to get good measurements of wide frequency spectra, as needed to get these limits. For this reason no-one has attempted to calculate  $\Pi_{pT}^{\text{linear}}$  from experimental data (to the author’s knowledge). However, in simulation this can be done as demonstrated by Nielsen [1999] and in Figure 4.3. Ellegaard [2005] showed that  $\Pi_{pT}^{\text{linear}}$  can be re-expressed as a single-frequency quantity  $\Lambda_{pT}(\omega)$  (see following section), more suited for experiments. This is published in Paper I.

The remainder of this chapter is a newly developed interpretation of “single parameter”-ness, based on  $\Lambda_{pT}(\omega)$ . In this interpretation, it is clear what is meant by “a single parameter”. In the classical understanding it is somewhat unclear what can be learned from a ratio close to unity but not exactly unity. In other words: What should a measured value of  $\Pi_{pT}^{\text{classic}}$  be compared to? Is  $\Pi = 1.2$  “significantly larger than unity” as concluded by Takahara et al. [1999]? It will become clear how we should interpret  $\Pi_{pT}^{\text{classic}} > 1$  (Subsection 4.1.3).

#### 4.1.1 Dynamic Prigogine-Defay ratio, $\Lambda(\omega)$

The dynamic Prigogine-Defay ratio  $\Lambda_{pT}(\omega)$  is an one-frequency test quantity for single parameter-ness. This was published in Paper I, based on the Ph.D. thesis of Ellegaard [2005]. It is defined from the frequency-dependent response functions. If  $c_p(\omega)''$ ,  $\kappa_T''(\omega)$  and  $\alpha_p''(\omega)$  are the imaginary parts (at a single frequency) of isobaric heat capacity per unit volume, isothermal compressibility and isobaric expansion coefficient respectively, then

$$\Lambda_{pT}(\omega) \equiv \frac{c_p''(\omega)\kappa_T''(\omega)}{T[\alpha_p''(\omega)]^2}. \quad (4.3)$$

It is in principle accessible through experiments, although it has not been measured yet. It is not at all trivial to measure frequency dependent response functions. As an example, a recent paper by Christensen et al. [2007] shows that conventional methods to measure frequency-dependent isobaric heat capacity  $c_p(\omega)$  fail.

---

Moynihan, 1980, Moynihan and Lesikar, 1981, Nieuwenhuizen, 1997, 2000, Ellegaard, 2005, Schmelzer and Gutzow, 2006, Pick, 2008] and Paper VI.

Table 4.1: Litterateur values of classical Prigogine-Defay ratios.

Material	$\Pi_{pT}$	$\Pi_{pT}^{-1/2}$	Ref.
Pure SiO <sub>2</sub> glass	10 <sup>3</sup> -2·10 <sup>5</sup>	0.03-0.002	a
Glycerol, C <sub>3</sub> H <sub>5</sub> (OH) <sub>3</sub>	9.4	0.33	b
Rubber	8.3	0.33	a
GeO <sub>2</sub>	6.9±1.3	0.38±0.04	h
16Na <sub>2</sub> O-10B <sub>2</sub> O <sub>3</sub> -74SiO <sub>2</sub>	4.9	0.45	f
B <sub>2</sub> O <sub>3</sub>	4.7	0.46	c/b
0.4Ca·NO <sub>3</sub> ·0.6KNO <sub>3</sub>	4.5	0.47	c/b
Glucose, OC <sub>6</sub> H <sub>7</sub> (OH) <sub>6</sub>	3.7	0.52	a
16Na <sub>2</sub> O-10CaO-74SiO <sub>2</sub>	3.6	0.53	f
Se	2.4	0.65	a/b
Se	2.0	0.71	j
ZrTiCuNiBe	2.4	0.65	e
26Na <sub>2</sub> O-74SiO <sub>2</sub>	2.3	0.66	f
Technical glasses	2.0-2.7	0.71-0.61	a
Polyvinylacetate	2.2(1.7)	0.67(0.77)	c/b
n-Propanol, C <sub>3</sub> H <sub>7</sub> OH	1.9	0.73	b
Polyvinylchlorid, PVC	1.7	0.77	b
Polystyrene, PS	1.3±0.1 (16)	0.88±0.03 (0.25)	d
OTP(75%)-TPCM(25%)	1.28	0.88	k
OTP(67%)-OPP(33%)	1.20±0.05	0.92±0.02	d
Polystyrene, PS	1.085	0.96	l
Phenoxy	1.03	0.99	g
Polycarbonate	1.02	0.99	g
Polysulfone	0.96	1.02	g
Polyarylate	0.90	1.05	g
Polyisobutene	0.9	1.05	b

Liquids are listed with decreasing classical Prigogine-Defay ratio. As discussed in details in Section 4.1.3 this separates van der Waals bonded liquids, with ratios close to unity, from the rest. References. a: [Nemilov, 1994]; b: [Donth, 1981]; c: [Gupta and Moynihan, 1976]; d: [Takahara et al., 1999]; e: [Samwer et al., 1999]; f: [Wondraczek and Behrens, 2007]; g: [Zoller, 1982]; h: [Dingwell et al., 1993]; i: [Hadac et al., 2007]; j: [Berg and Cooper, 1978]; k: Calculated by Ellegaard [2005] using data from Naoki et al. [1986]; l: [Oels and Rehage, 1977]. Abbreviations: OTP, o-terphenyl: C<sub>6</sub>H<sub>4</sub>(C<sub>6</sub>H<sub>5</sub>)<sub>2</sub>; TPCM, triphenylchloromethane: C(C<sub>6</sub>H<sub>5</sub>)<sub>3</sub>Cl; OPP, o-phenylphenol: C<sub>6</sub>H<sub>4</sub>(C<sub>6</sub>H<sub>5</sub>)OH; Polyvinylacetate: [-CH<sub>2</sub>(COOCH<sub>3</sub>)CH-]<sub>n</sub>; Polyvinylchlorid: [-C(CH<sub>2</sub>)CH<sub>2</sub>-]<sub>n</sub>; Polystyrene: [-CH(C<sub>6</sub>H<sub>5</sub>)CH<sub>2</sub>-]<sub>n</sub>; Phenoxy: [-CH<sub>2</sub>CH(OH)CH<sub>2</sub>O(C<sub>6</sub>H<sub>4</sub>)-]<sub>n</sub>; Polycarbonate: [-C<sub>2</sub>O(C<sub>6</sub>H<sub>4</sub>)C(CH<sub>3</sub>)<sub>2</sub>(C<sub>6</sub>H<sub>4</sub>)O-]<sub>n</sub>; Polysulfone: [-C(C<sub>6</sub>H<sub>4</sub>)SO<sub>2</sub>(C<sub>6</sub>H<sub>4</sub>)O(C<sub>6</sub>H<sub>4</sub>)C(CH<sub>3</sub>)<sub>2</sub>(C<sub>6</sub>H<sub>4</sub>)O-]<sub>n</sub>; Polyarylate: [-CO(C<sub>6</sub>H<sub>4</sub>)COO(C<sub>6</sub>H<sub>4</sub>)C(CH<sub>3</sub>)<sub>2</sub>(C<sub>6</sub>H<sub>4</sub>)O-]<sub>n</sub>.

#### 4. STRONGLY CORRELATING VISCOUS LIQUIDS

---

In Paper I it is shown that if  $\Pi_{pT}^{\text{linear}} = 1$  then  $\Lambda_{pT}(\omega) = 1$  at any  $\omega$ . Such liquids are referred to as “Single parameter liquids”. Moreover, if  $\Lambda(\omega)$  is unity in one ensemble, then it is unity in all ensembles:

$$1 = \Lambda_{pT}(\omega) = \Lambda_{VT}(\omega) = \Lambda_{pS}(\omega) = \Lambda_{VS}(\omega). \quad (4.4)$$

This is reasonable since it would be peculiar if “single parameter”-ness was ensemble dependent. However, if  $\Lambda_{pT}(\omega) > 1$  we cannot say that they are equal. Nevertheless, if one of the ratios is close to unity, the others are likely also to be close to unity, as demonstrated in simulations later.

An equivalent way of expressing “single parameter”-ness is<sup>3</sup>

$$\Delta\bar{p}(t) = \gamma_{pS}\Delta\bar{s}(t) \text{ when controlling } V \text{ and } T \quad (4.5)$$

where the bar indicates fluctuations on some relaxing time-scale. If the relation is exact, the bar is in principle not needed. Later, however, we will discuss a situation where these equations are approximate (replacing “=” with “ $\simeq$ ”). Then the bar makes a difference. Again, since “single parameter”-ness must be ensemble independent, it follows that

$$\Delta\bar{V}(t) = \gamma_{VS}\Delta\bar{s}(t) \text{ when controlling } p \text{ and } T, \quad (4.6)$$

$$\Delta\bar{p}(t) = \gamma_{VT}\Delta\bar{T}(t) \text{ when controlling } V \text{ and } S, \quad (4.7)$$

and

$$\Delta\bar{V}(t) = \gamma_{VT}\Delta\bar{T}(t) \text{ when controlling } p \text{ and } S. \quad (4.8)$$

The equations apply when the controlling parameters are held constant. Then the free parameters will fluctuate in a correlated manner (on the relaxing time-scale indicated by the bar). Also, the equations apply to perturbations (in the linear regime). Then relaxation of the free parameters follows the same (scaled) function.

Equations 4.5 to 4.8 answer the question: What is the single parameter? There is only one internal relaxing parameter in the system. Mechanical and thermal relaxation are slaves of this parameter. It is reasonable to speculate that other quantities, like dipole-moment, are also slaves of the single parameter. If dipole-moment is a slave, then dielectric measurements would reflect the “single parameter”-ness. This would make single parameter liquids even more interesting due to the simplicity.

All of the equations in this subsection (Equations 4.3 to 4.8) are equivalent, and any of them can be regarded as the definition of a single parameter liquid. It is easy to show from one of Equations 4.5 to 4.8 that a corresponding  $\Lambda_{XY}(\omega)$  is equal to unity. An example is given in next subsection. Showing it the other way, that one of Equations 4.5 to 4.8 can be derived from a cooresponding  $\Lambda_{XY}(\omega)$  being unity can also be shown. This is done in Paper I. In the following we will consider Equations 4.3 to 4.8 as the definition of a single parameter liquid.  $\Lambda_{XY}(\omega) = 1$  is regarded as a consequence. In future studies this way of thinking is recommended.

---

<sup>3</sup> $s = S/V$  is entropy per unit volume.

### 4.1.2 Connecting Prigogine-Defay ratio to a correlation coefficient

Single parameter liquids and strongly correlating *viscous* liquids are related as discussed in the following. The inverse square-root of the Prigogine-Defay ratio equals some correlation coefficient.

This will be demonstrated in the constant  $VT$  ensemble. To keep temperature constant, entropy has to be transferred between a heat-bath and the sample:  $\Delta S(t) = \Delta q(t)/T$  where  $q$  is heat. Since the volume is constant (no  $p\Delta V$  work) this heat is seen in the sample as a change of the total energy  $\Delta E$  and therefore  $\Delta E(t) = T\Delta S(t)$ . Since we will relate this to computer simulations, where total energy is easy to access, we will write energy instead of entropy.

If  $c_V''(\omega)$ ,  $K_T''(\omega)$  and  $\beta_V''(\omega)$  are the imaginary parts of the frequency dependent isochoric specific heat capacity per unit volume, isothermal bulk modulus and isochoric pressure coefficient<sup>4</sup> respectively, then the dynamic Prigogine-Defay ratio is (Appendix of Paper I)

$$\Lambda_{VT}(\omega) \equiv -\frac{c_V''(\omega)K_T''(\omega)}{T[\beta_V''(\omega)]^2}. \quad (4.9)$$

The fluctuation-dissipation theorem [Smit and Frenkel, 2001, Appendix C] connects equilibrium fluctuations to response functions. If  $\Delta E(t) = E(t) - \langle E \rangle$ ,  $\Delta p(t) = p(t) - \langle p \rangle$  and  $\mathcal{C}_\omega\{f(t)\} = \frac{1}{2\pi} \int f(t) \cos(\omega t) dt$  denotes the cosine transform of  $f(t)$ , then (Paper IV)

$$c_V''(\omega) = \frac{\omega}{Vk_B T^2} \mathcal{C}_\omega\{\langle \Delta E(0)\Delta E(t) \rangle_{VT}\}, \quad (4.10)$$

$$K_T''(\omega) = -\frac{\omega}{Vk_B T} \mathcal{C}_\omega\{\langle \Delta p(0)\Delta p(t) \rangle_{VT}\}, \quad (4.11)$$

$$\beta_V''(\omega) = \frac{\omega}{Vk_B T^2} \mathcal{C}_\omega\{\langle \Delta E(0)\Delta p(t) \rangle_{VT}\}. \quad (4.12)$$

Combining equation 4.9 to 4.12,  $\Lambda_{VT}(\omega)$  can be re-expressed as

$$\Lambda_{VT}(\omega) = \frac{\mathcal{C}_\omega\{\langle \Delta E(0)\Delta E(t) \rangle_{VT}\} \mathcal{C}_\omega\{\langle \Delta p(0)\Delta p(t) \rangle_{VT}\}}{[\mathcal{C}_\omega\{\langle \Delta E(0)\Delta p(t) \rangle_{VT}\}]^2}. \quad (4.13)$$

For later use, we will also define the frequency-dependent slope as

$$\gamma_{pE}(\omega) = V \sqrt{\frac{\mathcal{C}_\omega\{\langle \Delta p(0)\Delta p(t) \rangle_{VT}\}}{\mathcal{C}_\omega\{\langle \Delta E(0)\Delta E(t) \rangle_{VT}\}}} \quad (4.14)$$

that can be written (from Equations 4.10 and 4.11) as

$$\gamma_{pE}(\omega) = \sqrt{\frac{-K_T''(\omega)}{Tc_V''(\omega)}}. \quad (4.15)$$

<sup>4</sup>See the Appendix of Paper I for the definition of (all) the frequency-dependent response functions

#### 4. STRONGLY CORRELATING VISCOUS LIQUIDS

---

$\mathcal{C}_\omega(f(t))$  relates to fluctuations of  $f(t)$  on a  $1/\omega$  time-scale (similar to making a running-average over an  $1/\omega$  time-window) and thus,

$$(\Lambda_{VT}(\omega))^{-1/2} = \frac{\mathcal{C}_\omega\{\langle\Delta E(0)\Delta p(t)\rangle_{VT}\}}{\sqrt{\mathcal{C}_\omega\{\langle\Delta E(0)\Delta E(t)\rangle_{VT}\}\mathcal{C}_\omega\{\langle\Delta p(0)\Delta p(t)\rangle_{VT}\}}} \quad (4.16)$$

is a measure of how correlated  $p$  and  $E$  are on this time-scale. If we regard Equation 4.5 as our definition of a single parameter liquid, then it follows that  $(\Lambda_{VT}(\omega))^{-1/2} = 1$ .

In computer simulations, and conceptually, a more convenient way to study slow thermodynamic fluctuations is through time-correlation functions [Hansen and McDonald, 2006] and defining a time-dependent correlation coefficient as

$$R_{pE}(t) \equiv \frac{\langle\Delta E(0)\Delta p(t)\rangle_{VT}}{\sqrt{\langle\Delta E(0)\Delta E(t)\rangle_{VT}\langle\Delta p(0)\Delta p(t)\rangle_{VT}}} \quad (4.17)$$

and a time-dependent slope

$$\gamma_{pE}(t) = \sqrt{\frac{\langle\Delta p(0)\Delta p(t)\rangle_{VT}}{\langle\Delta E(0)\Delta E(t)\rangle_{VT}}}. \quad (4.18)$$

From the fluctuation dissipation theorem it follows that this is what could be derived from measurements of step experiments [Smit and Frenkel, 2001].

Let us set-up some equations to illustrate possible scenarios of equilibrium fluctuations. Let  $x(t)$  and  $y(t)$  be the conjugated variables of the fixed variables  $X$  and  $Y$  respectively. For simplicity, we will shift and normalize  $x$  and  $y$  so  $\langle x \rangle = \langle y \rangle = 0$  and  $\langle x^2 \rangle = \langle y^2 \rangle = 1$ . Imagine that  $x(t)$  and  $y(t)$  are sums of some hidden independent stochastic Debye processes  $f_1(t)$ ,  $f_2(t)$ ,  $s_1(t)$  and  $s_2(t)$ . They are independent so cross-correlation functions are zero. Let  $f_1$  and  $f_2$  be fast processes,  $\langle f_1(0)f_1(t) \rangle = \langle f_2(0)f_2(t) \rangle = \exp(-t)$ , and  $s_1$  and  $s_2$  be slow process,  $\langle s_1(0)s_1(t) \rangle = \langle s_2(0)s_2(t) \rangle = \exp(-t/100)$ . Write  $x(t)$  as

$$x(t) = G_{\lambda_x}\lambda_x f_1(t) + G_{\lambda_x}(1 - \lambda_x)s_1(t) \quad (4.19)$$

where  $\lambda_x$  ( $0 \leq \lambda_x \leq 1$ ) determines the relative size of the fast process, and

$$G_\lambda = 1/\sqrt{\lambda^2 + (1 - \lambda)^2}, \quad (4.20)$$

ensures normalization<sup>5</sup>,  $\langle x^2 \rangle = 1$ . In addition to  $f_1$  and  $s_1$ , let  $y(t)$  also depend on  $f_2$  and  $s_2$  to introduce some de-correlation between  $x$  and  $y$ :

$$\begin{aligned} y(t) &= G_{\lambda_y}G_{\lambda_f}\lambda_y[\lambda_f f_1(t) + (1 - \lambda_f)f_2(t)] \\ &+ G_{\lambda_y}G_{\lambda_s}(1 - \lambda_y)[\lambda_s s_1(t) + (1 - \lambda_s)s_2(t)]. \end{aligned} \quad (4.21)$$

where  $\lambda_y$  ( $0 \leq \lambda_y \leq 1$ ) determines the relative size of fast process.  $\lambda_f$  ( $0 \leq \lambda_f \leq 1$ ) and  $\lambda_s$  ( $0 \leq \lambda_s \leq 1$ ) determines the amount of correlation on fast and slow time-scales respectively. The time correlation functions for  $x$  and  $y$  are

$$\begin{aligned} \langle x(0)x(t) \rangle &= G_{\lambda_x}^2\lambda_x^2\langle f_1(0)f_1(t) \rangle \\ &+ G_{\lambda_x}^2(1 - \lambda_x)^2\langle s_1(0)s_1(t) \rangle, \end{aligned} \quad (4.22)$$

---

<sup>5</sup>Since  $\langle x^2 \rangle = G_{\lambda_x}^2[\lambda_x^2\langle f_1^2 \rangle + (1 - \lambda_x)^2\langle s_1^2 \rangle + 2\lambda_x(1 - \lambda_x)\langle f_1 s_1 \rangle] = 1$ ,  $\langle f_1^2 \rangle = \langle s_1^2 \rangle = 1$  and  $\langle f_1 s_1 \rangle = 0$  then  $G_\lambda = 1/\sqrt{\lambda^2 + (1 - \lambda)^2}$ , Equation 4.20.

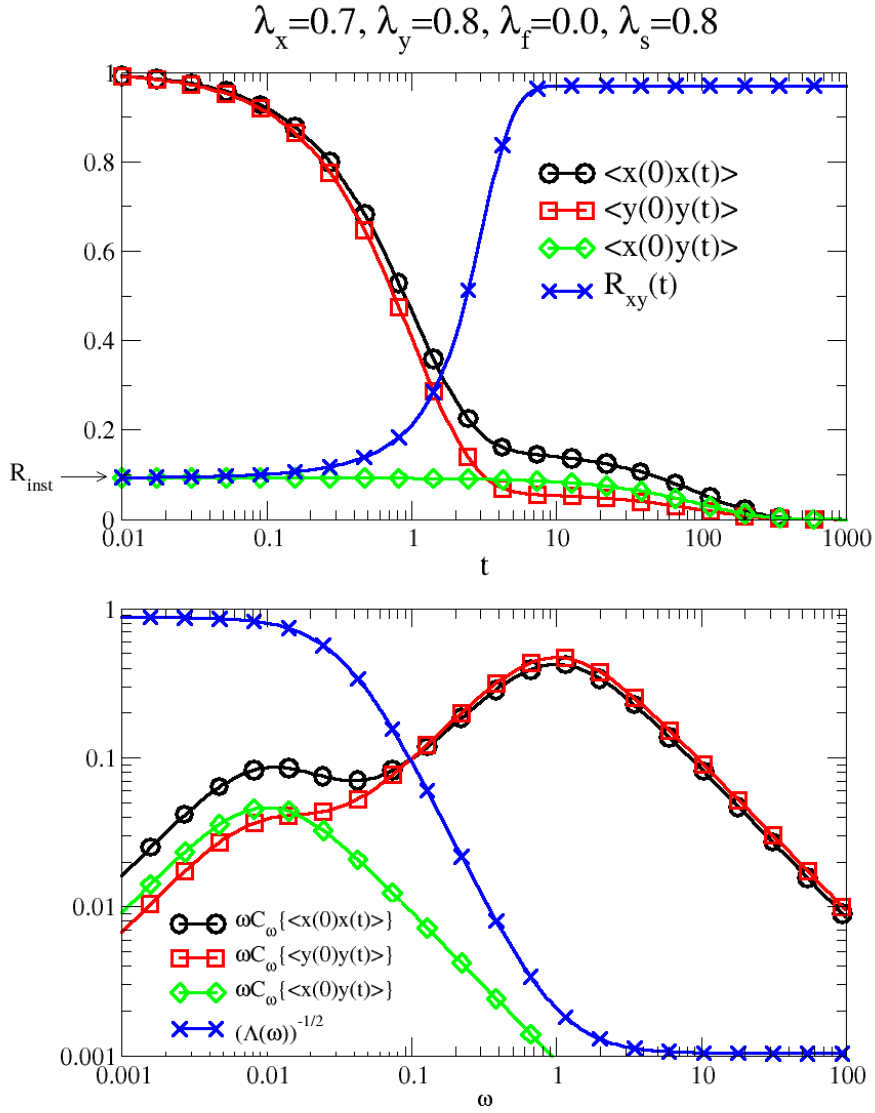


Figure 4.1: A possible scenario of thermodynamic fluctuations, Equations 4.19 and 4.21. In the parametrization shown,  $x$  and  $y$  are strongly correlated on long time-scales, but not on short time-scales. See also Figure 4.2.

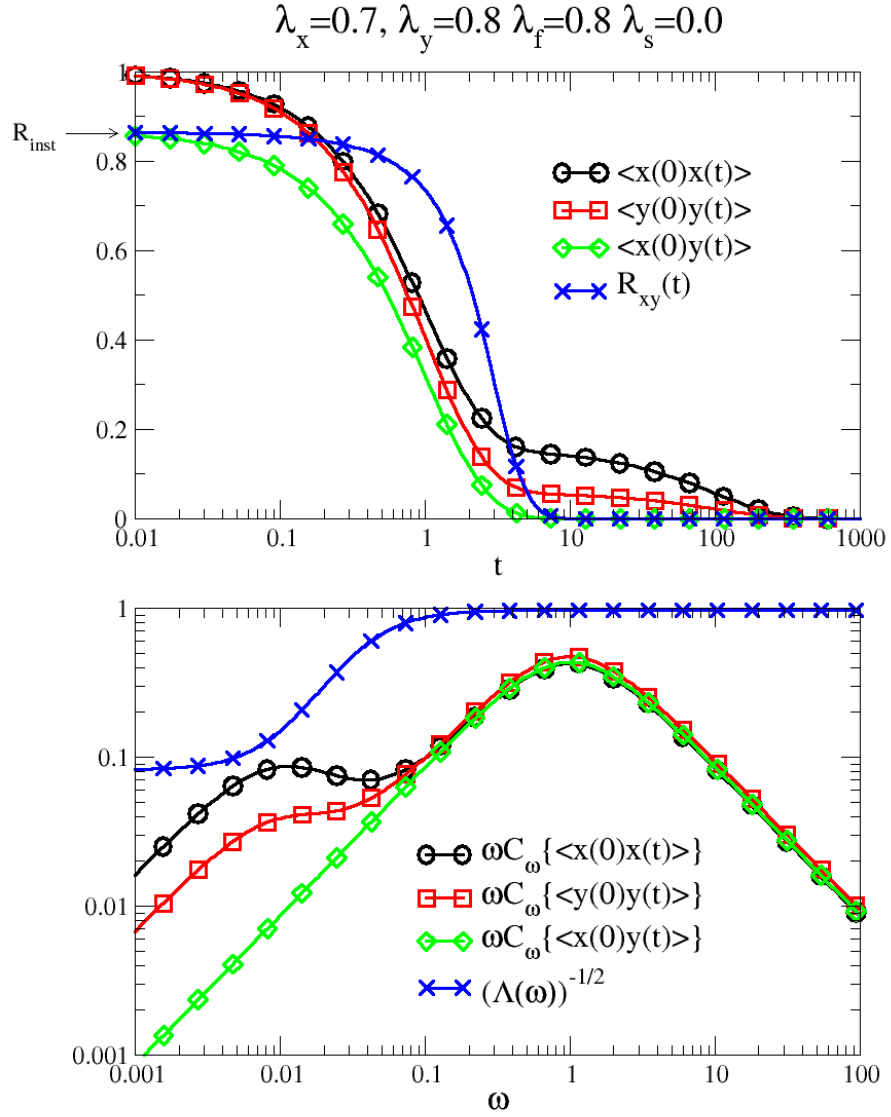


Figure 4.2: A possible scenario of thermodynamic fluctuations, Equations 4.19 and 4.21. In the parametrization shown,  $x$  and  $y$  are strongly correlated on short time-scales, but not on long time-scales. See also Figure 4.1.

$$\begin{aligned}
\langle y(0)y(t) \rangle &= G_{\lambda_y}^2 \lambda_y^2 G_{\lambda_f}^2 \lambda_f^2 \langle f_1(0)f_1(t) \rangle \\
&+ G_{\lambda_y}^2 \lambda_y^2 G_{\lambda_f}^2 (1 - \lambda_f)^2 \langle f_2(0)f_2(t) \rangle \\
&+ G_{\lambda_y}^2 (1 - \lambda_y)^2 G_{\lambda_s}^2 \lambda_s \langle s_1(0)s_1(t) \rangle \\
&+ G_{\lambda_y}^2 (1 - \lambda_y)^2 G_{\lambda_s}^2 (1 - \lambda_s) \langle s_2(0)s_2(t) \rangle
\end{aligned} \tag{4.23}$$

and

$$\begin{aligned}
\langle x(0)y(t) \rangle &= G_{\lambda_x} \lambda_x G_{\lambda_y} \lambda_y G_{\lambda_f} \lambda_f \langle f_1(0)f_1(t) \rangle \\
&+ G_{\lambda_x} (1 - \lambda_x) G_{\lambda_y} (1 - \lambda_y) G_{\lambda_s} \lambda_s \langle s_1(0)s_1(t) \rangle.
\end{aligned} \tag{4.24}$$

Since the auto-correlation functions of  $f_1$ ,  $f_2$ ,  $s_1$  and  $s_2$  is simply exponential relaxations it is straightforward to get an analytical expression of the time-dependent correlation coefficient  $R_{xy}(t)$ , Equation 4.17. Moreover, the cosine transform of exponential relaxation is given analytically [Spiegel and Liu, 1999],  $\mathcal{C}_\omega\{\exp(-t/\tau)\} = \Im\{\frac{1}{i\omega+1/\tau}\}$ , where  $\sqrt{-1} = i$  and  $\Im$  is the imaginary part. Thus, the dynamic Prigogine-Defay ratio  $\Lambda_{XY}(\omega)$ , Equation 4.13, also has an analytic expression. Three parametrization are shown on Figures 4.1, 4.2 and 4.5.

Now, consider a strongly correlating viscous liquid (Chapter 2). When  $\Lambda_{VT}(\omega)$  is evaluated, fast (picoseconds) kinetic parts of  $p$  and  $E$  are averaged out. Qualitatively this corresponds to the parametrization of Figure 4.1. Only the configurational parts survive so  $\bar{E}(t) = \bar{U}(t)$  and  $\bar{p}(t) = \bar{W}(t)/V$  (again, the bar indicates an average). A simple minded guess is therefore that  $(\Lambda_{VT}(\omega))^{-1/2}$  is equal to the  $W$ - $U$  energy correlation coefficient,  $R_{WU}$ . Strictly speaking, we cannot make this connection unless  $R_{WU}$  is exactly unity. To demonstrate this, think of  $x = W$  and  $y = U$  in Figure 4.1. Then the figure illustrates a situation where  $(\Lambda_{VT}(\omega))^{-1/2} > R_{WU}$ . The opposite situation,  $(\Lambda_{VT}(\omega))^{-1/2} < R_{WU}$ , is also possible as shown in Figure 4.2 (by changing the parametrization).

A realistic model system, the Kob-Andersen binary Lennard-Jones liquid, show, however, that to a good approximation

$$R_{pE}(t) \simeq R_{WU} \tag{4.25}$$

and

$$(\Lambda_{VT}(\omega))^{-1/2} \simeq R_{WU}, \tag{4.26}$$

as seen on Figure 4.3 and 4.4. This is a consequence of  $R_{WU}$  being close to unity. Moreover, the  $W$ - $U$  slope  $\gamma_{WU}$  can to a good approximation be calculated from

$$\gamma_{pE}(\omega) \simeq \gamma_{WU}, \tag{4.27}$$

and

$$\gamma_{pE}(t) \simeq \gamma_{WU}. \tag{4.28}$$

Before we move on, a final comment should be made. Measurements on viscous liquids typically reveal more than one relaxation processes. Think of a situation where a liquid has a slow  $\alpha$ -relaxation and a faster  $\beta$ -relaxation. Imagine that individually they are strongly correlating, but gives different strength to  $x$  and  $y$ . In other words, they have different slopes. Such a situation is shown on Figure 4.5. Note that in the region where the two processes mix, there is a decrease of correlation. Experimental data of  $\Lambda_{pT}(\omega)$  can in this way give some insight about the origin of relaxations.

## 4. STRONGLY CORRELATING VISCOUS LIQUIDS

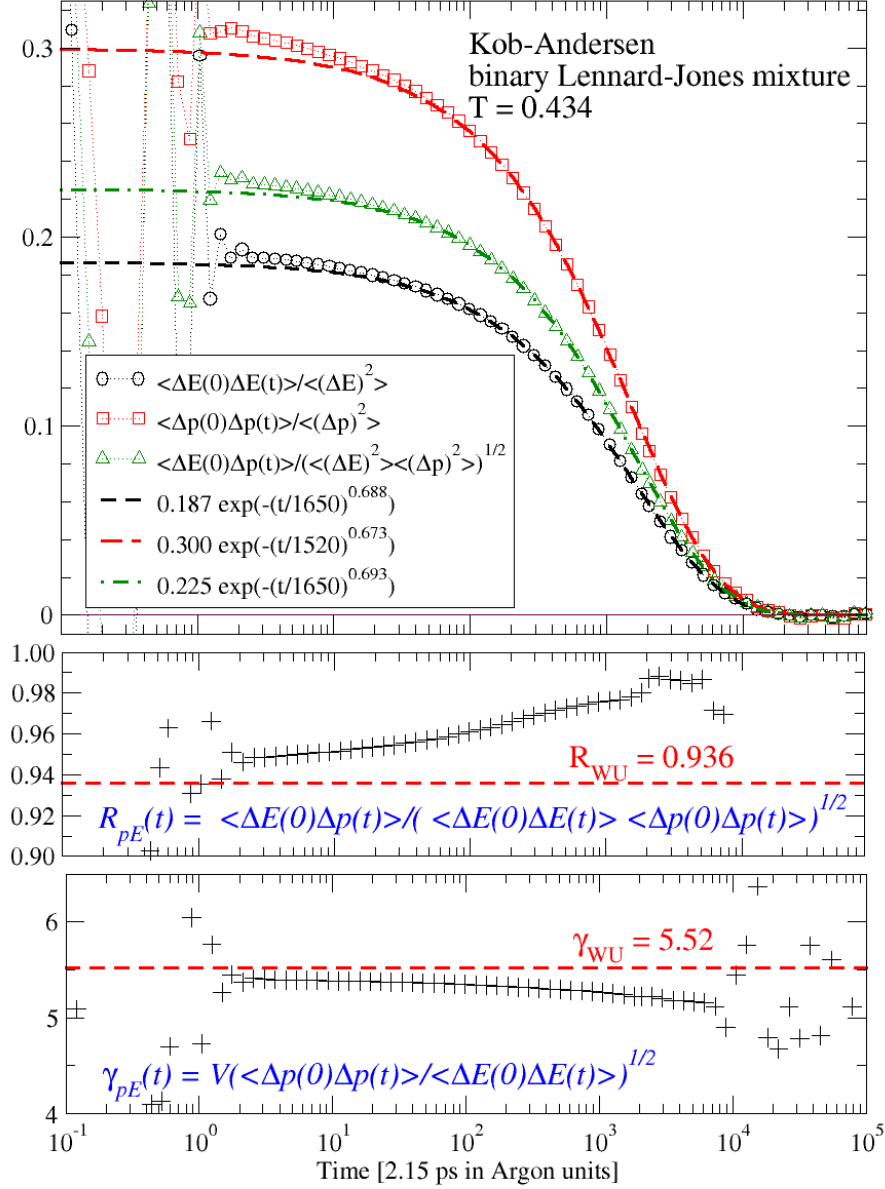


Figure 4.3: Auto- and cross correlation functions of (total) energy and pressure of the Kob-Andersen binary Lennard-Jones liquids at  $T = 0.434$ . A stretch exponential (fitted at  $t > 100$ ),  $A \exp(-(t/\tau)^{-\beta})$ , are shown. The linear Prigogine-Defay ratio (Equation 4.2) can be estimated as  $\Pi_{VT}^{\text{linear}} \simeq \frac{0.255}{\sqrt{0.187 \cdot 0.300}} = 1.08$  ( $(\Pi_{VT}^{\text{linear}})^{-1/2} \simeq 0.962$ ) using the prefactors of the fit. The lower panels shows the time dependent correlation coefficient  $R_{pE}(t)$  (Equation 4.17) and the corresponding slope (Equation 4.18). The  $W$ - $U$  correlation coefficient  $R_{WU} = 0.936$  and  $W$ - $U$  slope  $\gamma_{WU} = 5.52$  are indicated with dashed lines.

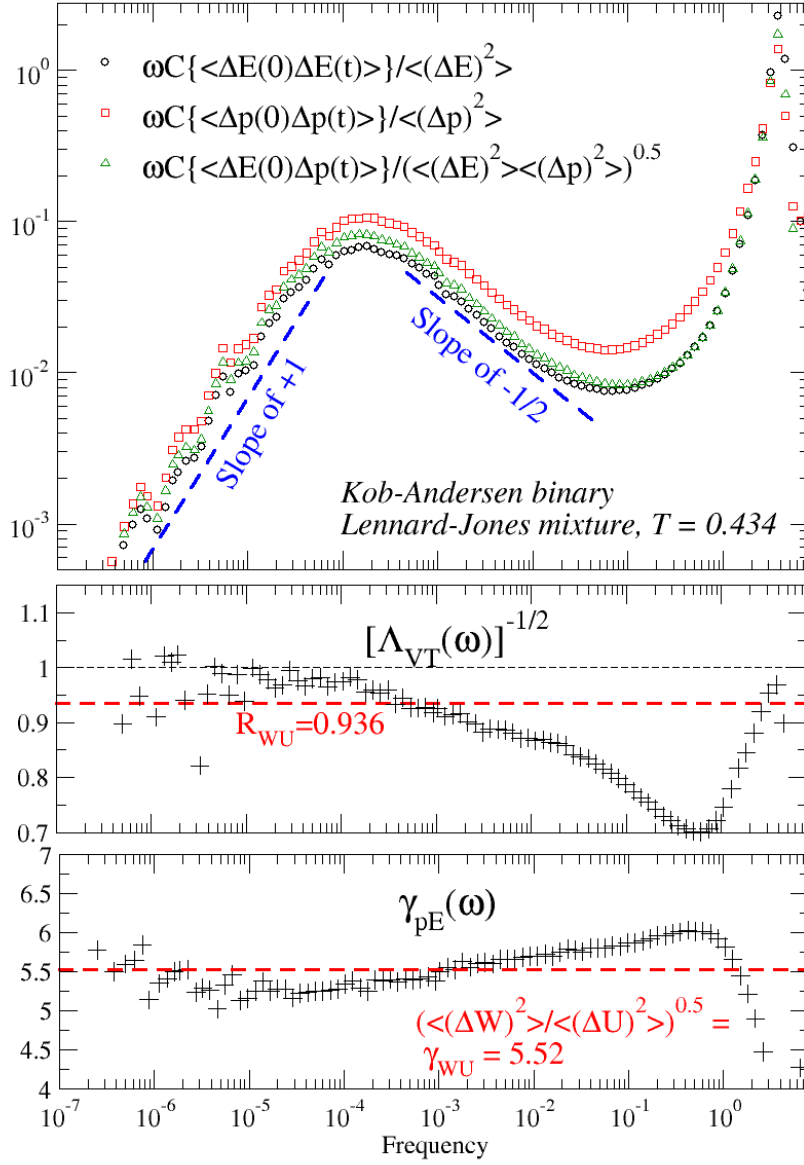


Figure 4.4: Normalized imaginary parts of natural response functions of the  $NVT$  ensemble (Equations 4.10 to 4.12) of the Kob-Andersen Lennard-Jones liquids at  $T = 0.434$ . The peak to the right is partially a consequence of the (artificial) Nosé-Hoover thermostat [Nosé, 1984, Hoover, 1985] and peak on the left is the structural relaxation peak. Note that the left-hand side of the structural relaxation peak has slope +1 and the right-hand side has close to slope  $-\frac{1}{2}$  (in the log-log representation). This is in good agreement with what is found in experiments [Nielsen et al., 2008] (note that the stretch exponential  $\beta$ , Figure 4.3, is somewhat larger than the limiting slope). The lower panels show the inverse square root of the dynamic Prigogine-Defay ratio (Equation 4.9) and the corresponding slope (Equation 4.14). The instantaneous  $W$ - $U$  correlation coefficient  $R_{WU} = 0.936$  and slope  $\gamma_{WU} = 5.52$  are indicated with red dashed lines.

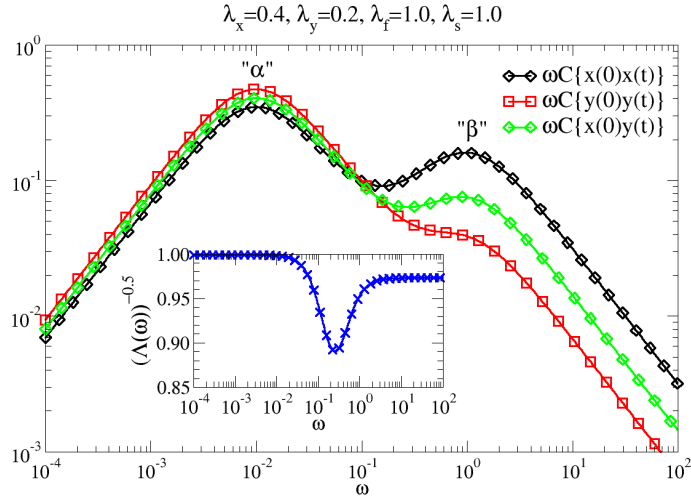


Figure 4.5: A possible scenario of thermodynamic fluctuations, Equations 4.19 and 4.21. Since  $\gamma_f = \gamma_s = 1$ , the fast and one slow Debye process would give perfect correlation between  $x$  and  $y$  if they were alone. Since  $\gamma_x = 0.4$  is different from  $\gamma_y = 0.2$  the slope of the fluctuations are different for the fast and the slow Debye relaxation. The consequence of this is that in the “mixing region” of the two internal Debye relaxations  $(\Lambda_{XY}(\omega))^{-1/2}$  have a dip.

### 4.1.3 Rethinking the classical Prigogine-Defay ratio

As discussed earlier, the classic Prigogine-Defay ratio  $\Pi_{pT}^{\text{classic}}$ , Equation 4.1 page 29, is not strictly well-defined. However, let us assume that the values of the (static) response functions of the liquid correspond to the  $\omega \rightarrow 0$  limits and the (static) response functions of the glass<sup>6</sup> correspond to the  $\omega \rightarrow \infty$  limits of the frequency-dependent response functions of the equilibrium liquid at  $T_g$ . This would make  $\Pi_{pT}^{\text{classic}}$  equal to the well-defined linear Prigogine-Defay ratio  $\Pi_{pT}^{\text{linear}}$ , Equation 4.2 (page 30). Then, the inverse square root of the classical Prigogine-Defay ratio reflects a correlation coefficient,

$$(\Pi_{pT}^{\text{classic}})^{-1/2} \simeq R_{VS}(\text{of slow fluctuations}), \quad (4.29)$$

and

$$(\Pi_{VT}^{\text{classic}})^{-1/2} \simeq R_{pS}(\text{of slow fluctuations}), \quad (4.30)$$

or, as argued in the previous section,

$$(\Pi_{VT}^{\text{classic}})^{-1/2} \simeq R_{WU}. \quad (4.31)$$

This is a novel interpretation of  $\Pi^{\text{classic}}$ . Also, the  $W$ - $U$  slope can be estimated from the same data as

$$\gamma_{WU} \simeq \gamma_{VT}^{\text{classic}} = \sqrt{\frac{-\Delta K_T}{T \Delta c_V}}. \quad (4.32)$$

<sup>6</sup>Since a glass can be prepared in numerous ways, there is no unique value of the glass response functions. How this affects the approximation is a matter of future studies.

Equations 4.31 and 4.32 are verified for the Kob-Andersen binary Lennard-Jones liquid, Figure 4.6. This is a useful approximation, since values of the classical ratio are available in literature. A revisit of  $\Pi^{\text{classic}}$  enable us to investigate the conjecture of Section 2.2 (page 17). This conjecture speculates that van der Waals bonded liquids are strongly correlating liquids.

First, we investigate  $\Pi^{\text{classic}}$  of some model systems. The Kob-Andersen binary Lennard-Jones liquid have a ratio close to unity, Figure 4.6. Clarke [1979] reported  $\Pi_{pT}^{\text{classic}} \simeq 1$  for the (single component) Lennard-Jones liquid and Cape and Woodcock [1980] argue that the ratio must be unity in soft-sphere systems (consistent with Chapter 3). These authors noted that this was not in agreement with the wisdom of that time – that Prigogine-Defay ratios typically had values between 2 and 4 [Gupta and Moynihan, 1976]. However, in the light of strongly correlating liquids, a ratio close to unity is expected in all of these model systems. Thus, simulations support the claim that strongly correlating viscous liquids have  $\Pi_{pT}^{\text{classic}} \simeq 1$ .

Now, let us reexamine the classical Prigogine-Defay found experimentally, Table 4.1. Some  $\Pi_{pT}^{\text{classic}}$  are in fact close to unity. In Table 4.1 liquids are listed with decreasing  $\Pi_{pT}^{\text{classic}}$ . Note that the lowest values are for the van der Waals bonded liquids – exactly as it is claimed by the conjecture. As an example, Takahara et al. [1999] have measured  $\Pi_{pT}^{\text{classic}} = 1.20 \pm 0.05$  corresponding to a correlation coefficient of  $(\Pi_{pT}^{\text{classic}})^{-\frac{1}{2}} = 0.92 \pm 0.02$  for OTP (67%) mixed with OPP (33%). This supports the conjecture that van der Waals bonded liquids are strongly correlating liquids. Unfortunately this the only value of a van der Waals bonded molecular liquid. However, the van der Waals bonded polymers also have  $\Pi_{pT}^{\text{classic}}$  close unity.

Another supporting observation relates to n-propanol, with one OH-group, and glycerol with three OH-groups. Both molecules are approximately the same size having a backbone of three carbon atoms. With an increasing number of OH-groups  $\Pi_{pT}^{\text{classic}}$  is expected to increase since correlation is destroyed by hydrogen bonds. Indeed  $\Pi_{pT}^{\text{classical}}(\text{glycerol}) = 9.4$  is significantly larger than  $\Pi_{pT}^{\text{classical}}(\text{n-propanol}) = 1.9$ .

There is at present time little interest for  $\Pi_{pT}^{\text{classical}}$ . Presumably, this is due to the negative result of Gupta and Moynihan [1976]. However, the presented rethinking and revisit of the Prigogine-Defay ratio, demonstrates that interesting information can be extracted from the ratio. As we shall see in the following section the slope  $\gamma_{WU}$  is an important quantity for strongly correlating viscous liquid. This is accessible though equation 4.32. Experimentalists are therefore urged to regain interest in the Prigogine-Defay ratio – both the classical and the more well-defined frequency-dependent version.

## 4.2 Hidden scale invariance

In this section, in Paper VII and in Paper XIII it is argued that strongly correlating liquids have a hidden scale invariance: State points with the same

$$\Gamma \equiv \rho^{\gamma_s} / T \quad (4.33)$$

have (approximately) the same dynamics and structure (in scaled units). The scaling exponent  $\gamma_s$  is the same as  $\gamma_{WU}$ , however, since  $\gamma_{WU}$  is slightly state

#### 4. STRONGLY CORRELATING VISCOUS LIQUIDS

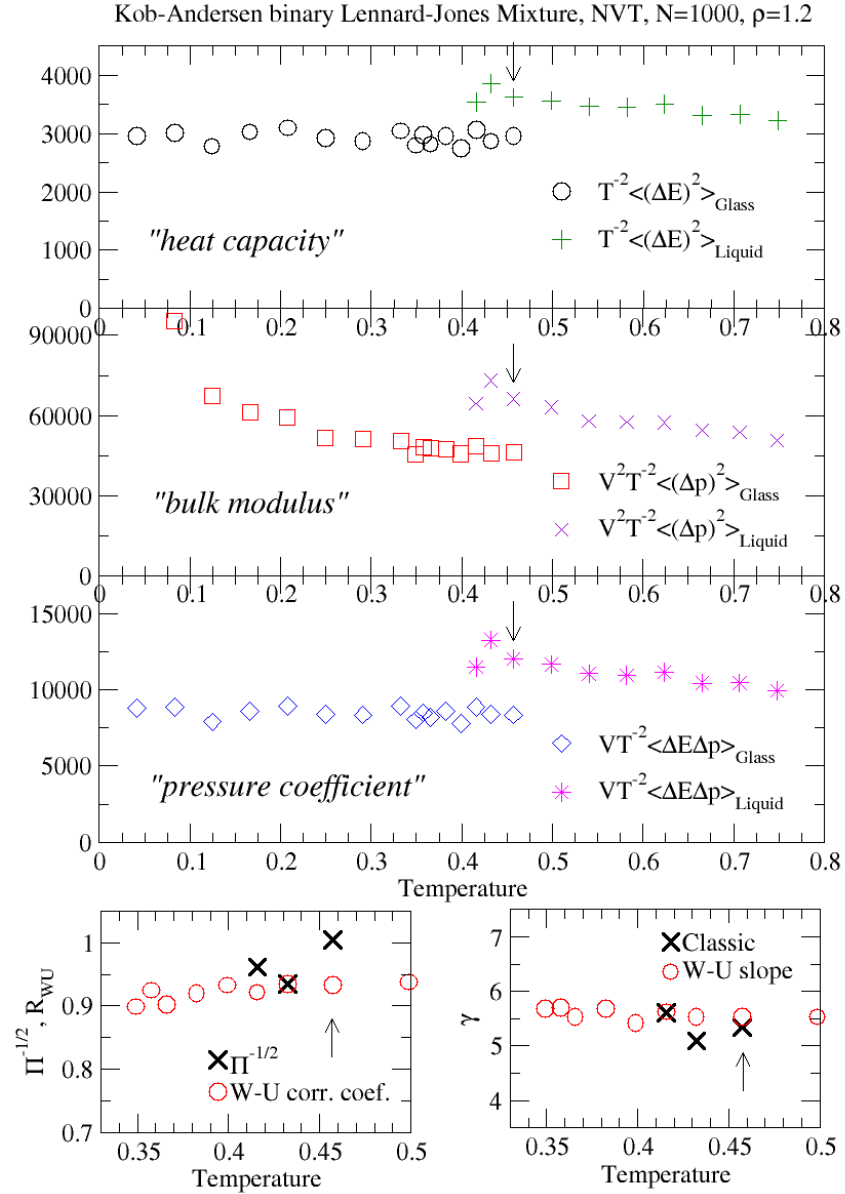


Figure 4.6: Classical approach to obtain the Prigogine-Defay ratio and slope of the Kob-Andersen binary Lennard-Jones liquid. A glass at temperature  $T$  was made from a quenched structure (cooled instantaneous to  $T = 0$ ) taken from a configuration in equilibrium at  $T = 0.457$  (marked by a arrow). After 500 ps of equilibration, 1000 ps of  $E$  and  $p$  fluctuations were used to calculate  $\langle(\Delta E)^2\rangle_{\text{Glass}}$ ,  $\langle(\Delta p)^2\rangle_{\text{Glass}}$  and  $\langle\Delta E\Delta p\rangle_{\text{Glass}}$ .  $E$  and  $p$  showed no drift (annealing of the glass) compared to the size of the fluctuations. Within statistical error, the classical approach reproduces the  $W$ - $U$  correlation coefficient and  $W$ - $U$  slope of instantaneously fluctuations.

point dependent, scaling can only be approximate. Nevertheless, as shown below in simulations,  $\gamma_s$  chosen to be the average  $\gamma_{WU}$  of the state points of interest gives good scaling.

The theoretical explanation for hidden scale invariance is as follows: First, recall the work of Hoover and coworkers [Hoover et al., 1970, Hoover and Ross, 1971, Hoover et al., 1971] showing the simplicity of soft-sphere liquids where particles interact pairwise via an inverse power-law,

$$U^{\text{pow}}(r_{ij}) = \varepsilon \left( \frac{r_{ij}}{\sigma} \right)^{-n}. \quad (4.34)$$

In such a systems, physical quantities expressed in units of the characteristic velocity

$$v_s \equiv \sqrt{\frac{k_B T}{m}} \quad (4.35)$$

and the characteristic length

$$l_s \equiv \left( \frac{N}{V} \right)^{-1/3} \quad (4.36)$$

are the same for state points with the same  $\Gamma$  (Equation 4.33) [Hoover et al., 1971]. Thus, in scaled units state points with the same  $\Gamma$  are identical, having the same structure and dynamics. Therefore, soft-sphere liquids are said to have scale invariance.

Now, consider a strongly correlating liquid and recall the origin of the  $W$ - $U$  correlation given in Chapter 3. The pair energy can be written as

$$U(r_{ij}) = U^{\text{pow}}(r_{ij}) + br_{ij} + U^{\text{diff}}(r_{ij}) \quad (4.37)$$

where  $U^{\text{pow}}$  is referred to as the effective inverse power-law. Let us consider state points with the same  $\Gamma$  in the  $NVT$  ensemble. The trajectory at these state points (and in general) is determined by the visited energy surface  $U(\vec{R}(t)) = \sum_{\text{pairs}} U(r_{ij})$ , where  $\vec{R}(t)$  is the  $3N$  coordinate vector of the system,  $\vec{R}(t) = \{\vec{r}_1(t), \vec{r}_2(t), \dots, \vec{r}_N(t)\}$ . As argued in Chapter 3,  $\sum_{\text{pairs}} [br + U^{\text{diff}}(r_{ij})]$  does not fluctuate (at constant volume) and

$$U(\vec{R}(t)) \simeq U^{\text{pow}}(\vec{R}(t)) + U_0(V). \quad (4.38)$$

$U_0(V)$  is only a function of volume  $V$ . Assume that  $U^{\text{pow}}$  is not too state point dependent ( $\gamma_{WU}$  nearly constant). Then, strongly correlating liquids inherit the scale invariance of structure and dynamics of soft sphere liquids. It should be noted that strongly correlating liquids are not as simple soft-sphere liquids. For soft-sphere liquids the pressure can be related directly to the energy,  $\frac{3}{n}(pV/(Nk_B T) - 1) = (E/(Nk_B T) - \frac{3}{2})$  or  $\frac{3}{n}W = U$  (Appendix A.1); this is not the case for strongly correlating liquids as discussed in Chapter 2 (Figure 2.2 page 15). Nevertheless, scale invariance is found in simulations and experiments as discussed in the following.

Figure 4.7 show the  $W$ - $U$  correlation coefficient  $R_{WU}$  and the  $W$ - $U$  slope  $\gamma_{WU}$  of the Lewis-Wahnström OTP model for a range of state points. Since  $R_{WU}$  is close to unity ( $0.90 < R_{WU} < 0.93$ ) this is a strongly correlating liquid. Moreover, the slope  $\gamma_{WU}$  only varies 7% about 7.9 for the investigated

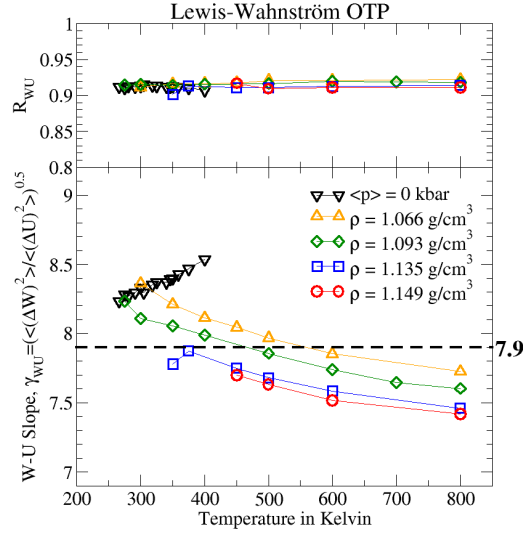


Figure 4.7:  $W$ - $U$  correlation coefficient (top) and  $W$ - $U$  slope (bottom) of the Lewis-Wahnström OTP model. The correlation is strong  $0.90 < R_{WU} < 0.93$  and the slope varies only slightly around  $7.9 (\pm 7\%)$ .

state points. For comparison,  $\gamma_{WU}$  is about 5.9 with the same spread for the asymmetric dumbbell model (Paper VII and Paper XIII). Therefore, we should expect the Lewis-Wahnström OTP liquid to have scale invariance of structure and dynamics with  $\gamma_s = 7.9$ .

Figure 4.8 shows the radial distribution function of three selected state points. Two of the state points have same  $\Gamma$  and the same radial distribution function as a function of scaled length  $r' = r(N/V)^{1/3}$  (although the scaling is not perfect, see legend of Figure 4.8). Thus structure can be scaled as expected. The third of the shown state points has the same temperature as the first, and the same pressure as the second. However, for this third state point, scaling of structure fails since  $\Gamma$  is different from that of the two other state points. In Paper XIII it is shown that structure of the asymmetric dumbbell model can be scale as well (simulations conducted by Thomas B. Schröder).

Scaling of dynamics can be investigated through the diffusion constant. Figure 4.9 shows scaling of the reduced (using  $v_s$  and  $l_s$  defined in Equations 4.35 and 4.36) diffusion constant  $D^* = D(N/V)^{1/3}(k_B T/m)^{-1/2}$  [Rosenfeld, 1999, Coslovich and Roland, 2008] of the Lewis-Wahnström OTP model. Scaling of the the asymmetric dumbbell model is shown in Paper VII and Paper XIII. A equivalent scaling of dynamics has been reported experimentally [Tölle, 2001, Dreyfus et al., 2003, Alba-Simionesco et al., 2004, Casalini and Roland, 2004, Roland et al., 2005]. For van der Waals bonded liquids, the structural relaxation is only a function of  $\rho^{\gamma_s}/T$ :

$$\tau_\alpha = g(\rho^{\gamma_s}/T). \quad (4.39)$$

However, before this study, it was not known that  $\gamma_s \simeq \gamma_{WU}$  could be calculated from two response function (see previous section). At first, it was believed that

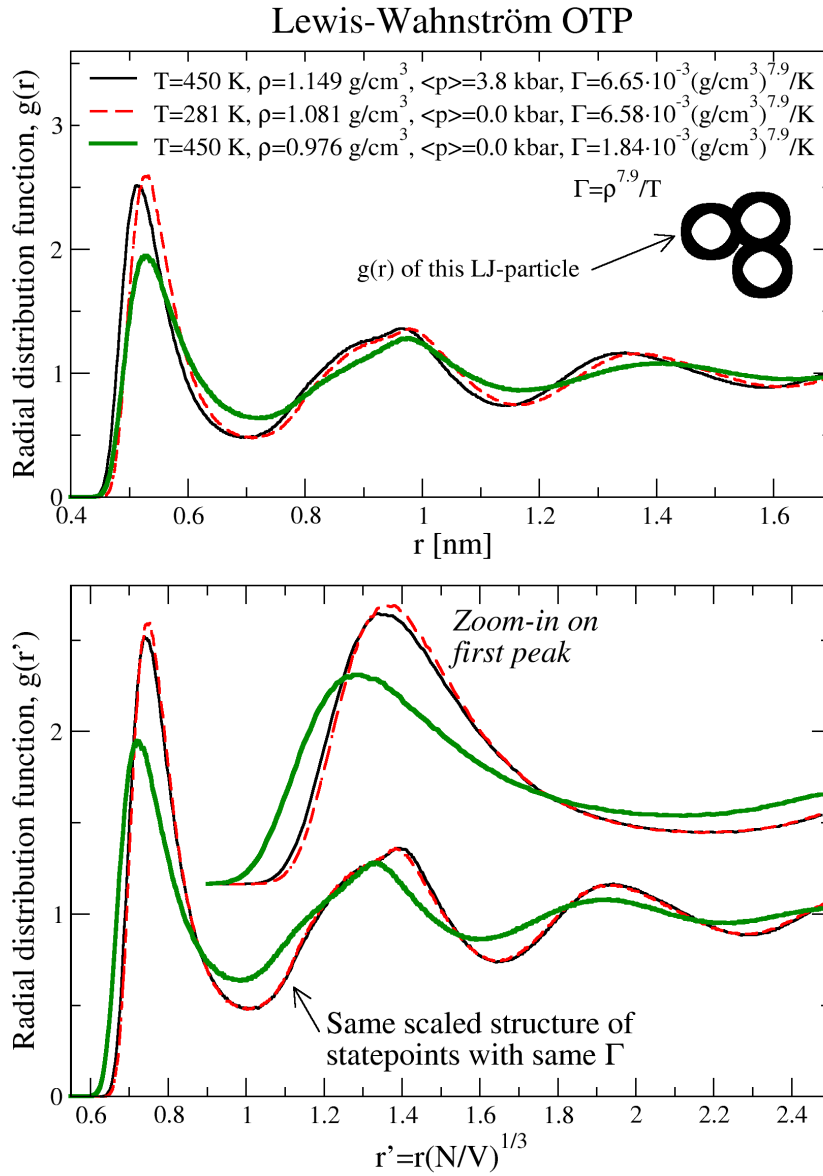


Figure 4.8: The radial distribution function  $g(r)$  (top) at three state points of the Lewis-Wahnström OTP model. The definition of  $g(r)$  is given in 3.2. In the bottom panel it is shown that when  $\Gamma$  is the same, then the structure is also the same in scaled units. The inset show a zoom-in on the first peak. Note that the scaling is not perfect. This is presumably a consequence of rigid bonds connecting Lennard-Jones particles not scaling.

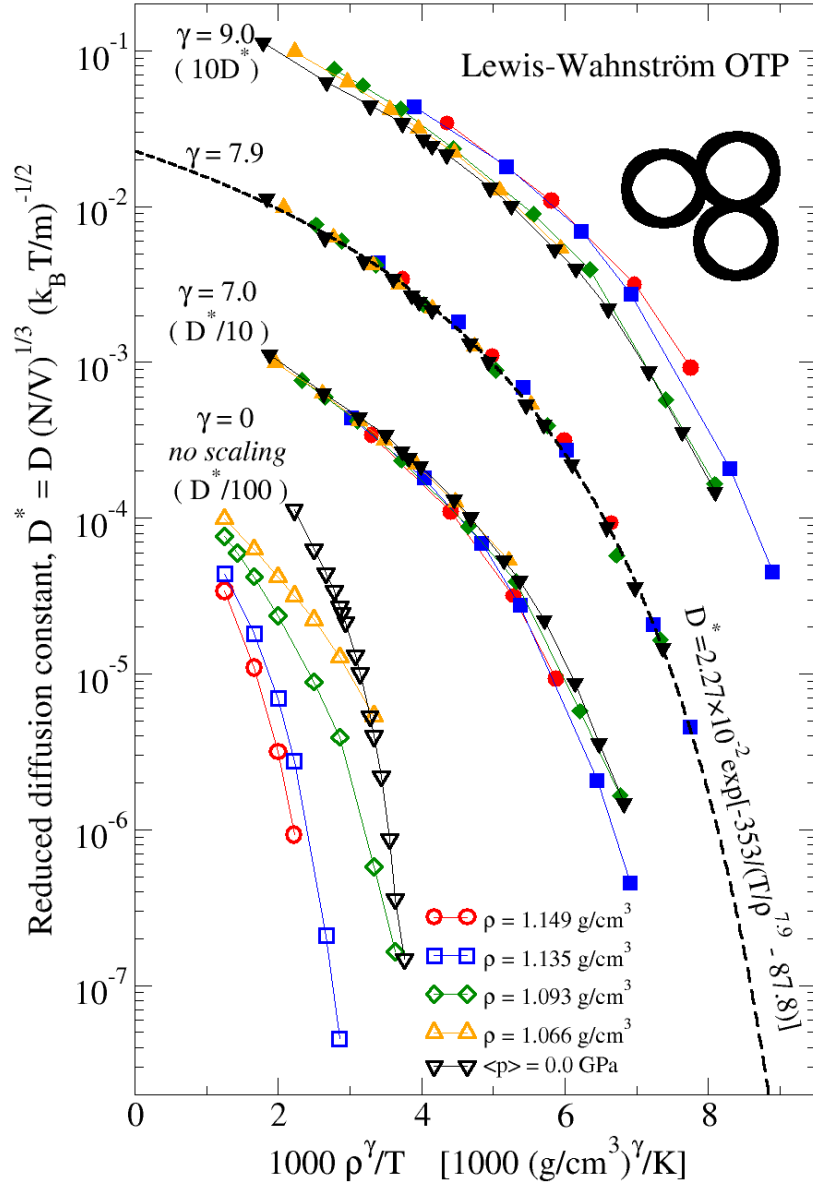


Figure 4.9: Scaling of the reduced diffusion constant of the Lewis-Wahnström OTP model. Note that the scaling works when the scaling exponent equals the  $W$ - $U$  slope  $\gamma_s = 7.9 \simeq \gamma_{WU}$ , see Figure 4.7.

the scaling worked in general for viscous liquids. However, it is now realized that density scaling does not work for hydrogen bonded and covalent bonded liquids [Ferrer et al., 1998, Hensel-Bielowka et al., 2002, Roland et al., 2006, Le Grand et al., 2007, Roland et al., 2008]. This agrees with the theoretical framework given here, since these liquids are not strongly correlating. In Paper VII the failure of scaling for non-strongly correlating liquids is demonstrated by adding charges to the asymmetric dumbbell model (simulations conducted by Thomas B Schröder).

Finally, it should be noted that Coslovich and Roland [2009] in a recent paper also confirms the theoretical framework given here in simulations of viscous binary Lennard-Jones mixtures.



## Chapter 5

# Volume-energy fluctuations of phospholipid membranes

This chapter reports a simulation study of phospholipid membranes. Some membranes have strong correlations between the slow volume and energy fluctuations. The origin of the correlation can be traced to the van der Waals bonded core (the fatty acyl chains). Thus, strong correlations of membranes have the same origin as those of strongly correlating simple liquids (Chapter 3). This demonstrates that complex systems, exemplified by phospholipid membranes, can have properties similar to that of strongly correlating simple liquids (discussed in previous chapters).

Results of this chapter can also be found in Paper V and Paper X.

### 5.1 Motivation

A phospholipid is an amphiphilic molecule, thus having a hydrophilic and hydrophobic part. In water, phospholipids can self-organize into membranes, where hydrophobic acyl-chains are shielded from water as sketched in Figure 5.1.

Figure 5.2 shows two snapshots of all-atom molecular dynamics simulations of such two phospholipid membranes (details are given later). The acyl-chains are disordered in the membrane to the left, and are ordered in the membrane to the right. Two such phases are also found in nature, and are referred to as the (disordered)  $L_\alpha$  and the (ordered)  $L_\beta$  phase [Zhang et al., 1995, Nielsen et al., 2007].

The  $L_\beta \rightarrow L_\alpha$  phase transition is seen as a dramatic increase of response functions. Figure 5.3 shows excess (caused by the transition) compressibility  $\Delta\kappa_T(T)$ , and excess heat capacity  $\Delta c_p(T)$  over the  $L_\alpha \rightarrow L_\beta$  phase transition of a di-myristoyl-phosphatidyl-choline (DMPC) membrane. As seen in the figure,  $\Delta\kappa_T(T)$  and  $\Delta c_p(T)$  can be superimposed,

$$\Delta\kappa_T(T) = \frac{(\gamma_{HV})^2 T}{\bar{V}(T)} \Delta c_p(T). \quad (5.1)$$

Such a proportionality is a natural consequence if

$$\Delta V_i = \gamma_{HV} \Delta H_i \quad (5.2)$$

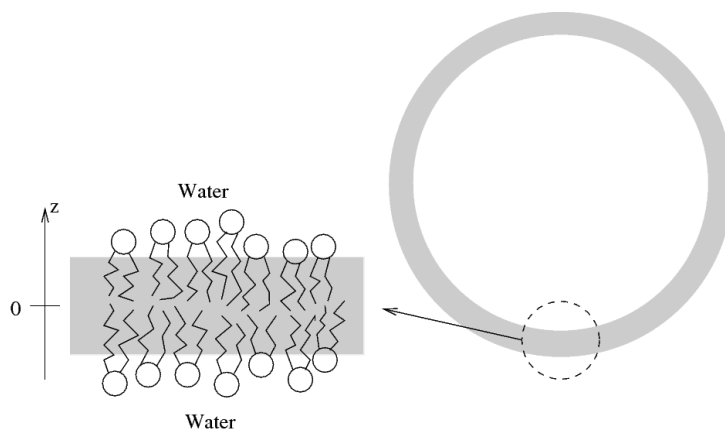


Figure 5.1: Sketch of phospholipids forming a spherical vesicle. Extruded phospholipids form such vesicles. Often phospholipid vesicles serve as a simple model of a biological cell [Alberts et al., 2002]. Hydrophilic head-groups of lipids are drawn as circles, and hydrophobic fatty acyl-chains as lines. The gray area represents a hydrophobic region, separating “in-site” water from “out-site” water. The figure is copied from my master thesis [Pedersen, 2005]. Figure 5.2 show a snap-shot from a simulation of such a phospholipid membrane.

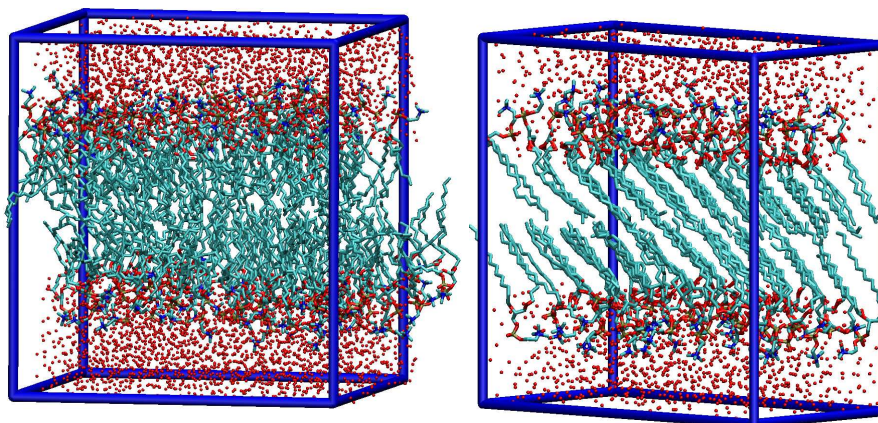


Figure 5.2: Snap-shot from all-atom simulations of two fully-hydrated DMPC membranes. The membrane on the left is in a disordered phase whereas the membrane on the right is in an ordered phase. Hydrogen is not shown for clarity, but is included in the actual simulations. The blue wire-frame indicates the periodic boundary box. This figure can also be found in Paper X.

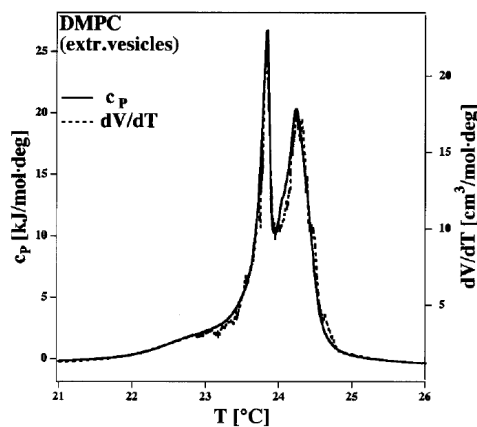


Figure 5.3: Heat capacity and volume expansion coefficient of extruded DMPC vesicles (Figure 5.1) at the phase transition. The two curves can be superimposed, Equation 5.1. This figure is copied from Ebel et al. [2001].

for available micro-states [Ebel et al., 2001, Heimburg, 1998]. Note that this equation is similar to Equations 4.5-4.8 (page 32). This suggests a connection between strongly correlating liquids and membranes. As a part of my master thesis, I simulated phospholipid membranes [Pedersen, 2005, Pedersen et al., 2007] and it was therefore natural to revisit the simulated membranes to investigate the above proportionality.

Before moving on, the importance for biological membranes (where the major constituents are phospholipids), of a proportionality should be mentioned. The conventional wisdom is that nerve signals are carried as electrical signals as formulated in the theory by Hodgkin and Huxley [1952]. However, recently Heimburg and Jackson [2005] showed that biological membranes may carry solitonic sound waves, and subsequently speculated that nerve signals may be carried this way [Heimburg and Jackson, 2007]. An element in the Heimburg-Jackson theory of nerve signals is that enthalpy and volume are correlated in their slow thermal fluctuations.

## 5.2 A simulation study

The following study includes simulations of seven membranes (simulations conducted by Günther H. Peters). The following abbreviations are used:

**DMPC-f:** fully hydrated di-myristoyl-phosphatidyl-choline membrane in fluid phase. The initial configuration is taken from Reference [Pedersen et al., 2007].

**DMPC-g:** fully hydrated di-myristoyl-phosphatidyl-cholin membrane in ordered phase. The initial configuration is built from a configuration in Reference [Venable et al., 2000].

**DPPC-f:** fully hydrated di-palmitoyl-phosphatidyl-choline membrane in fluid phase. The initial configuration is taken from Reference [Somme et al., 2007].

**DPPC-g:** fully hydrated di-palmitoyl-phosphatidyl-choline membrane ordered phase. The initial configuration is built from a configuration in Reference [Venable et al., 2000].

**DPPG:** fully hydrated di-palmitoyl-phosphatidyl-glycerol membrane in fluid phase with calcium counter ions. Initial configuration is taken from Reference [Pedersen et al., 2006].

**DPPE:** fully hydrated di-myristoyl-phosphatidyl-serine membrane in fluid phase with calcium counter ions. Initial configuration is taken from Reference [Pedersen et al., 2006].

**DMPSH:** fully hydrated and protonated di-myristoyl-phosphatidyl-serine membrane in fluid phase. Initial configuration is taken from Reference [Pedersen et al., 2006].

Some simulation details are given in Table 5.1, however, for more details the reader is referred to Paper X and References [Pedersen, 2005, Pedersen et al., 2006, 2007].

It is not feasible to have the simulation temperature at the phase transition and test Equation 5.1 directly since relaxation time of the membrane simply exceeds the simulation time. However, as demonstrated in the following, volume-energy correlations are also present in the fluid and the ordered phase (where “quasi” equilibrium states can be reached).

Figure 5.4 shows a time-series of slow thermal fluctuation of volume and energy (of the DMPC-f membrane). Volume and energy are strongly correlated with a correlation coefficient of

$$R_{\bar{V}\bar{U}} = \frac{\langle \Delta \bar{U} \Delta \bar{V} \rangle}{\sqrt{\langle (\Delta \bar{U})^2 \rangle \langle (\Delta \bar{V})^2 \rangle}} = 0.77, \quad (5.3)$$

where the bar indicates an averaging window of  $\frac{1}{2}$  ns. This averages out fast fluctuations. If no averaging is done, the correlation coefficient is reduced to  $R_{VU} = 0.35$ . As seen in the following, this is partially due to fast fluctuations of the water (recall that water is not a strongly correlating liquid as shown in Figure 2.3 page 16).

Table 5.1 list  $R_{\bar{V}\bar{U}}$  and Figure 5.5 shows the time-dependent correlation coefficient,

$$R_{VU}(t) = \frac{\langle \Delta U(0) \Delta V(t) \rangle}{\sqrt{\langle \Delta U(0) \Delta U(t) \rangle \langle \Delta V(0) \Delta V(t) \rangle}}, \quad (5.4)$$

of the seven membranes. Five of the membranes, DMPC-f, DPPC-f, DPPC-g, DMPG and DMPSH, have strong correlations in the slow volume-energy fluctuations with  $R_{\bar{V}\bar{U}} \geq 0.75$  and  $R_{VU}(t > 0.5 \text{ ns}) > 0.75$ . The origin of the correlation can be traced to the hydrophobic (van der Waals bonded) core of the membrane. This can be quantified as done in the following:

First, the atoms are divided into three groups, using the following subscripts:

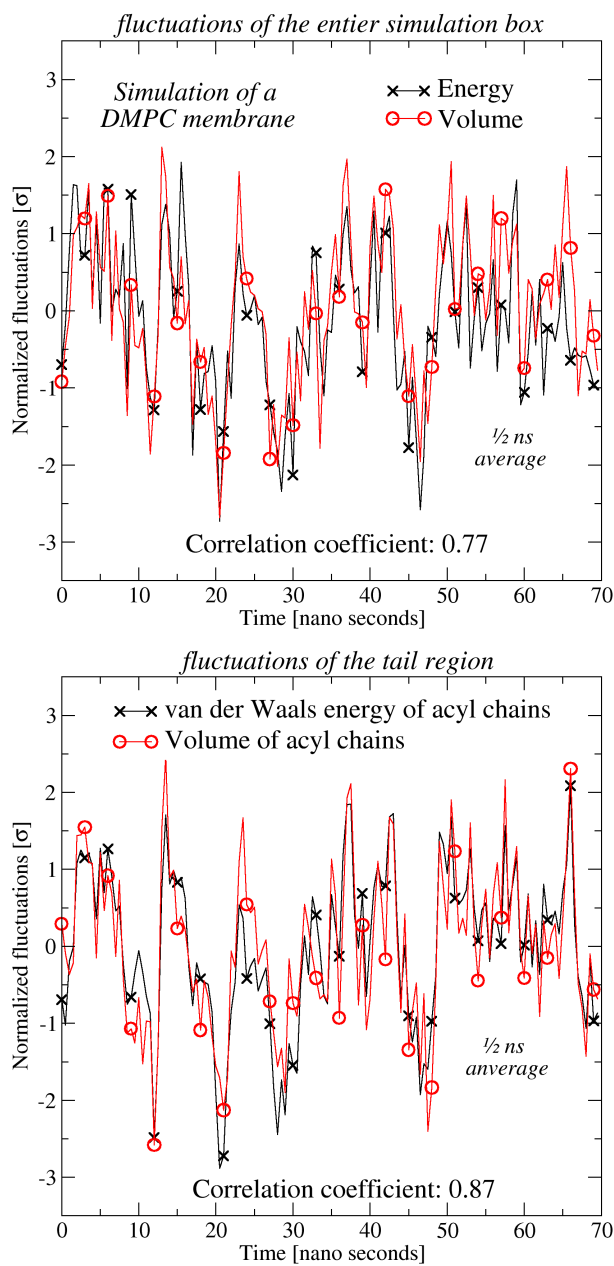


Figure 5.4: The top panel shows normalized fluctuation of volume,  $\Delta\bar{V}(t)/\sigma_{\bar{V}}$ , and energy,  $\Delta\bar{U}(t)/\sigma_{\bar{U}}$  of the DMPC-f membrane. The bar indicates a  $\frac{1}{2}$  ns averaging window.  $\Delta\bar{V}$  and  $\Delta\bar{U}$  are strongly correlated with a correlation coefficient of  $R_{\bar{V},\bar{U}} = 0.77$ . The bottom panel shows normalized fluctuations of the Voronoi volume of the tail region,  $\Delta\bar{V}_t(t)/\sigma_{\bar{V}_t}$ , and Lennard-Jones energy of tail-region,  $\Delta U_t^{\text{LJ}}(t)/\sigma_{U_t^{\text{LJ}}}$ . The correlation coefficient is  $R_{\bar{V}_t, U_t^{\text{LJ}}} = 0.87$ . These figures can also be found in Paper X.

Table 5.1: Overview of simulation details and results

	$t_{sim}$ [ns]	$t_{prod}$ [ns]	$N_{lip}$	$T$ [K]	$\frac{N_{wat}}{N_{lip}}$	$R_{\bar{V}\bar{U}}$	$\gamma_{\bar{V}\bar{U}}$	$R_{\bar{U}\bar{U}_t}$
DMPC-f	151	121	128	330	33	0.77	6.7	0.82
DMPC-g	65	36	64	286	33	0.47	4.3	0.31
DPPC-f	180	124	72	325	29	0.87	7.1	0.89
DPPC-g	78	48	64	304	33	0.75	4.6	0.71
DMPG	149	49	128	330	33	0.82	5.9	0.80
DMPS	139	49	128	340	36	0.59	5.3	0.64
DMPSH	136	35	128	340	37	0.78	9.2	0.84

$t_{sim}$ : Total simulation time in nanoseconds;  $t_{prod}$ : Length of production run in nanoseconds (only membranes in quasi-equilibrium, i.e., with no detectable drift in the area per molecule, were included in the data analysis);  $N_{lip}$ : Number of lipid molecules;  $T$ : Temperature in Kelvin;  $N_{wat}/N_{lip}$ : Number of water molecules per lipid molecule;  $R_{\bar{V}\bar{U}}$ : Energy-Volume correlation coefficient;  $\gamma_{\bar{V}\bar{U}}$ : Energy-volume scaling factor in  $\text{\AA}^3 \text{ mol/kcal}$ ;  $R_{\bar{U}\bar{U}_t}$ : Energy-“Energy of acyl groups” correlation coefficient.

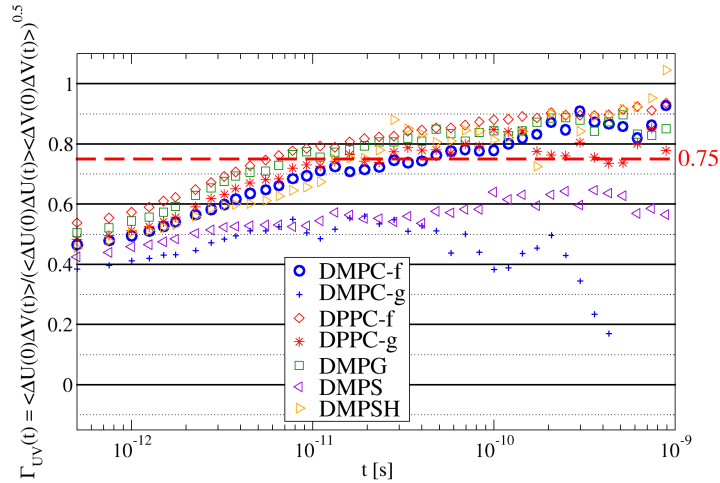


Figure 5.5: Time-dependent correlation function of volume-energy (Equation 5.3). DMPC-f, DPPC-f, DPPC-g, DMPG and DMPSH membranes have strong volume-energy correlation in the slow fluctuations,  $R_{VU}(t > 0.5 \text{ ns}) > 0.75$ . This figure can also be found in Paper X.

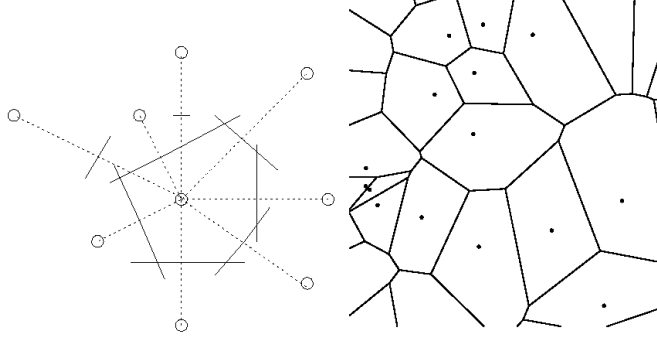


Figure 5.6: The principle of construction of Voronoi polyhedrons [Voronoi, 1908]. For simplicity, a construction in two dimensions is shown. On the left, circles represent particles. The Voronoi polygon of the center atom is drawn with full lines. Points included in this volume have the center particles as the closest particle. The Voronoi polygons of a collection of particles are shown on the right. Note that the Voronoi polygons tile space. The total area is therefore the sum of Voronoi areas. In three dimensions polygons become polyhedra and the total volume is the sum of the Voronoi volumes. This figure is copied from my master thesis [Pedersen, 2005].

**t** for “tail”. Atoms of  $-\text{CH}_2-$  and  $-\text{CH}_3$  groups of the fatty acyl-chains. Shown as light blue atoms in Figure 5.2.

**h** for “head”. The remainder of the lipid atoms. As seen in Figure 5.2, these atoms are located in the interface and are in close contact with water.

**w** for “water”. Shown as red spheres in Figure 5.2. Note that water is excluded from the core of the membrane.

The volume of a given region is calculated by summing Voronoi volumes [Voronoi, 1908] of the heavy atoms (excluding hydrogen);  $V = V_t + V_h + V_w$ . The principle of construction Voronoi polyhedrons are given in Figure 5.6. Also, energy can be split up in three contributions;  $U = U_t + U_h + U_w$  where

$$U_x = U_x^{\text{intra}} + \frac{1}{2} \sum_{i=x} \sum_{j=\text{all}} U_{ij}^{\text{coul}} + \frac{1}{2} \sum_{i=x} \sum_{j=\text{all}} U_{ij}^{\text{LJ}}, \quad (5.5)$$

with  $x$  either tail, head, or water.  $U_x^{\text{intra}}$  is the energy of intra-molecular bonds,

$$U_{ij}^{\text{coul}} = q_i q_j / (4\pi\epsilon_0 r_{ij}), \quad (5.6)$$

is the Coulomb energy of two pairs, and

$$U_{ij}^{\text{LJ}} = 4\epsilon_{ij}((\sigma_{ij}/r_{ij})^{12} - (\sigma_{ij}/r_{ij})^6) \quad (5.7)$$

is the Lennard-Jones pair energy.

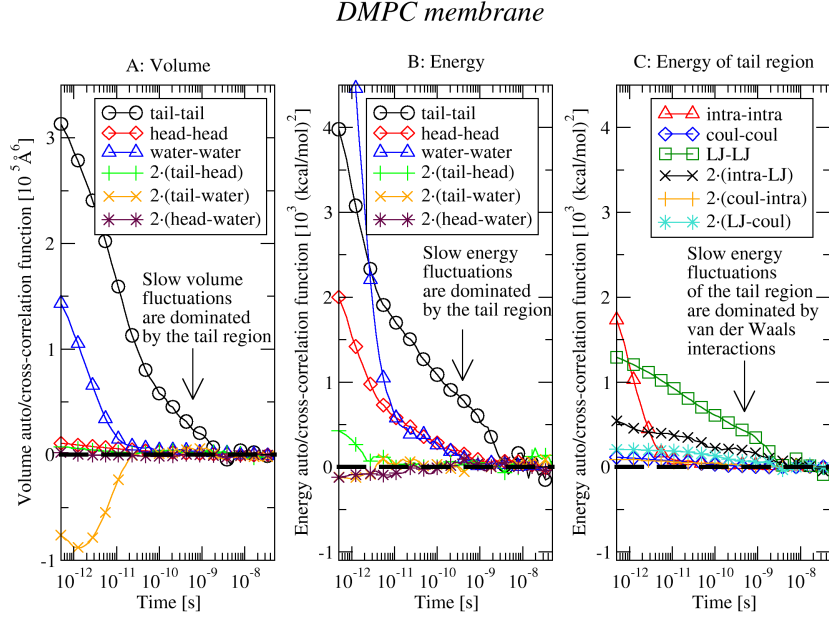


Figure 5.7: Terms of equation 5.8 for the DMPC-f membrane. See text after this equation for more details. This figures can also be found in Paper X.

The auto-correlation functions of volume and energy (Equation 5.4), can now be split into six terms:

$$\begin{aligned}
 \langle \Delta \mathcal{V}(0) \Delta \mathcal{V}(t) \rangle &= \langle \Delta \mathcal{V}_t(0) \Delta \mathcal{V}_t(t) \rangle \\
 &+ \langle \Delta \mathcal{V}_h(0) \Delta \mathcal{V}_h(t) \rangle \\
 &+ \langle \Delta \mathcal{V}_w(0) \Delta \mathcal{V}_w(t) \rangle \\
 &+ 2 \langle \Delta \mathcal{V}_t(0) \Delta \mathcal{V}_h(t) \rangle \\
 &+ 2 \langle \Delta \mathcal{V}_t(0) \Delta \mathcal{V}_w(t) \rangle \\
 &+ 2 \langle \Delta \mathcal{V}_h(0) \Delta \mathcal{V}_w(t) \rangle,
 \end{aligned} \tag{5.8}$$

with  $\mathcal{V}$  either  $E$  or  $V$ . Figure 5.7 shows the six terms of volume and energy respectively (DMPC-f membrane). The only non-vanishing term of slow ( $t \gtrsim \frac{1}{2}$  ns) fluctuations of volume is  $\langle \Delta \mathcal{V}_t(0) \Delta \mathcal{V}_t(t) \rangle$ , showing that slow fluctuations of volume are dominated by the tail-region, as expected. Also slow energy fluctuations are dominated by the tail region. However, it should be noted that the contributions to fluctuations from water and head-region are significant. As discussed later, this weakens the (total) volume-energy correlation of a given membrane, explaining that some membranes have stronger  $\bar{U}$ - $\bar{V}$  correlation than others.

Also, Figure 5.7 shows an additional splitting of the tail-energy in inter-molecular bond energy, Lennard-Jones (or van der Waals) energy and Coulomb energy (similar to that of Equation 5.8). As expected, slow fluctuations are

dominated by the Lennard-Jones contribution.

The analysis suggests that the origin of the (total) volume-energy correlation can be traced to the van der Waals bonded tail region:

$$\Delta\bar{V}_t \propto \Delta\bar{U}_t^{LJ}, \quad (5.9)$$

where

$$U_t^{LJ} = \frac{1}{2} \sum_{i=\text{tails}} \sum_{j=\text{all}} U_{ij}^{LJ} \quad (5.10)$$

Remember, however, that we throw away some non-vanishing energy terms. Nevertheless,  $R_{\bar{V}_t, \bar{U}_t^{LJ}} = 0.87$  is larger than  $R_{\bar{V}\bar{U}} = 0.78$  strengthens this conclusion. As mentioned earlier, the correlation is weakened by the tail-energy not completely dominating slow fluctuations. To investigate this further,  $R_{\bar{U}\bar{U}_t}$  can be used as a measure of how much of the energy fluctuations comes from the tail region. Comparing  $R_{\bar{V}\bar{U}}$  with  $R_{\bar{U}\bar{U}_t}$ , as done in Table 5.1, shows that large values of  $R_{\bar{U}\bar{U}_t}$  is followed by  $R_{\bar{V}\bar{U}}$  and vice versa.

Finally, a volume-energy scaling factor (or slope) can be calculated from the simulations as

$$\gamma_{\bar{V}\bar{U}} = \sqrt{\frac{\langle(\Delta\bar{V})^2\rangle}{\langle(\Delta\bar{U})^2\rangle}} \quad (5.11)$$

The experimental value (Equations 5.1) is found to be  $(7.788 \pm 0.110) \times 10^{-4}$  mL/J =  $(5.418 \pm 0.077)$  Å·mol/kcal for DMPC membranes [Ebel et al., 2001]. This roughly agrees with the values calculated in simulations, as seen in Table 5.1. One caveat is that  $\gamma_{\bar{V}\bar{U}}$  of the fluid membranes is approximately two times that of the ordered membrane. From the scaling given by Equation 5.1 it is expected that they should be the same. More work is needed to clarify this.

Finally it should be noted that energy and volume generally do not have significant correlation with membrane area or the chain order parameter defined as [Tieleman and Berendsen, 1996]

$$S_{CD} = \left| \left\langle \frac{3}{2} \cos^2(\theta_{CD}) - \frac{1}{2} \right\rangle_{ch} \right| \quad (5.12)$$

where  $\theta_{CD}$  is the angle between the membrane normal and the C-H bond of a given methylene group, and  $\langle \dots \rangle_{ch}$  denotes an average over all methylene groups in all chains<sup>1</sup>. Correlation coefficients are listed in Table 5.2.

To conclude this chapter: It has been demonstrated that a complex system can have properties similar to that of a strongly correlating liquid. Note, the importance of *separation of time-scales*. What happens is that a strongly correlating element of the system dominates fluctuations on some time-scale. In membranes, slow fluctuations of energy and volume are dominated by van der Waals bonded core. Qualitatively this corresponds to what is shown in Figure 4.1 (page 35).

<sup>1</sup>Note that usually a static  $S_{CD}$  is reported, and for individual methyl-groups. Here a dynamic version is defined.

Table 5.2: Correlation coefficients

	$R_{\bar{V}\bar{U}\bar{V}}$	$\gamma_{\bar{V}\bar{U}}$	$R_{\bar{U}\bar{U}_t}$	$R_{\bar{U}\bar{A}}$	$R_{\bar{V}\bar{A}}$	$R_{\bar{A}\bar{S}_{CD}}$	$R_{\bar{U}\bar{S}_{CD}}$	$R_{\bar{V}\bar{S}_{CD}}$
DMPC-f	0.77	6.7	0.82	0.50	0.57	-0.75	-0.49	-0.54
DMPC-g	0.47	4.3	0.31	0.02	0.05	-0.64	0.12	0.14
DPPC-f	0.87	7.1	0.89	-0.29	-0.36	0.00	-0.61	-0.71
DPPC-g	0.75	4.6	0.71	-0.16	0.12	-0.67	0.09	-0.07
DMPG	0.82	5.9	0.80	0.41	0.40	-0.76	0.01	0.08
DMPS	0.59	5.3	0.64	0.30	0.28	-0.71	0.04	0.20
DMPSH	0.78	9.2	0.84	0.43	0.51	-0.50	0.05	0.14

$R_{\bar{V}\bar{U}}$ : Energy-Volume correlation coefficient;  $\gamma_{\bar{V}\bar{U}}$ : Energy-volume scaling factor in  $\text{\AA}^3 \text{ mol/kcal}$ ;  $R_{\bar{U}\bar{U}_t}$ : Energy-“Energy of acyl groups” correlation coefficient;  $R_{\bar{U}\bar{A}}$ : Energy-Area correlation coefficient;  $R_{\bar{V}\bar{A}}$ : Volume-Area correlation coefficient;  $R_{\bar{A}\bar{S}_{CD}}$ : Area-“chain order-parameter” correlation coefficient;  $R_{\bar{U}\bar{S}_{CD}}$ : Energy-“chain order-parameter” correlation coefficient;  $R_{\bar{V}\bar{S}_{CD}}$ : Volume-“chain order-parameter” correlation coefficient.

## Chapter 6

# Stability of a binary mixture

Long-time simulations are important for computational studies of viscous liquids. It is now possible to investigate low temperature liquids with several decade of relaxation times. Nowadays, simulation times of 0.1 ms are within reach for a system of 1000 particles, Figure 1.7 (page 8). As shown below, however, some of the standard models used in the computational community of viscous liquids crystallize on these time-scale. Paper II reports crystallization of the Wahnström binary Lennard-Jones liquid [Wahnström, 1991]. Toxværd et al. [2007] report crystallization<sup>1</sup> of the Kob-Andersen Lennard-Jones liquid [Kob and Andersen, 1994, 1995a,b]. Also the ortho-terphenyl model suggested by Lewis and Wahnström [1994] crystallizes as seen in Figure 6.1.

The following sections gives a detailed investigation of the stability of the Wahnström binary Lennard-Jones liquid. A paper including these results are at the moment in the process of being written in collaboration with Peter Harrowell (School of Chemistry, University of Sydney). The stability of the Kob-Andersen Lennard-Jones liquid is only briefly discussed. More details can be found in Paper XI. Crystallization mechanism of the Lewis-Wahnström o-terphenyl model have not been investigated in details. However, the structure of the formed crystal is shown in Figure 6.1.

### 6.1 The Wahnström binary Lennard-Jones mixture

This mixture was originally suggested by Wahnström [1991] to study viscous liquid dynamics. It consists of two kinds of Lennard-Jones particles, labeled A and B, where the diameter of B particles is  $\sigma_{BB}/\sigma_{AA} = 1.2$  that of the A particles. The composition is equimolar,  $N_A = N_B$ . See section 1.2.1, Paper II and Figure 1.4 for more details.

---

<sup>1</sup>In the final days before handing in the thesis, it was realized that the force parameters for simulating the Kob-Andersen liquid was implemented wrong. The Lennard-Jones binding energies simulated were  $\epsilon'_{\alpha\beta} = \sigma_{\alpha\beta}\epsilon_{\alpha\beta}$  where  $\sigma_{\alpha\beta}$  and  $\epsilon_{\alpha\beta}$  are the original Kob-Andersen parameters. Thus, the binding energies of BB pairs,  $\epsilon'_{BB} = \sigma_{BB}\epsilon_{BB} = 0.88 \cdot 0.5 = 0.44$ , and AB,  $\epsilon'_{AB} = \sigma_{AB}\epsilon_{AB} = 0.8 \cdot 1.5 = 1.2$ , pairs were reduced. A reduction of the AB binding energy will increase composition fluctuations, and thereby making the system more prone to crystallization. It is therefore still an open question on what time scale the Kob-Andersen mixture will crystallize.

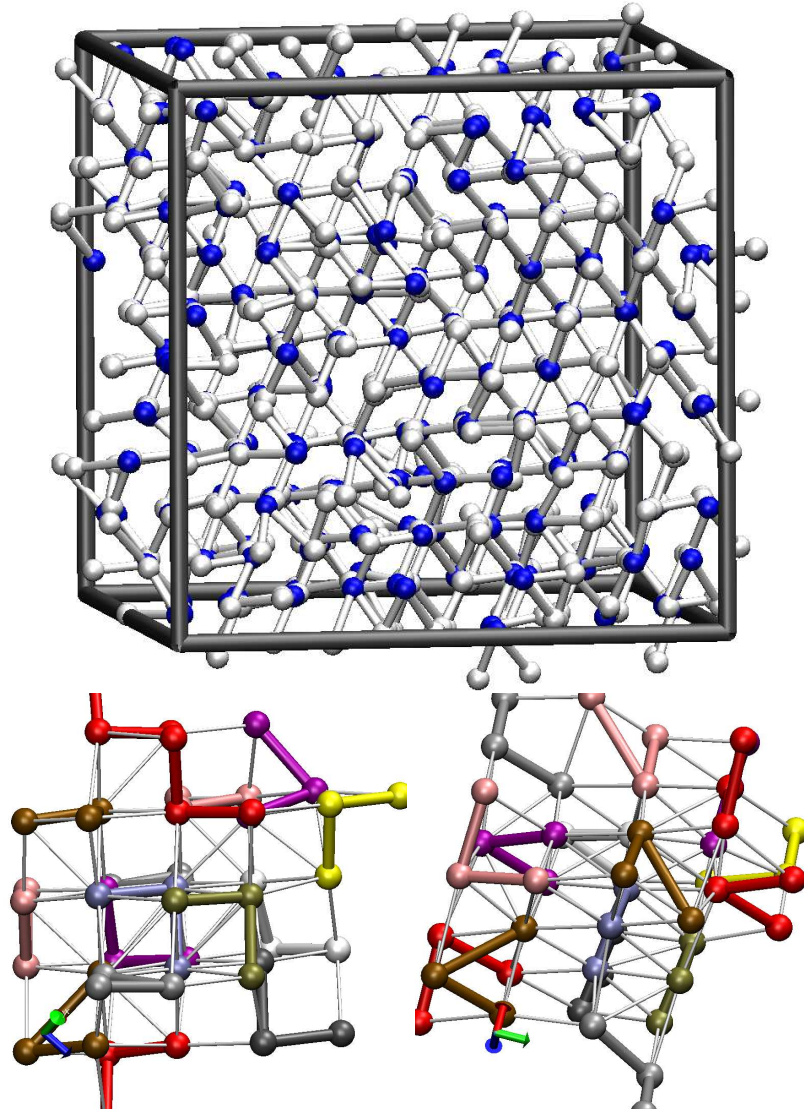


Figure 6.1: Crystal formed spontaneously from the melt of the Lewis-Wahnström o-terphenyl model [Lewis and Wahnström, 1994] (three Lennard-Jones particles placed in an isosceles triangle with an angle of  $75^\circ$ , see Figure 1.5). As seen in the upper part of the figure, all of the 324 molecules are arranged in an ordered structure (center particles are colored blue). A part of crystal viewed from two angles is shown in the lower part of the figure. The gray lines are guidelines for the eye.

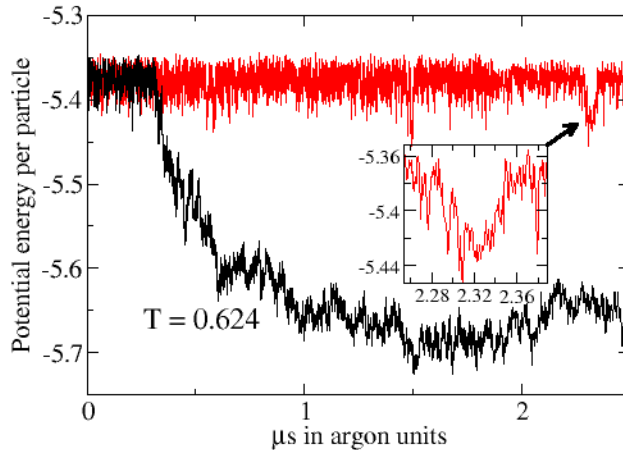


Figure 6.2: Time series of energy in two (selected) simulations of the Wahnström binary Lennard-Jones liquid at  $T = 0.624$ . The dramatic drop in energy is a consequence of crystallization. The structural relaxation time of the liquid is of the order of a nanosecond.

## 6.2 The crystal

The Wahnström binary Lennard-Jones mixture can spontaneously form a crystal from the melt. This is seen as a dramatic drop in energy as shown in Figure 6.2. An inspection of particle positions, as done in Figure 6.3, reveals a large crystal with  $\text{MgZn}_2$  structure<sup>2</sup> (and defects). The  $\text{MgZn}_2$  structure is not built into the model, and was not, to the authors' knowledge, predicted. Table 6.2 lists the energy and volume of some close-packed crystal structures. This analysis indeed suggests that the  $\text{MgZn}_2$  structure is the true ground state.

The crystal is one of the so-called Laves phases that comprise the largest group of inter-metallic phases [Stein et al., 2004, 2005]. Understanding crystallization of a Laves structure is therefore important in its own right.  $\text{MgZn}_2$  has optimal packing of hard-spheres when the size ratio is  $\sigma_B/\sigma_A = \sqrt{3}/2 \simeq 1.22$ , close to the size ratio  $\sigma_B/\sigma_A = 1.2$  of the Wahnström mixture. This close-packing feature of  $\text{MgZn}_2$  makes crystallization related to packing.

The crystal formed is remarkable on two accounts: i) The AB liquid is off-composition compared to the  $\text{A}_2\text{B}$  crystal. Hence, a significant composition fluctuation must accompany crystal formation. ii) The crystal structure is quite complex, having a unit cell of 12 particles. In the light of this, it is remarkable that the crystal forms at all. This is naturally also the reason why crystallization of this model has not been reported before.

<sup>2</sup> $\text{MgZn}_2$  structure (C14) have a trigonal, hexagonal unit-cell with  $\text{P6}_3/\text{mm}$  symmetry with six A particles on the  $h$  position, two A particles on the  $a$  position and four B particles on the  $f$  position, where  $h$ ,  $a$  and  $f$  are the Wyckoff letters [Pearson, 1972, page 657].

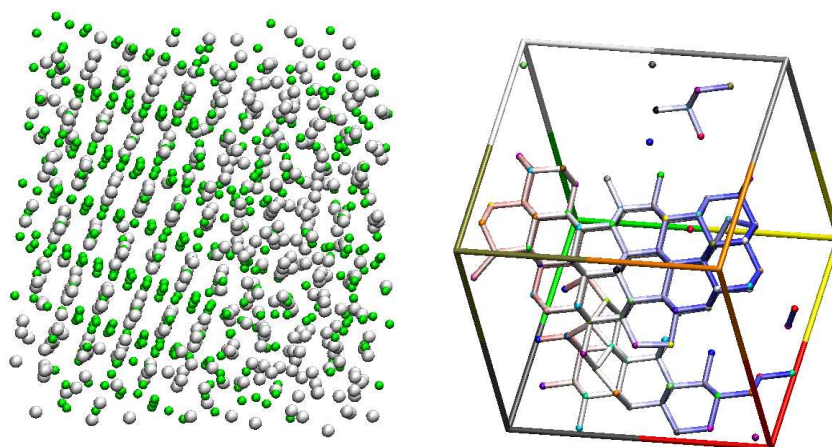


Figure 6.3: Crystal formed spontaneously from the melt of the Wahnström binary Lennard-Jones liquid. B particles are colored white (light gray) and A particles are colored green (dark gray). The coordinates are the quenched structure taken at the last point of the black curve in Figure 6.2. The left hand side of the figure shows the positions of all the particles. The crystal fills roughly half of the box. The remainder of the box is filled with a B-rich liquid since the total composition is AB whereas that of the crystal is  $A_2B$ . The structure of the crystal is  $MgZn_2$  is shown in Figure 6.5. The right hand side of the figure shows the formed crystal represented as Frank-Kasper bonds (see Figure 6.7). Configurations are rotated for maximum clarity.

### 6.3 Mechanism of crystallization

First, define the first shell as particles within the first peak of the radial distribution function  $g(r)$  using the first minimum as cutoff, as shown in Figure 6.4. Then, define local composition as  $\chi_B^{fs} = Z_B/Z$ , where  $Z_B$  is the number of B particles, and  $Z$  is the total number of particles in the first shell.

Let us take a closer look at the  $MgZn_2$  crystal structure shown in Figure 6.5. The smaller A particles have distorted icosahedral first shells with a local composition of  $\chi_B^{fs} = 0.5$ . Figure 6.6 shows the distribution of first shell arrangements of the liquids. Note that the most common is of the same kind as the crystal. Coslovich and Pastore [2007] also noted the high abundant of this arrangement. So the local arrangement around A particles is roughly the same in liquid and crystal. On the other hand, crystalline B particles have a first shell that is very different from the liquid. The crystalline B particles have a high coordination of 16 particles and a local composition of  $\chi_B^{fs} = 0.25$ . This first shell arrangement is unusual in the liquid (Figure 6.6). Thus, the structural fluctuation leading to crystallization implies a significant change of the first shells of B particles. Note that the composition fluctuation needed is only seen around B particles.

To undertake a study of the rearrangement associated with crystallization, we need to characterize local structure. I have extended the common neighbor

Table 6.1: Energy and packing of Wahnström crystals.

Crystal	$V/N$ [ $\sigma_{AA}^3$ ]	$U/N$ [ $\epsilon_{AA}$ ]	First shell compositions
Pure A			
FCC <sup>†</sup> (A)	0.93663	-7.26293	A-12-0
A <sub>2</sub> B mixture			
(Laves) MgCu <sub>2</sub>	1.13351	-7.28515	A-6-6 and B-12-4
(Laves) MgZn <sub>2</sub>	1.13193	-7.29910	A-6-6 and B-12-4
(Laves) MgNi <sub>2</sub>	1.13275	-7.29179	A-6-6 and B-12-4
MoPt <sub>2</sub>	1.16593	-6.83436	A-9-5 and B-10-4
MoSi <sub>2</sub>	1.16594	-6.83429	A-9-5 and B-10-4
AB mixture			
Liquid	1.33341	-5.37896	Figure 6.6
CuAu	1.26577	-6.84244	A-3-8 and B-8-6
FeB	1.26449	-6.84971	A-4-8 and B-8-6
$\frac{3}{4}$ MgZn <sub>2</sub> (A <sub>2</sub> B) + $\frac{1}{4}$ FCC(B)	1.23842	-7.20207	A-6-6, 75% B-12-4 and 25% B-0-12
$\frac{3}{4}$ CuZr <sub>2</sub> (AB <sub>2</sub> ) + $\frac{1}{4}$ FCC(A)	1.26088	-6.91559	75% A-4-8, 25% A-12-0 and B-4-9
$\frac{1}{2}$ Cu(A) + $\frac{1}{2}$ FCC(B)	1.24726	-7.08695	A-12-0 and B-0-12
AB <sub>2</sub> mixture			
CuZr <sub>2</sub>	1.36896	-6.79967	A-4-8 and B-4-9
$\frac{3}{8}$ MgZn <sub>2</sub> (A <sub>2</sub> B) + $\frac{5}{8}$ FCC(B)	1.39815	-7.05651	A-6-6, 37.5% B-12-4 and 62.5% B-4-9
Pure B			
FCC(B)*	1.55788	-6.91096	B-0-12

Energies and volumes were calculated on the basis of  $NpT$  simulations of pure crystals: FCC<sup>†</sup> of A particles, MgCu<sub>2</sub>, MgZn<sub>2</sub>, MgNi<sub>2</sub>, MoPt<sub>2</sub>, MoSi<sub>2</sub>, CuAu, FeB, AB<sub>2</sub>, CuZr<sub>2</sub> and a FCC of B particles. Crystals were simulated at  $T = 0.624$  and  $p = 4.7$  (same as liquid).

All these crystals are stable at this temperature and pressure (in the simulated time interval of some nanoseconds). The candidates for structures were selected from Reference [Kummerfeld et al., 2008] and private correspondence with Toby S. Hudson. Note that at all the investigated compositions, MgZn<sub>2</sub> in combination with a pure FCC crystal (A or B) has lowest energy and volume, thus this is a good candidate for the true ground state of the system (of-course, Gibbs free energies are the appropriate quantities to compare). <sup>†</sup>FCC: face center cubic or Cu. \*The energy of the FCC crystals (pure A and pure B) are different although  $\epsilon_{AA} = \epsilon_{BB}$ . The difference is an artifact of the truncation of the potential.

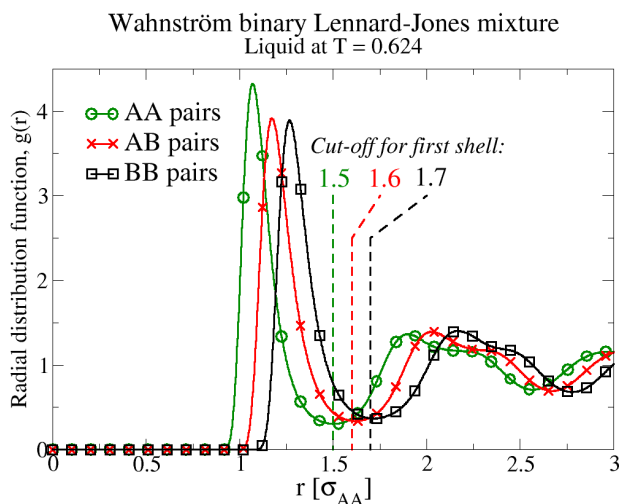


Figure 6.4: Radial distribution function  $g(r)$  of the liquid at  $T = 0.624$ . The first minimum is used as cut-off for when defining particles of the first shell.

analysis suggested by Honeycutt and Andersen [1986] so it takes the two kinds of particles into account: Consider two neighbor particles and their common neighbors as shown in Figure 6.7. Six integers is used to characterize such a (two colored) bi-pyramid graph,  $Rn_A n_B s_{AA} s_{AB} s_{BB}$ . Where  $R$  is the type of neighbor pair so  $R = 1$  for AA,  $R = 2$  for AB and  $R = 3$  for BB,  $n_A$  and  $n_B$  is the number of A and B common neighbors respectively, and  $s_{AA}$ ,  $s_{AB}$  and  $s_{BB}$  is the number of AA, AB and BB contacts amongst common neighbors. We will refer to such a local arrangement as a bond. For later use, the stability of a common neighbor arrangement is measured as the time interval of the first and the last observation. This is referred to as the lifetime. Note that in this time interval a particle can leave the arrangement as long as it returns at a later time.

The crystal is made up of just five types of bonds. Three AA bonds, 114023, 123122 and 132221, an AB bond, 232140, and a BB bond, 360600. In the following the 360600 BB bond will play an important role in the analysis. As seen in Figure 6.5 the  $\text{MgZn}_2$  crystal structure can be viewed as a hexagonal diamond structure of B particles connected by such bonds. Hence, each B has four 360600-bonds pointing to the corners of a tetrahedron as seen on Figure 6.5. The 360600-tetrahedron is the basic element of all the Laves structures. The difference between the structures is how the 360300-bonds are connected. Such an analysis was the subject of the celebrated work by Frank and Kasper [1958, 1959]. In acknowledgment of their work we will henceforth refer to 360600 bonds as Frank-Kasper bonds. A Frank-Kasper bond is shown in Figure 6.7.

Let us return to the liquid (at  $T = 0.624$ ). Figure 6.8 shows the average lifetime and abundance of bonds in the liquid. The most common and stable AA and AB bonds are the ones with five bonded common neighbors,  $n_A + n_B =$

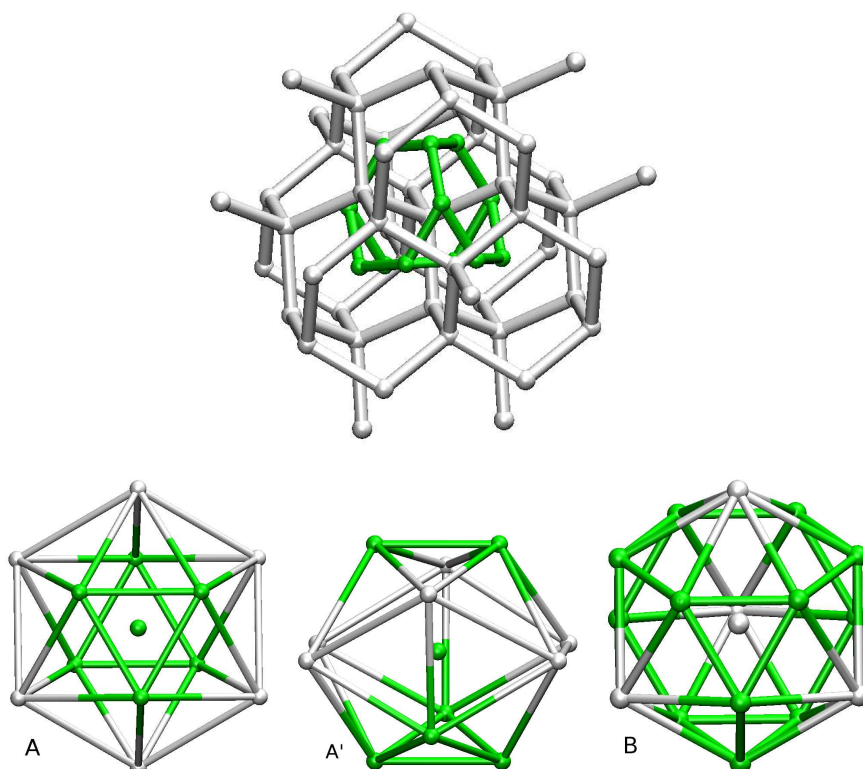


Figure 6.5: The  $\text{MgZn}_2$  crystal structure of the Wahnström binary Lennard-Jones liquid. The white B particles are arranged in a hexagonal diamond structure, connected with Frank-Kasper bonds (see Figure 6.7). Only first shell green A particles of the central B are shown for clarity. Particles have three kind of first shells shown in the lower part of the figure.

$s_{AA} + s_{AB} + s_{BB} = 5$ . These are of the same kind as the bonds of the crystal. This is consistent with the previous conclusion, that the local environment of A particles is similar to that of the crystal. These bonds are not only abundant; they are also the most stable. This is an interesting observation. Some crystal structure is built into the liquid, and, moreover gives stability to the liquid. We will return to this when discussing long-lived structural fluctuations of the liquid, Subsection 6.4.

One BB bond is different from the others, and that is the Frank-Kasper bond (Figure 6.7). As seen in Figure 6.8, there are only about six of these bonds, but when they are there, they are long-lived. The low abundance makes Frank-Kasper bond ideal for investigating the onset of crystallization. Figure 6.9 shows the number of Frank-Kasper bond at the crystallization event and at some points where the liquid experience transient dips in energy. At the onset of crystallization there is, as expected, a large increase of Frank-Kasper bonds. However, also in the meta-stable liquid, large transient clusters of Frank-Kasper bonds appear. If two B particles, having one or more Franks-Kasper bonds, shares A particles, that are a part of these bonds, we will consider the two B

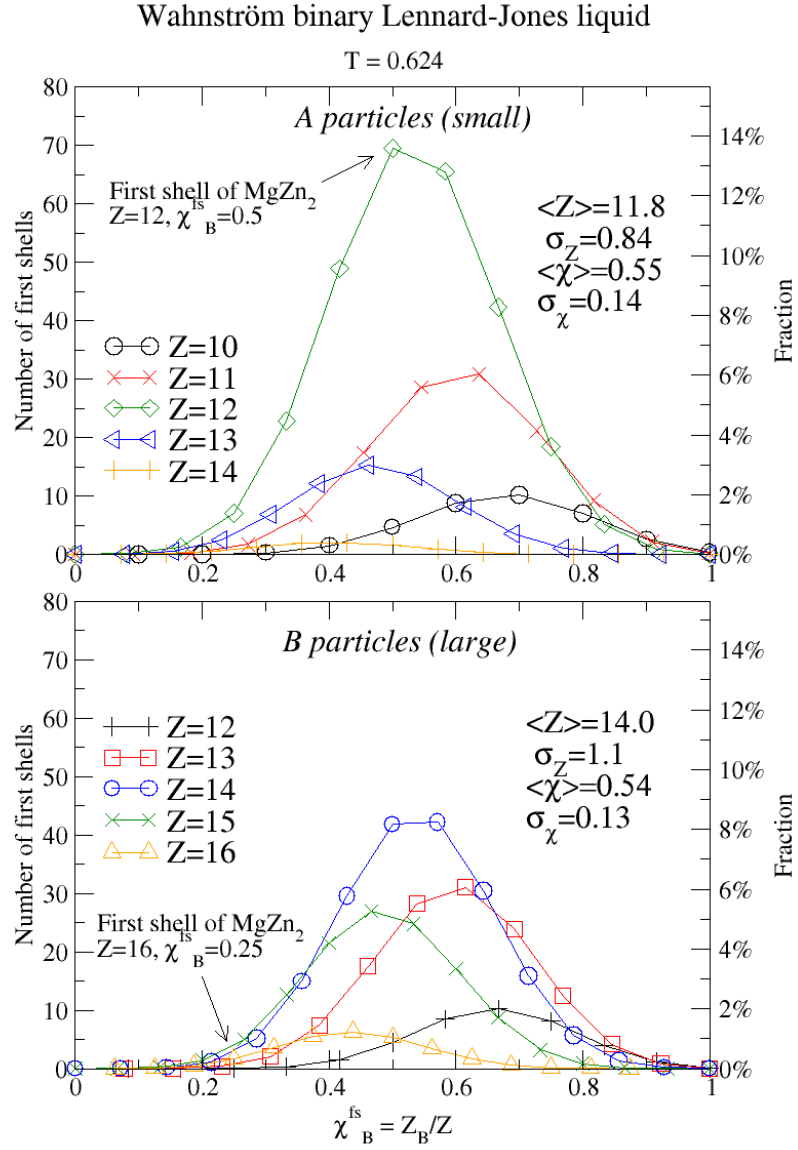


Figure 6.6: Distribution of first shells of Wahnström binary Lennard-Jones liquid. Note that the most frequent first shell of A particles are the same as in the crystal, whereas this is not the case for the B particles.

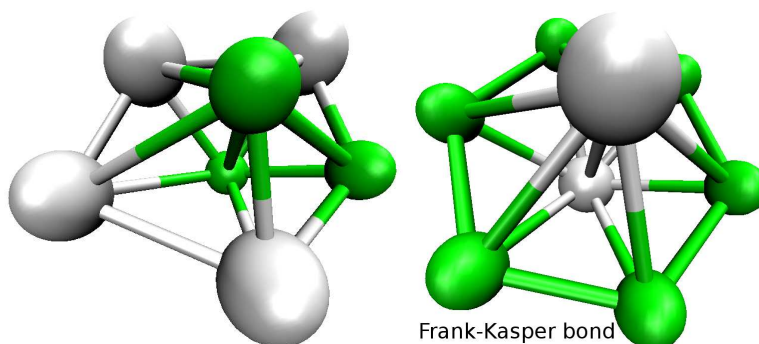


Figure 6.7: Neighboring particles and their common neighbors characterize by six integers,  $Rn_A n_B s_{AA} s_{AB} s_{BB}$ . The arrangement on the left is a AA pair,  $R = 1$ , with one common A,  $n_A = 1$  and four common B particles,  $n_B = 4$ . The common neighbors have none AA contacts,  $s_{AA} = 0$ , two AB contacts,  $s_{AB} = 2$ , and three BB contacts  $s_{BB} = 3$ . Thus, this is a 114023-bond. The arrangement on the right is a 360600-bond referred to as a Frank-Kasper bond.

particles to be in the same cluster. Figure 6.10 shows the largest clusters at the transient dips in energy shown in Figure 6.9. Some of the clusters are dense and similar to the crystal, whereas others are open structure not similar to the crystal. Clearly such an open structure hinders crystallization. Also, clusters tend to have (broken) pentagons of Frank-Kasper bonds. This is not a feature of the crystal, and will hinder crystallization. In other words, besides forming the Frank-Kasper bonds, the bonds also have to be arranged in the right way.

The onset of crystallization must be accompanied by a significant composition fluctuation. Figure 6.11 shows the average local composition of B particles with zero to four Frank-Kasper bonds. Note that a substantial part of the composition fluctuation takes place at the formation of just a single Frank-Kasper bond.

We now have a rather complete picture of the crystallization of the Wahnström binary Lennard-Jones liquid. Let us summarize. Local crystalline-like structure of A particles are built into the liquid as distorted icosahedra with  $\chi_B^{\text{fs}} = 0.5$ . However, B particles are not in a local crystalline-like environment. The formation of a Frank-Kasper bond, accompanied by a composition fluctuation sets the onset of a possible crystallization event. A cluster will form, and if it is compact it can continue to grow and eventually lead to non-reversible growth.

## 6.4 Long-lived structural fluctuations stabilizing the liquid

This section addresses the question: What are the long-lived structural fluctuations stabilizing the metastable liquid? We will address this question by an investigation of the 10% of particles with the longest lifetimes of first shells. Figure 6.12 shows a cluster analysis of these particles. Stable particles are not randomly distributed, but are formed in extended clusters. With decreasing tem-

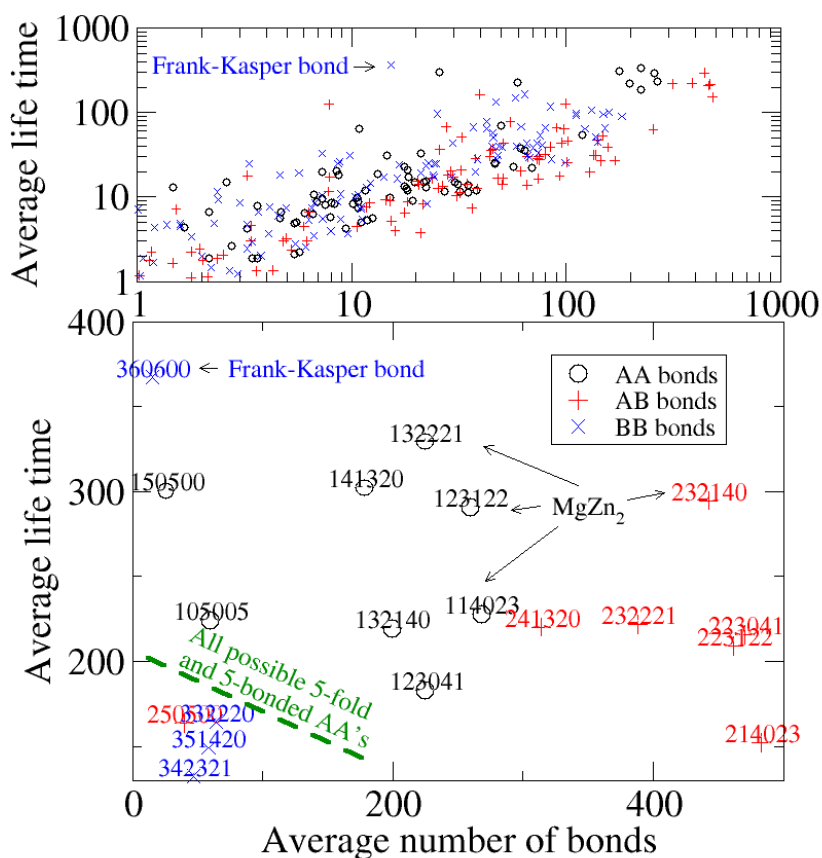


Figure 6.8: Scatter plot of frequency and average lifetime of common neighbor bi-pyramids. See text for more details.

perature the characteristic size of these cluster grow. This is an example of the well-known heterogeneity of viscous liquids [Ediger, 2000].

Figure 6.13 show the first shell distribution of stable particles, relative to the overall distribution. It is possible to identify a particular stable local arrangement: the distorted icosahedra ( $Z = 12$ ) first shells of A particles. Coslovich and Pastore [2007] also note that the frequency of this arrangement grows with decreasing temperature and associated this with the non-Arrhenius growth of the structural relaxation time (although they use a Voronoi construction to investigate neighboring particles, see Figure 5.6). The most stable first shells of B particles are less distinguishable. Nevertheless, a high coordination number tends to give stability. Note that the more crystalline-like the arrangement is, the more stability it gives. In other words, the crystal and the liquid use the same kind of arrangement to get stability. Stability is gained both for the liquid and crystal by the same kind of local packing. This is an interesting observation. Often, properties of the liquid are regarded as disconnected from

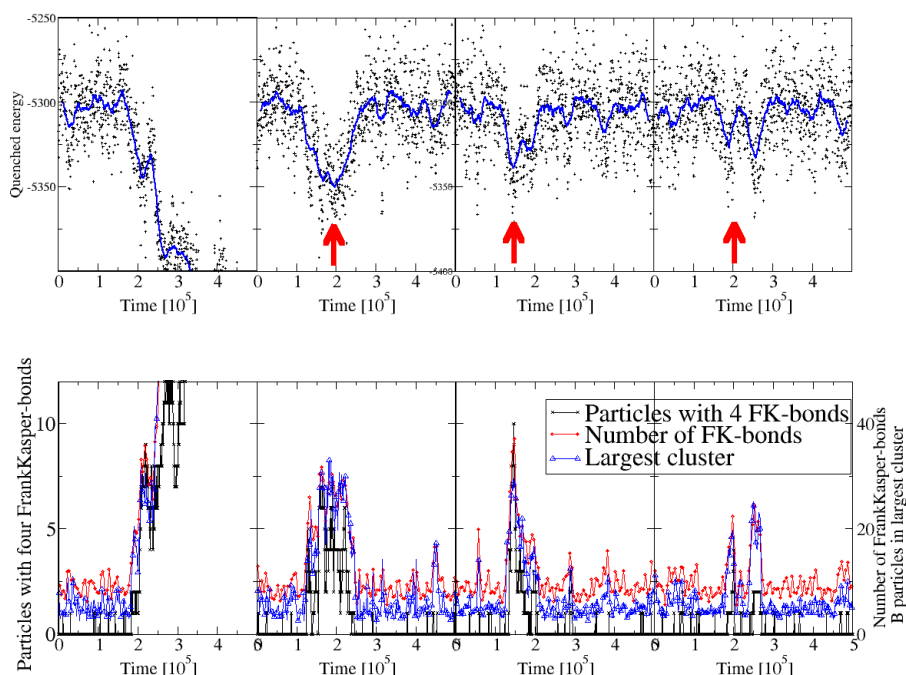


Figure 6.9: The top panels show quenched energy. In Panel 1A the drop in energy is a result of crystallization. In the remaining panels reversible drops in energy are observed. The lower panels show that the drops in energy are accompanied by the formation of extended Frank-Kasper cluster. Clusters at times marked with arrows are shown in Figure 6.10.

the crystal. Here, a connection is demonstrated. The reason why the liquid and crystal can use the same kind of local arrangements is the complexity of the crystal. The locally preferred arrangement can be assembled in many ways, without forming a crystal. The liquid could be said to have “entropic frustration”. This phrase is inspired by “geometric frustration”, used to explain metastability of the single component Lennard-Jones liquid (in three dimensions<sup>3</sup>). The locally preferred structure of the liquid is a perfect icosahedron. Icosahedra cannot tile space to make a crystal, and the liquid is said to have “geometric frustration” [Sadoc and Mosseri, 1999, Tarjus et al., 2005] (the crystal has the face centered cubic structure). The locally preferred structure of a liquid with entropic frustration can tile space, however, many non-crystal structures can also be build (high entropy). Other systems with some complexity of the crystal could also have entropic frustration.

<sup>3</sup>In two dimensions there is no frustration of a single particle liquid. The locally preferred structure is a hexagon. Hexagons can tile space to make a crystal.

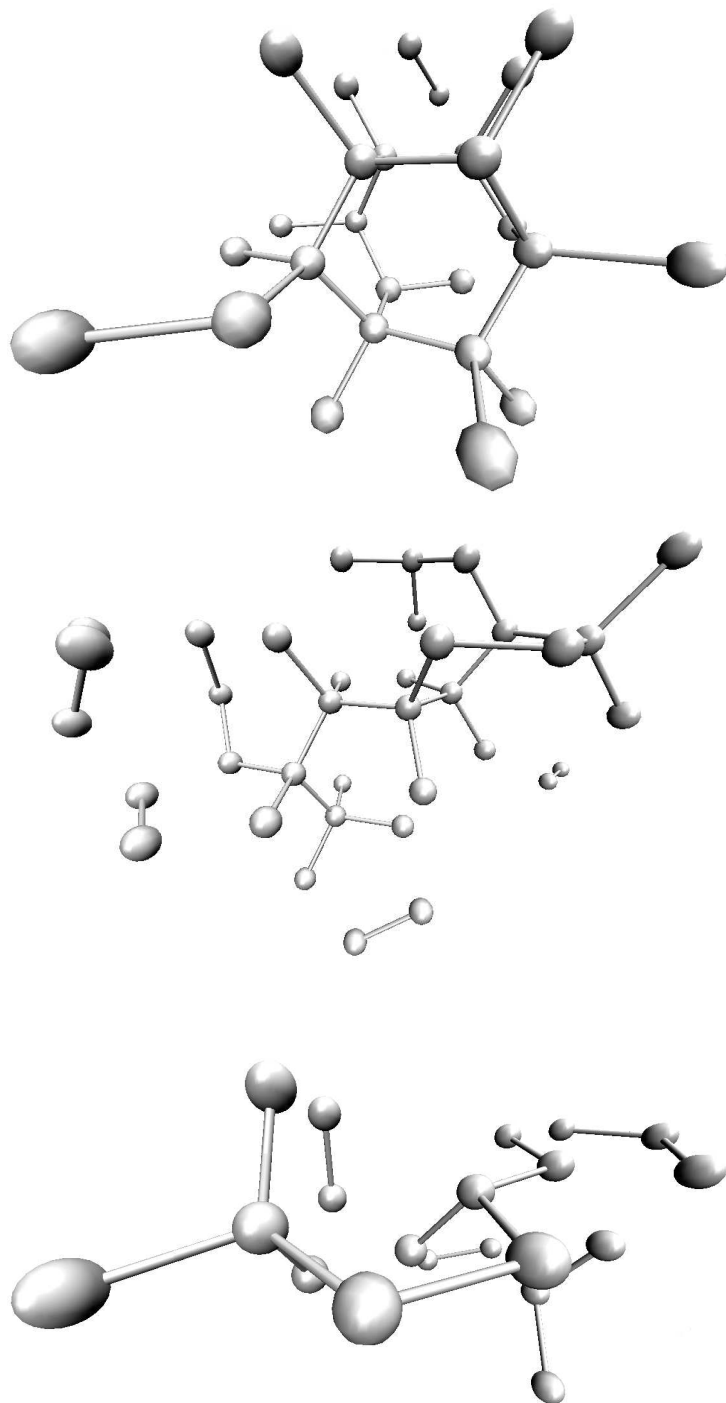


Figure 6.10: Representative transient Frank-Kasper clusters. See the legend of Figure 6.9 for details about the shown clusters. The cluster at the top is dense and similar to the crystal. The middle cluster has a more open structure. Note also the broken pentagon central in the cluster. This is not a feature of the crystal, and will clearly hinder crystallization. The bottom cluster have an even more open structure, not similar to the crystal.

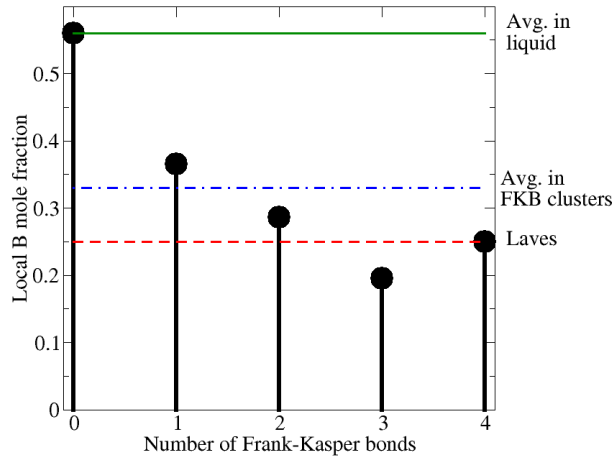


Figure 6.11: Local composition,  $\chi_B^{fs}$ , of B particles. Note that a large composition fluctuation is associated with the formation of a single Frank-Kasper bond.

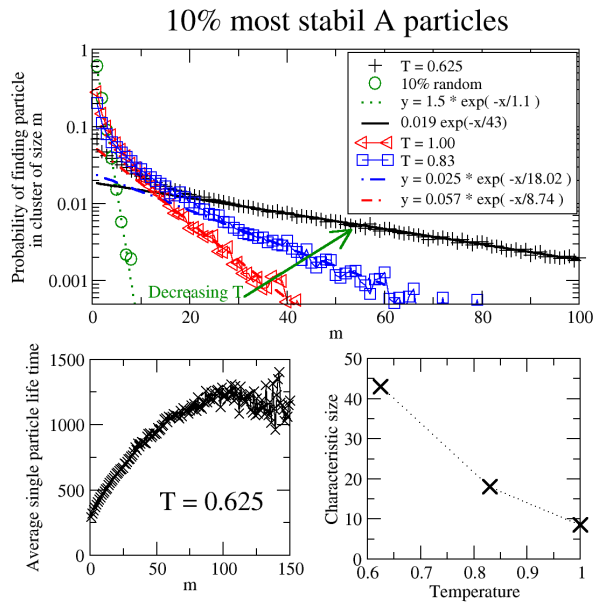


Figure 6.12: Cluster analysis of 10% most long-lived first shells. The top panel shows the cluster distribution at different temperatures. The lower left panel shows that long-lives particles tends to be in large cluster. The lower panel to the right shows that the characteristic cluster size increase when temperature is lowered.

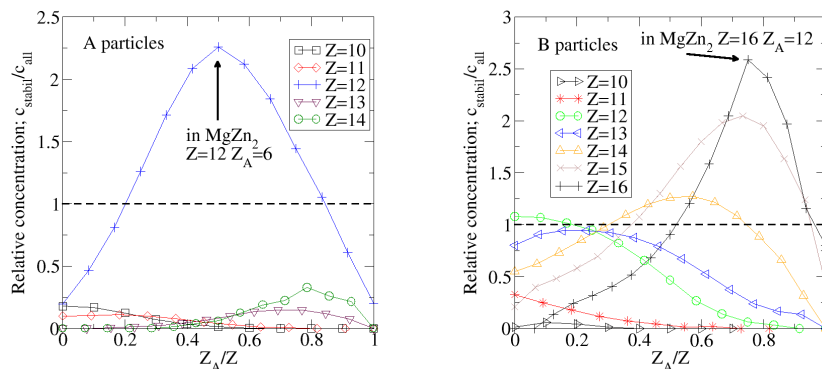


Figure 6.13: First shell of 10% most long-lived first shells. Note that particles with coordination of  $Z=12$  especially stable.

## 6.5 Kob-Andersen binary Lennard-Jones mixture

The crystallization of the Kob-Andersen binary Lennard-Jones liquid is discussed briefly in the following. The reader is referred to Paper XI for more details.

For both the Wahnström and the Kob-Andersen binary Lennard-Jones liquid the size ratio of particles is about 1.2. However, a difference is that the latter strongly disobeys the Lorentz-Berthelot rule, resulting in a strong AB attraction (see Figure 1.4 on page 6). Usually the Kob-Andersen mixture is simulated at  $A_4B_1$  composition where B refers to the smaller particle<sup>4</sup>, but if it is simulated at AB composition it will quickly crystallize in a CsCl structure. Figure 6.14 shows the distribution of first shells of the Kob-Andersen binary Lennard-Jones liquid at the  $A_4B_1$  composition. Note that strong AB attraction reduce composition fluctuations (compare to the Wahnström mixture, Figure 6.6). This prevents the AB crystal from forming at  $\chi_B = 0.20$ . However, a composition fluctuation can lead to crystallization of A particles in a face centered cubic (FCC) structure as demonstrated by Toxværd et al. [2007, and Paper XI]. Crystallization into a pure FCC crystal of A particles and a mixed CsCl crystal was foreseen by Fernandez and Harrowell [2003]. The FCC crystal is simple with only a single particle in the unit-cell. Thus, the crystal do not have the complexity of the Wahnström binary Lennard-Jones liquid, making the crystallization mechanism simpler.

Crystallization is avoided, if the AA and BB pair potential is truncating at the minimum and leave the AB pair potential untouched (Paper XI, simulations conducted by Søren Toxværd). See Paper XI for more details on this.

<sup>4</sup>The standard notation is used for classifying small and large particles. For the Wahnström liquid the larger particles are B's and smaller particles are A's. For the Kob-Andersen liquid the standard notation is the opposite so larger particles are A's and smaller particles are B's.

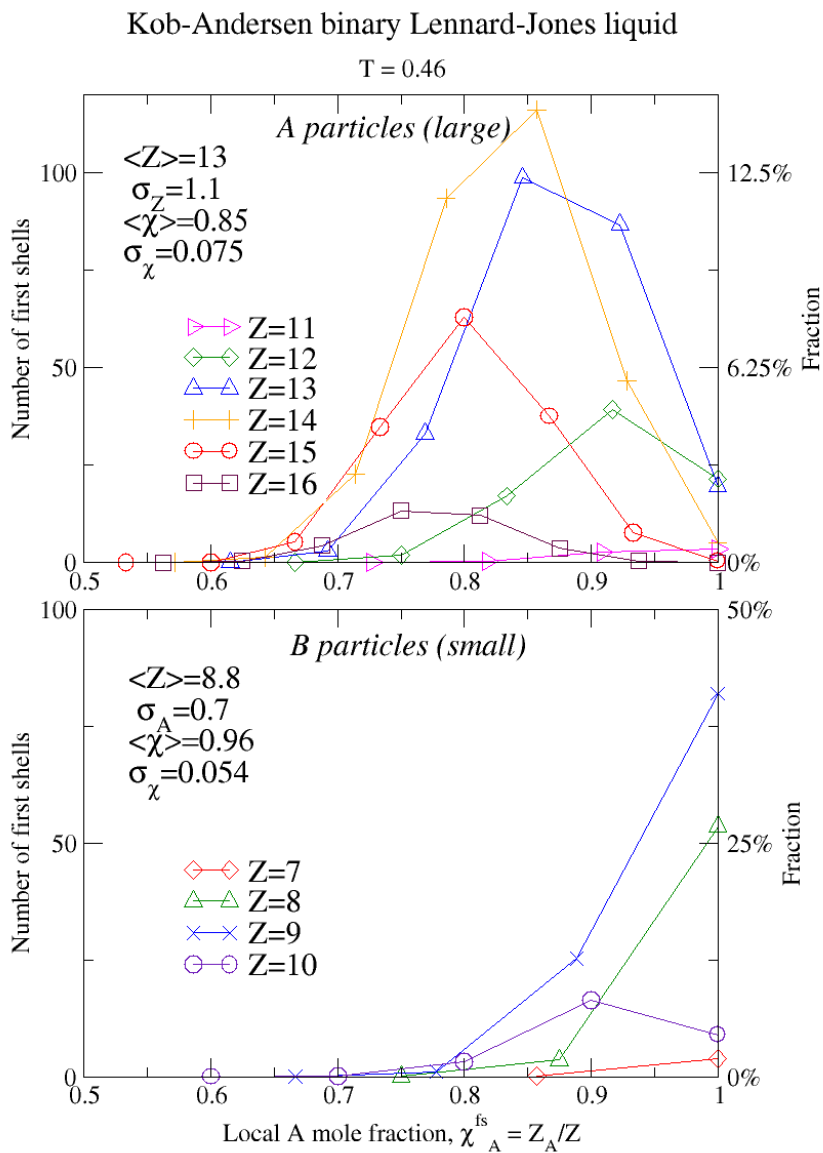


Figure 6.14: First shells of the Kob-Andersen binary Lennard-Jones liquid. Note that local composition fluctuations  $\sigma_{\chi_A^{\text{fs}}}$  are small compared the Wahnström mixture, Figure 6.6. This is a consequence of strong AB attraction, see text. The most frequent first shells are different from the crystal (CsCl and pure A FCC), see text.



## Chapter 7

# Outlook

As a summary of the thesis, this chapter provides a list of open questions and future research projects that would be a natural continuation.

- A:** The model systems investigated (see Figure 2.3 on page 16) in the study of thermodynamic fluctuations do not take quantum effects explicitly into account. First principles molecular dynamics simulations (like the method suggested by Car and Parrinello [1985]), would be valuable to get a better understanding of the thermodynamic correlations of real systems.
- B:** Strong  $W$ - $U$  correlations of the Lennard-Jones liquid are explained by an effective inverse power law (Chapter 3). Paper XIII test and confirms the effective inverse power law explanation for the asymmetric dumbbell model. However, this should also be done for more molecular systems.
- C:** The revising of the classical Prigogine-Defay ratio supported the conjecture of Section 2.2, that van der Waals bonded liquids are strongly correlating liquids. This raises the question: What other kinds of liquids are strongly correlating? Simulations of the metallic systems Cu and MgCu exhibit correlation coefficients of  $R_{WU} = 0.926$  ( $T = 2340$  K and  $\rho = 125.8$  mol/l) and  $R_{WU} = 0.797$  ( $T = 650$  K and  $\rho = 85$  mol/l) respectively (Paper VIII). The metallic mixture ZrTiCuNiBe has a classic Prigogine-Defay ratio of  $\Pi_{pT}^{\text{classic}} = 2.4$ , corresponding to a correlation coefficient of  $(\Pi_{pT}^{\text{classic}})^{-1/2} = 0.65$ . Simulations and experiments can be used to clarify if some metallic systems should be included in the class of strongly correlating liquids.
- D:** Relaxation of strongly correlating viscous liquids are simpler than that of viscous liquids in general. This has been demonstrated for relaxation of thermodynamic quantities like  $V$ ,  $E$ ,  $p$ ,  $T$ . It would be interesting if structural quantities follow the same relaxation. This can be investigated in simulations. In fact, some preliminary studies (data not shown) of the Wahnström binary Lennard-Jones liquid suggest that the number of 12 coordinated A particles,  $N_{A^{12}}$ , (Section 6.4) follows the (thermodynamic) single parameter. If this is the case, it reasonable to refer to the single parameter as a structural order parameter.

## 7. OUTLOOK

---

- E:** Let us assume that  $N_{A12}$  follows the (thermodynamic) single parameter. Recall that 12-coordinated A particles were important for the stability of the Wahnström binary Lennard-Jones liquid (Section 6.4). Thus, the single parameter determines how fast the liquid relaxes at a given instant. This may be related to the so-called internal clock of a viscous liquid [Olsen et al., 2008].
- F:** Values of the static  $NpT$  response functions of the glass and liquid at  $T_g$  can be found in literature for numerous liquids. These values can not only be used to calculate the classical Progomine-Defay ratio (Table 4.1), but also estimate a  $\gamma_{WU}$ -slope (see Subsection 4.1.3 on 40). This estimated  $\gamma_{WU}$  is expected to be equal to  $\gamma_s$  determined from scaling of structural relaxation time (Section 4.2).
- G:** Figure 4.8 (page 45) shows scaling of the radial distribution function of the Lewis-Wahnström OTP model of two state points with the same  $\Gamma$ . However, the scaling is not perfect as seen in the inset zooming in on the first peak. It is speculated that this is due to intramolecular bonds. This should be investigated further.
- H:** As discussed in Section 4.1.3, the classical approach of investigating strongly correlating viscous liquids is approximate. Experimentally measured frequency dependent or time dependent response function is a more direct approach. This is an ongoing work of the Glass and Time group.
- I:** The study of phospholipid membranes demonstrated that strong correlations are present in the slow thermodynamic fluctuations of membranes. One caveat is that  $\gamma_{UV}$  is not the same for the ordered and the disordered phase. This should be investigated further.
- J:** Other complex systems, where slow dynamics can be traced to a van der Waals bonded region, could have strong thermodynamic correlations (on some time scale). Proteins could be such systems.
- K:** Chapter 6 reports crystallization of the Lewis-Wahnström OTP model. More work is needed to identify the crystal structure (Figure 6.1) and to undertake a study of the crystallization. A part of this would include defining an orderparameter. Understanding the crystallization mechanism of this one-component system is interesting: Experimentally, OTP shows an interesting mechanics for crystallization close to the glass transition. In the most of the supercooled regime, the growth rate is limited by molecular diffusion. However, Mapes et al. [2006] have reported that close to the glass transition crystal growth is not limited by diffusion, but takes place faster. Apparently, local molecular motion is sufficient for the crystal to form. It is an open question whether the Lewis-Wahnström OTP model exhibits such crystallization mechanism.
- L:** Investigating the crystallization of the Wahnström binary Lennard-Jones liquid in terms of Frank-Kasper bonds has translated a problem of packing into a problem of forming a network (Section 6.3). However, more work should be made on clarifying which clusters lead to crystallisation and which do not. This investigation may be compared with crystallization of network forming liquids.

# Bibliography

- C. Alba-Simionesco, A. Cailliaux, A. Alegria, and G. Tarjus. Scaling out the density dependence of the  $\alpha$  relaxation in glass-forming polymers. *EUROPHYSICS LETTERS*, 68(1):58–64, OCT 2004. ISSN 0295-5075. doi: 10.1209/epl/i2004-10214-6.
- B. Alberts, A. Johnson, J. Lewis, M. Raff, K. Roberts, and P. Walter. *Molecular Biology of the Cell*. Garland, fourth edition, 2002. ISBN 0815332181.
- M. P. Allen and D. J. Tildesley. *Computer Simulations of Liquids*. Oxford Science Publications, 1987.
- H. C. Andersen, J. D. Weeks, and D. Chandler. Relationship between hard-sphere fluid and fluids with realistic repulsive forces. *Physical Review A: Atomic, Molecular, and Optical Physics*, 4(4):1597, 1971.
- C. A. Angell. Relaxations in complex systems. In K. L. Ngai and G. B. Wright, editors, *Strong and fragile liquids*, pages 3–11. U.S. GPO, Washington, D. C., 1985.
- P. Atkins and J. de Paula. *Physical Chemistry*. Oxford University Press, 2002.
- N. P. Bailey, J. Schiotz, and K. W. Jacobsen. Simulation of Cu-Mg metallic glass: Thermodynamics and structure. *Physical Review B: Condensed Matter and Materials Physics*, 69(14), Apr 2004. ISSN 1098-0121. doi: 10.1103/PhysRevB.69.144205.
- R. Becker and W. Doring. Kinetic treatment of germ formation in supersaturated vapour. *Annalen der Physik*, 24(8):719–752, Dec 1935. ISSN 0003-3804.
- D. Ben-Amotz and G. Stell. Analytical implementation and critical tests of fluid thermodynamic perturbation theory. *Journal of Chemical Physics*, 119(20):10777–10788, Nov 22 2003. ISSN 0021-9606. doi: 10.1063/1.1620995.
- H. J. C. Berendsen, J. R. Grigera, and T. P. Straatsma. The missing term in effective pair potentials. *Journal of Physical Chemistry*, 91(24):6269–6271, Nov 19 1987. ISSN 0022-3654.
- J. I. Berg and A. R. Cooper. Linear Non-Equilibrium Thermodynamic Theory of Glass-Transition Kinetics. *Journal of Chemical Physics*, 68(10):4481–4485, 1978. ISSN 0021-9606.
- J. N. Cape and L. V. Woodcock. Glass-transition in a soft-sphere model. *Journal of Chemical Physics*, 72(2):976–985, 1980. ISSN 0021-9606.

## BIBLIOGRAPHY

---

- R. Car and M. Parrinello. Unified Approach for Molecular-Dynamics and Density-Functional Theory. *Physical Review Letters*, 55(22):2471–2474, 1985. ISSN 0031-9007.
- R. Casalini and C. M. Roland. Thermodynamical scaling of the glass transition dynamics. *Physical Review E: Statistical, Nonlinear, and Soft Matter Physics*, 69(6, Part 1), JUN 2004. ISSN 1063-651X. doi: 10.1103/PhysRevE.69.062501.
- T. Christensen, N. B. Olsen, and J. C. Dyre. Conventional methods fail to measure  $c(p)(\omega)$  of glass-forming liquids. *PHYSICAL REVIEW E*, 75(4, Part 1), Apr 2007. ISSN 1539-3755. doi: 10.1103/PhysRevE.75.041502.
- J. H. R. Clarke. Molecular-dynamics studies of glass-formation in the Lennard-Jones model of argon. *Journal of Chemical Society - Faraday Transactions II*, 75(Part 10):1371–1387, 1979. ISSN 0300-9238.
- D. Coslovich and G. Pastore. Understanding fragility in supercooled Lennard-Jones mixtures. I. Locally preferred structures. *Journal of Chemical Physics*, 127(12):124504, Sep 28 2007. ISSN 0021-9606. doi: 10.1063/1.2773716.
- D. Coslovich and C. M. Roland. Pressure-energy correlations and thermodynamic scaling in viscous Lennard-Jones liquids. *Journal of Chemical Physics*, 130(1):014508, 7 Jan 2009. doi: 10.1063/1.3054635.
- D. Coslovich and C. M. Roland. Thermodynamic scaling of diffusion in supercooled Lennard-Jones liquids. *Journal of Physical Chemistry B*, 112(5):1329–1332, Feb 7 2008. ISSN 1520-6106. doi: 10.1021/jp710457e.
- R. O. Davies and G. O. Jones. Thermodynamic and kinetic properties of glasses. *Advances In Physics*, 2(7):370–410, 1953a. ISSN 0001-8732.
- R. O. Davies and G. O. Jones. The irreversible approach to equilibrium in glasses. *Proceedings Of The Royal Society Of London Series A: Mathematical And Physical Sciences*, 217(1128):26–42, 1953b.
- P. Debenedetti and F. Stillinger. Supercooled liquids and the glass transition. *Nature*, 410(6825):259–267, Mar 8 2001. ISSN 0028-0836.
- P. G. Debenedetti. Thermodynamics - When a phase is born. *Nature*, 441(7090):168–169, May 11 2006. ISSN 0028-0836. doi: 10.1038/441168a.
- E. A. DiMarzio. Validity of Ehrenfest relation for a system with more than one order parameter. *Journal of Applied Physics*, 45(10):4143–4145, 1974. ISSN 0021-8979.
- D. B. Dingwell, R. Knoche, and S. L. Webb. A volume temperature relationship for liquid  $\text{GeO}_2$  and some geophysically relevant derived parameters for network liquids. *Physics and Chemistry of Minerals*, 19(7):445–453, Feb 1993. ISSN 0342-1791.
- E.-J. Donth. Der glasübergang. In *Wissenschaftliche Taschenbücher Mathematik-Physik*, volume 271. Akademie-Verlag, Berlin, 1981.

- 
- C. Dreyfus, A. Aouadi, J. Gapinski, M. Matos-Lopes, W. Steffen, A. Patkowski, and R. M. Pick. Temperature and pressure study of Brillouin transverse modes in the organic glass-forming liquid orthoterphenyl. *Physical Review E: Statistical, Nonlinear, and Soft Matter Physics*, 68:011204, 2003.
- J. C. Dyre. Colloquium: The glass transition and elastic models of glass-forming liquids. *Reviews of Modern Physics*, 78(3):953–972, Jul-Sep 2006. ISSN 0034-6861. doi: 10.1103/RevModPhys.78.953.
- S. U. Dzhaliilo and K. I. Rzaev. On Phenomenon Of Selenium Vitrification. *Physica Status Solidi*, 20(1):261, 1967. ISSN 0031-8957.
- M. Dzugutov. Glass-formation in a simple monatomic liquid with icosahedral inherent local order. *Physical Review A: Atomic, Molecular, and Optical Physics*, 46(6):R2984–R2987, Sep 15 1992. ISSN 1050-2947.
- H. Ebel, P. Grabitz, and T. Heimburg. Enthalpy and volume changes in lipid membranes. I. The proportionality of heat and volume changes in the lipid melting transition and its implication for the elastic constants. *Journal of Physical Chemistry B*, 105(30):7353–7360, Aug 2 2001. ISSN 1089-5647. doi: 10.1021/jp010515s.
- M. D. Ediger. Spatially heterogeneous dynamics in supercooled liquids. *Annual Review of Physical Chemistry*, 51:99–128, 2000. ISSN 0066-426X.
- N. L. Ellegaard. *Energy landscape approaches to the dynamics of supercooled liquids*. PhD thesis, Institut for studiet af Matematik og Fysik samt deres Funktioner i Undervisning, Forskning og Anvendelser (IMFUFA), Roskilde University, Denmark, 2005.
- S. E. Feller, Y. H. Zhang, R. W. Pastor, and B. R. Brooks. Constant-Pressure Molecular-Dynamics Simulation - The Langevin Piston Method. *Journal of Chemical Physics*, 103(11):4613–4621, Sep 15 1995. ISSN 0021-9606.
- J. R. Fernandez and P. Harrowell. Crystal phases of a glass-forming Lennard-Jones mixture. *Physical Review E: Statistical, Nonlinear, and Soft Matter Physics*, 67(1, Part 1), Jan 2003. ISSN 1063-651X. doi: 10.1103/PhysRevE.67.011403.
- M. L. Ferrer, C. Lawrence, B. Demirjian, D. Kivelson, C. Alba-Simionesco, and G. Tarjus. Supercooled liquids and the glass transition: Temperature as the control variable. *Journal of Chemical Physics*, 109(18):8010–8015, Nov 8 1998. ISSN 0021-9606.
- N. Foloppe and A. D. MacKerell. All-atom empirical force field for nucleic acids: I. Parameter optimization based on small molecule and condensed phase macromolecular target data. *Journal of Computational Chemistry*, 21(2):86–104, Jan 30 2000. ISSN 0192-8651.
- F. C. Frank and J. S. Kasper. Complex Alloy Structures Regarded as Sphere Packings .1. Definitions and Basic Principles. *Acta Crystallographica*, 11(3): 184–190, 1958. ISSN 0108-7673.

## BIBLIOGRAPHY

---

- F. C. Frank and J. S. Kasper. Complex Alloy Structures Regarded as Sphere Packing .2. Analysis and Classification of Representative Structures. *Acta Crystallographica*, 12(7):483–499, 1959. ISSN 0108-7673.
- M. Goldstein. Validity of Ehrenfest equation for a system with more than one ordering parameter - critique of a paper by Dimarzio. *Journal of Applied Physics*, 46(10):4153–4156, 1975. ISSN 0021-8979.
- P. K. Gupta and C. T. Moynihan. Prigogine-Defay ratio for systems with more than one order parameter. *Journal of Chemical Physics*, 65(10):4136–4140, 1976. ISSN 0021-9606.
- J. Hadac, P. Slobodian, P. Riha, P. Saha, R. W. Rychwalski, I. Emri, and J. Kubat. Effect of cooling rate on enthalpy and volume relaxation of polystyrene. *Journal of Non-Crystalline Solids*, 353(28):2681–2691, Sep 1 2007. ISSN 0022-3093. doi: 10.1016/j.jnoncrysol.2007.05.017.
- J.-P. Hansen and I. McDonald. *Theory of Simple Liquids*. Academic Press, third edition, 2006.
- T. Hecksher, A. I. Nielsen, N. B. Olsen, and J. C. Dyre. Little evidence for dynamic divergences in ultraviscous molecular liquids. *Nature Physics*, 4(9):737–741, Sep 2008. ISSN 1745-2473. doi: 10.1038/nphys1033.
- T. Heimburg. Mechanical aspects of membrane thermodynamics. Estimation of the mechanical properties of lipid membranes close to the chain melting transition from calorimetry. *Biochimica et Biophysica Acta, Biomembranes*, 1415(1):147–162, Dec 9 1998. ISSN 0005-2736.
- T. Heimburg and A. D. Jackson. On soliton propagation in biomembranes and nerves. *Proceedings of the National Academy of Sciences of the United States of America*, 102(28):9790–9795, Jul 12 2005. ISSN 0027-8424. doi: 10.1073/pnas.0503823102.
- T. Heimburg and A. D. Jackson. The thermodynamics of general anesthesia. *Biophysical Journal*, 92(9):3159–3165, May 1 2007. ISSN 0006-3495. doi: 10.1529/biophysj.106.099754.
- S. Hensel-Bielowka, M. Paluch, J. Ziolo, and C. M. Roland. Dynamics of sorbitol at elevated pressure. *Journal of Physical Chemistry B*, 106(48):12459–12463, DEC 5 2002. ISSN 1520-6106. doi: 10.1021/jp0264228.
- B. Hess, H. Bekker, H. J. C. Berendsen, and J. G. E. M. Fraaije. LINCS: A linear constraint solver for molecular simulations. *Journal of Computational Chemistry*, 18(12):1463–1472, Sep 1997. ISSN 0192-8651.
- A. L. Hodgkin and A. F. Huxley. A Quantitative Description of Membrane Current and its Application to Conduction and Excitation in Nerve. *Journal of Physiology, London*, 117(4):500–544, 1952. ISSN 0022-3751.
- J. D. Honeycutt and H. C. Andersen. Small System Size Artifacts in The Molecular-Dynamics Simulation of Homogeneous Crystal Nucleation in Supercooled Atomic Liquids. *Journal of Physical Chemistry*, 90(8):1585–1589, Apr 10 1986. ISSN 0022-3654.

- 
- W. G. Hoover. Canonical Dynamics - Equilibrium Phase-Space Distributions. *Physical Review A: Atomic, Molecular, and Optical Physics*, 31(3):1695–1697, 1985. ISSN 1050-2947.
- W. G. Hoover and M. Ross. Statistical Theories Of Melting. *Contemporary Physics*, 12(4):339, 1971. ISSN 0010-7514.
- W. G. Hoover, M. Roos, K. W. Johnson, D. Henderson, J. A. Barker, and B. C. Brown. Soft-sphere equation of state. *Journal of Chemical Physics*, 52(10):4931, 1970. ISSN 0021-9606.
- W. G. Hoover, S. G. Gray, and K. W. Johnson. Thermodynamic Properties of Fluid and Solid Phases force Inverse Power Potentials. *Journal of Chemical Physics*, 55(3):1128, 1971. ISSN 0021-9606.
- W. Humphrey, A. Dalke, and K. Schulten. VMD – Visual Molecular Dynamics. *Journal of Molecular Graphics*, 14:33–38, 1996.
- K. W. Jacobsen, J. K. Nørskov, and M. J. Puska. Interatomic Interactions In The Effective-Medium Theory. *Physical Review B: Condensed Matter and Materials Physics*, 35(14):7423–7442, May 15 1987. ISSN 0163-1829.
- K. W. Jacobsen, P. Stoltze, and J. K. Nørskov. A semi-empirical effective medium theory for metals and alloys. *Surface Science*, 366(2):394–402, Oct 20 1996. ISSN 0039-6028.
- W. L. Jorgensen, J. D. Madura, and C. J. Swenson. Optimized intermolecular potential functions for liquid hydrocarbons. *Journal of the American Chemical Society*, 106(22):6638–6646, 1984. ISSN 0002-7863.
- L. Kale, R. Skeel, M. Bhandarkar, R. Brunner, A. Gursoy, N. Krawetz, J. Phillips, A. Shinozaki, K. Varadarajan, and K. Schulten. NAMD2: Greater scalability for parallel molecular dynamics. *Journal of Computational Physics*, 151(1):283–312, May 1 1999. ISSN 0021-9991.
- W. Kob and H. C. Andersen. Scaling behavior in the  $\beta$ -relaxation regime of a supercooled Lennard-Jones mixture. *Physical Review Letters*, 73(10):1376–1379, Sep 1994. doi: 10.1103/PhysRevLett.73.1376.
- W. Kob and H. C. Andersen. Testing mode-coupling theory for a supercooled binary Lennard-Jones mixture I: The van Hove correlation function. *Physical Review E: Statistical, Nonlinear, and Soft Matter Physics*, 51(5):4626–4641, May 1995a. doi: 10.1103/PhysRevE.51.4626.
- W. Kob and H. C. Andersen. Testing Mode-Coupling Theory for a Supercooled Binary Lennard-Jones Mixture .2. Intermediate Scattering Function and Dynamic Susceptibility. *Physical Review E: Statistical, Nonlinear, and Soft Matter Physics*, 52(4, Part B):4134–4153, Oct 1995b. ISSN 1063-651X.
- J. K. Kummerfeld, T. S. Hudson, and P. Harrowell. The densest packing of AB binary hard-sphere homogeneous compounds across all size ratios. *Journal of Physical Chemistry B*, 112(35):10773–10776, Sep 4 2008. ISSN 1520-6106. doi: 10.1021/jp804953r.

## BIBLIOGRAPHY

---

- A. Le Grand, C. Dreyfus, C. Bousquet, and R. M. Pick. Scaling of the structural relaxation in simulated liquid silica. *Physical Review E: Statistical, Nonlinear, and Soft Matter Physics*, 75(6, Part 1), Jun 2007. ISSN 1539-3755. doi: 10.1103/PhysRevE.75.061203.
- E. W. Lemmon, M. O. McLinden, and D. G. Friend. Thermophysical properties of fluid systems. In P. J. Linstrom and W. G. Mallard, editors, *Chemistry WebBook, NIST Standard Reference Database Number 96*. National Institute of Standards and Technology, Gaithersburg MD, 20899, 2005. URL <http://webbook.nist.gov>.
- J. E. Lennard-Jones. Cohesion. *Proceedings of the Physical Society*, 43(Part 1):461–482, Jan 1931. ISSN 0959-5309.
- A. V. Lesikar and C. T. Moynihan. Some relations connecting volume and enthalpy relaxation in the order parameter model of liquids and glasses. *Journal of Chemical Physics*, 72(12):6422–6423, 1980. ISSN 0021-9606.
- L. J. Lewis and G. Wahnström. Molecular-dynamics study of supercooled ortho-terphenyl. *Physical Review E: Statistical, Nonlinear, and Soft Matter Physics*, 50(5):3865–3877, Nov 1994. ISSN 1063-651X.
- M. W. Mahoney and W. L. Jorgensen. A five-site model for liquid water and the reproduction of the density anomaly by rigid, nonpolarizable potential functions. *Journal of Chemical Physics*, 112(20):8910–8922, May 22 2000. ISSN 0021-9606.
- M. Mapes, S. Swallen, and M. Ediger. Self-diffusion of supercooled o-terphenyl near the glass transition temperature. *JOURNAL OF PHYSICAL CHEMISTRY B*, 110(1):507–511, JAN 12 2006. ISSN 1520-6106. doi: 10.1021/jp0555955.
- C. T. Moynihan and P. K. Gupta. Order parameter model for structural relaxation in glass. *Journal of Non-Crystalline Solids*, 29(2):143–158, 1978. ISSN 0022-3093.
- C. T. Moynihan and A. V. Lesikar. Comparison and analysis of relaxation processes at the glass-transition temperature. *Annals of the New York Academy of Sciences*, 371(Oct):151–169, 1981. ISSN 0077-8923.
- C. T. Moynihan, P. B. Macedo, C. J. Montrose, P. K. Gupta, M. A. Debolt, J. F. Dill, B. E. Dom, P. W. Drake, A. J. Eastal, P. B. Elterman, R. P. Moeller, H. Sasabe, and J. A. Wilder. Structural relaxation in vitreous materials. *Annals of the New York Academy of Sciences*, 279(Oct 15):15–35, 1976. ISSN 0077-8923.
- M. Naoki, K. Matsumoto, and M. Matsushita. Factors Determining Relaxation-Time and Glass-Transition .2. Triphenylchloromethane Ortho-Terphenyl Mixture. *Journal of Physical Chemistry*, 90(18):4423–4427, Aug 28 1986. ISSN 0022-3654.
- S. V. Nemilov. *Thermodynamic and Kinetic Aspects of the Vitreous State*. CRS, London, 1994.

- 
- A. I. Nielsen, T. Christensen, B. Jakobsen, K. Niss, N. B. Olsen, R. Richert, and J. C. Dyre. Prevalence of approximate  $\sqrt{t}$  relaxation for the dielectric  $\alpha$  process in viscous organic liquids. *arXiv*, 0811.1116v1 [cond-mat.soft], 2008. URL <http://arxiv.org/abs/0811.1116>.
- J. K. Nielsen. Linear response theory for thermodynamic properties. *Physical Review E: Statistical, Nonlinear, and Soft Matter Physics*, 60(1):471–481, Jul 1999. ISSN 1063-651X.
- L. K. Nielsen, T. Bjornholm, and O. G. Mouritsen. Thermodynamic and real-space structural evidence of a 2D critical point in phospholipid monolayers. *Langmuir*, 23(23):11684–11692, Nov 6 2007. ISSN 0743-7463. doi: 10.1021/la7016352.
- T. M. Nieuwenhuizen. Ehrenfest relations at the glass transition: Solution to an old paradox. *Physical Review Letters*, 79(7):1317–1320, Aug 18 1997. ISSN 0031-9007.
- T. M. Nieuwenhuizen. Thermodynamic picture of the glassy state. *Journal of Physics: Condensed Matter*, 12(29):6543–6552, Jul 24 2000. ISSN 0953-8984. Workshop on Unifying Concepts in Glass Physics, Trieste, Italy, Sep 15-18, 1999.
- S. Nosé. A Molecular-Dynamics Method for Simulations in the Canonical Ensemble. *Molecular Physics*, 52(2):255–268, 1984. ISSN 0026-8976.
- H. J. Oels and G. Rehage. Pressure-volume-temperature measurements on atactic polystyrene - thermodynamic view. *Macromolecules*, 10(5):1036–1043, 1977. ISSN 0024-9297.
- N. B. Olsen, T. Hecksher, K. Niss, and J. C. Dyre. Physical ageing studied by a device allowing for rapid thermal equilibration. *arXiv.org*, pages arXiv:0811.0994v1 [cond-mat.soft], 2008. URL <http://arxiv.org/abs/0811.0994>.
- A. E. Owen. The glass transition. In N. H. March, R. A. Street, and M. P. Tosi, editors, *Amorphous Solids and The Liquid State*, pages 395–432. Kluwer Academic Publishers Group, 1985.
- W. B. Pearson. *The Crystal Chemistry and Physics of Metals and Alloys*. Wiley-Interscience, New York, 1972.
- U. R. Pedersen. Strukturelle ændringer af en phospholipidmembran perturberet med n-alkohol undersøgt med md-simuleringer og saxs. Master's thesis, Roskilde University, Postbox 260, DK-4000 Roskilde, Denmark, Dec 2005. In danish. English title: Structural changes of a phospholipidmembran perturbed with n-alcohol investigated by MD-simulations and SAXS.
- U. R. Pedersen, C. Leidy, P. Westh, and G. H. Peters. The effect of calcium on the properties of charged phospholipid bilayers. *Biochimica et Biophysica Acta, Biomembranes*, 1758(5):573–582, May 2006. ISSN 0005-2736. doi: 10.1016/j.bbamem.2006.03.035.

## BIBLIOGRAPHY

---

- U. R. Pedersen, G. H. Peters, and P. Westh. Molecular packing in 1-hexanol-DMPC bilayers studied by molecular dynamics simulation. *Biophysical Chemistry*, 125(1):104–111, Jan 2007. ISSN 0301-4622. doi: 10.1016/j.bpc.2006.07.005.
- R. M. Pick. The Prigogine-Defay ratio and the microscopic theory of supercooled liquids. *Journal of Chemical Physics*, 129(12), Sep 28 2008. ISSN 0021-9606. doi: 10.1063/1.2969899.
- I. Prigogine and R. Defay. *Chemical thermodynamics*. Longmans, Green and Co, New York, 1954.
- R. J. Roe. Thermodynamics of glassy state with multiple order parameters. *Journal of Applied Physics*, 48(10):4085–4091, 1977. ISSN 0021-8979.
- C. M. Roland, S. Hensel-Bielowka, M. Paluch, and R. Casalini. Supercooled dynamics of glass-forming liquids and polymers under hydrostatic pressure. *Reports on Progress in Physics*, 68(6):1405–1478, Jun 2005. ISSN 0034-4885. doi: 10.1088/0034-4885/68/6/R03.
- C. M. Roland, S. Bair, and R. Casalini. Thermodynamic scaling of the viscosity of van der Waals, H-bonded, and ionic liquids. *Journal of Chemical Physics*, 125(12), Sep 28 2006. ISSN 0021-9606. doi: 10.1063/1.2346679.
- C. M. Roland, R. Casalini, R. Bergman, and J. Mattsson. Role of hydrogen bonds in the supercooled dynamics of glass-forming liquids at high pressures. *Physical Review B: Condensed Matter and Materials Physics*, 77(1), Jan 2008. ISSN 1098-0121. doi: 10.1103/PhysRevB.77.012201.
- Y. Rosenfeld. A quasi-universal scaling law for atomic transport in simple fluids. *Journal of Physics: Condensed Matter*, 11(28):5415–5427, Jul 19 1999. ISSN 0953-8984.
- J. F. Sadoc and R. Mosseri. *Geometric Frustration*. Cambridge University Press, 1999.
- K. Samwer, R. Busch, and W. L. Johnson. Change of compressibility at the glass transition and Prigogine-Defay ratio in ZrTiCuNiBe alloys. *Physical Review Letters*, 82(3):580–583, Jan 18 1999. ISSN 0031-9007.
- J. W. P. Schmelzer and I. Gutzow. The prigogine-defay ratio revisited. *Journal of Chemical Physics*, 125(18), Nov 14 2006. ISSN 0021-9606. doi: 10.1063/1.2374894.
- B. Smit and D. Frenkel. *Understanding Molecular Simulation: from Algorithms to Applications*. Academic Press; 2nd edition (October 15, 2001), second edition, 2001.
- J. Sonne, M. O. Jensen, F. Y. Hansen, L. Hemmingsen, and G. H. Peters. Reparameterization of all-atom dipalmitoylphosphatidylcholine lipid parameters enables simulation of fluid bilayers at zero tension. *Biophysical Journal*, 92(12):4157–4167, Jun 2007. ISSN 0006-3495. doi: 10.1529/biophysj.106.087130.

- 
- M. R. Spiegel and J. Liu. Mathematical handbook of formulars and tables. In *Schaum's Outline Series*. McGraw-Hill, 2nd edition, 1999.
- F. Stein, M. Palm, and G. Sauthoff. Structure and stability of Laves phases. Part I. Critical assessment of factors controlling Laves phase stability. *Intermetallics*, 12(7-9, Sp. Iss. SI):713–720, Jul-Sep 2004. ISSN 0966-9795. doi: 10.1016/j.intermet.2004.02.010.
- F. Stein, A. Palm, and G. Sauthoff. Structure and stability of Laves phases part II - structure type variations in binary and ternary systems. *Intermetallics*, 13(10):1056–1074, Oct 2005. ISSN 0966-9795. doi: 10.1016/j.intermet.2004.11.001.
- S. Takahara, M. Ishikawa, O. Yamamuro, and T. Matsuo. Structural relaxations of glassy polystyrene and o-terphenyl studied by simultaneous measurement of enthalpy and volume under high pressure. *Journal of Physical Chemistry B*, 103(5):792–796, Feb 4 1999. ISSN 1089-5647.
- G. Tarjus, S. A. Kivelson, Z. Nussinov, and P. Viot. The frustration-based approach of supercooled liquids and the glass transition: a review and critical assessment. *Journal of Physics: Condensed Matter*, 17(50):R1143–R1182, Dec 21 2005. ISSN 0953-8984. doi: 10.1088/0953-8984/17/50/R01.
- P. R. ten Wolde and D. Frenkel. Computer simulation study of gas-liquid nucleation in a Lennard-Jones system. *Journal of Chemical Physics*, 109(22):9901–9918, Dec 8 1998. ISSN 0021-9606.
- D. P. Tieleman and H. J. C. Berendsen. Molecular dynamics simulations of a fully hydrated dipalmitoyl phosphatidylcholine bilayer with different macroscopic boundary conditions and parameters. *Journal of Chemical Physics*, 105(11):4871–4880, Sep 15 1996. ISSN 0021-9606.
- A. Tölle. Neutron scattering studies of the model glass former ortho-terphenyl. *Reports on Progress in Physics*, 64(11):1473–1532, Nov 2001. ISSN 0034-4885.
- S. Toxværd, T. B. Schrøder, and J. C. Dyre. Crystallization of the Kob-Andersen binary Lennard-Jones liquid. *arXiv*, 0712.0377v2 [cond-mat.soft], Dec 2007. URL <http://arxiv.org/abs/0712.0377>.
- D. van der Spoel, E. Lindahl, B. Hess, A. R. van Buuren, E. Apol, P. J. Meulenhoff, D. P. Tieleman, A. L. Sijbers, K. A. Feenstra, R. van Drunen, and H. J. Berendsen. *GROMACS user manual version 3.3*, 2006. URL [www.gromacs.org](http://www.gromacs.org).
- W. F. van Gunsteren, S. R. Billeter, A. A. Eising, P. H. Hunenberger, P. Kruger, A. E. Mark, W. R. P. Scott, and I. G. Tironi. *Biomolecular simulation: The GROMOS96 manual and user guide*. vdf Hochschulverlag AG an der ETH Zurich and BIOMOS b.v., Zurich, Groningen, 1996.
- R. M. Venable, B. R. Brooks, and R. W. Pastor. Molecular dynamics simulations of gel (L-beta I) phase lipid bilayers in constant pressure and constant surface area ensembles. *Journal of Chemical Physics*, 112(10):4822–4832, Mar 8 2000. ISSN 0021-9606.

## BIBLIOGRAPHY

---

- M. Volmer and A. Weber. Germ-formation in oversaturated figures. *Zeitschrift für Physikalische Chemie-Stoichiometrie und Verwandtschaftslehre*, 119(3/4): 277–301, Mar 1926. ISSN 0372-8501.
- G. Voronoi. New parametric applications concerning the theory of quadratic forms - second announcement. *Journal für die Reine und Angewandte Mathematik*, 134:198–287, 1908.
- G. Wahnström. Molecular-Dynamics Study of a Supercooled 2-Component Lennard-Jones System. *Physical Review A: Atomic, Molecular, and Optical Physics*, 44(6):3752–3764, Sep 15 1991. ISSN 1050-2947.
- L. Wondraczek and H. Behrens. Molar volume, excess enthalpy, and Prigogine-Defay ratio of some silicate glasses with different (P,T) histories. *Journal of Chemical Physics*, 127(15), Oct 21 2007. ISSN 0021-9606. doi: 10.1063/1.2794745.
- E. Zaccarelli, G. Foffi, K. A. Dawson, S. V. Buldyrev, F. Sciortino, and P. Tartaglia. Confirmation of anomalous dynamical arrest in attractive colloids: A molecular dynamics study. *Physical Review E: Statistical, Nonlinear, and Soft Matter Physics*, 66(4, Part 1), Oct 2002. ISSN 1063-651X. doi: 10.1103/PhysRevE.66.041402.
- E. Zaccarelli, F. Sciortino, and P. Tartaglia. Numerical study of the glass-glass transition in short-ranged attractive colloids. *Journal of Physics: Condensed Matter*, 16(42, Sp. Iss. SI):S4849–S4860, Oct 27 2004. ISSN 0953-8984. doi: 10.1088/0953-8984/16/42/004. Workshop on Structural Arrest Transitions in Colloidal Systems with Short-Range Attractions, Messina, ITALY, DEC 17-20, 2003.
- R. T. Zhang, W. J. Sun, S. Tristramnagle, R. L. Headrick, R. M. Suter, and J. F. Nagle. Critical Fluctuations in Membranes. *Physical Review Letters*, 74(14):2832–2835, Apr 3 1995. ISSN 0031-9007.
- P. Zoller. A study of the pressure-volume-temperature relationships of four related amorphous polymers: Polycarbonate, polyarylate, phenoxy, and polysulfone. *Journal of Polymer Science, Part B: Polymer Physics*, 20:1453–1464, 1982. doi: 10.1002/pol.1982.180200811.

# Appendix A

## Calculations

### A.1 Energy-pressure correlations in a soft-sphere liquid

In soft-sphere liquid where particles interact via a inverse power-law potential<sup>1</sup>,

$$U_{ij}^{pow} = a_{ij}r_{ij}^{-n}. \quad (\text{A.1})$$

where  $r_{ij}$  is the distance between particle  $i$  and  $j$ , and  $a_{i,j}$ 's and  $b$  are constants. The total potential energy of a system of  $N$  particles is

$$U^{pow} = \sum_{i>j}^N U_{ij}^{pow} \quad (\text{A.2})$$

The virial is given by

$$W = \frac{1}{3} \sum_{ih} r_{ij} F_{ij} \quad (\text{A.3})$$

where

$$F_{ij} = -\frac{d}{dr} U_{ij} = na_{ij}r_{ij}^{-n} \quad (\text{A.4})$$

is the force between particle  $i$  and  $j$ . Thus, virial is proportional to potential energy,

$$W^{pow}(t) = \gamma_{WU}^{pow} U^{pow}(t), \quad (\text{A.5})$$

with a proportionality constant of

$$\gamma_{WU}^{pow} = n/3. \quad (\text{A.6})$$

### A.2 Fitting inverse power-law to the generalized Lennard-Jones potential

At distance  $r_s$  ( $r_s < 1$ ) we can fit and inverse power-law plus a constant,

$$U_{ij}^{pow} = ar^{-p} + c, \quad (\text{A.7})$$

---

<sup>1</sup>Note that we here uses index  $ij$  on the prefactor  $a_{ij}$  for the sake of generality. So perfect correlation goes for a poly-disperse system as well as a mono-disperse.

## A. CALCULATIONS

---

to the generalized Lennard-Jones potential (having a global minimum of  $-1$  at  $r = 1$ ),

$$U_{ij}^{LJ} = (nr^{-m} - mr^{-n})/(m - n), \quad (\text{A.8})$$

by matching pair energy ( $U_{ij}$ ), virial ( $W_{ij} = -r \frac{d}{dr} U_{ij}$ ) and hyper-virial ( $X_{ij} = -r \frac{d}{dr} W_{ij}$ ). First, put  $\frac{X_{ij}^{LJ}(r_s)}{W_{ij}^{LJ}(r_s)} = \frac{X_{ij}^{\text{pow}}(r_s)}{W_{ij}^{\text{pow}}(r_s)}$  and isolate the exponent,

$$p = (mr_s^{-m} - nr_s^{-n})/(r_s^{-m} - r_s^{-n}). \quad (\text{A.9})$$

Then put  $W_{ij}^{LJ}(r_s) = W_{ij}^{\text{pow}}(r_s)$  and isolate the pre-factor,

$$a = mn(r_s^{-m} - r_s^{-n})/[(m - n)pr_s^{-p}]. \quad (\text{A.10})$$

Finally put  $U_{ij}^{LJ}(r_s) = U_{ij}^{\text{pow}}(r_s)$  to get the constant,

$$c = (nr_s^{-m} - mr_s^{-n})/(m - n) - ar_s^{-p}. \quad (\text{A.11})$$

If  $p$  is known and not  $r_s$ , then isolate  $r_s$  from equation A.9,

$$r_s = [(n - p)/(m - p)]^{1/(n-m)}. \quad (\text{A.12})$$

The inverse power-law fitted to the standard Lennard-Jones potential (with  $m = 12$  and  $n = 6$ ) at the characteristic distance  $r_s = 2^{-1/6}$  where  $U_{ij}^{LJ}(r_s) = 0$  is

$$U_{ij}^{\text{pow}} = \frac{1}{6}r^{-18} + \frac{4}{3}. \quad (\text{A.13})$$

Rescaling the Lennard-Jones potential to get the minimum to  $2^{1/6}$  ( $r' = 2^{1/6}r$ ) we get

$$U_{ij}^{\text{pow}} = \frac{4}{3}r'^{-18} + \frac{4}{3} \quad (\text{A.14})$$

shown on Figure 3.1 page 20.